Bone Tissue Engineering using Colloidal Gels and Native Extracellular Matrix Biomaterials

By

S. Connor Dennis

B. S., Chemical and Petroleum Engineering, The University of Kansas, 2010

Submitted to the Bioengineering Program
and the Graduate Faculty of the University of Kansas
in partial fulfillment of the degree requirements for the degree of
Doctor of Philosophy

Committee Members:

_____
Dr. Cory J. Berkland, Committee Chair

_____
Dr. Michael Detamore

_____
Dr. Sarah Kieweg

_____
Dr. Teruna Siahaan

_____
Dr. Stevin Gehrke

January 12th, 2015
Date defended

The Dissertation Committee for Stephen Connor Dennis certifies that this is the approved version of the following dissertation:

Bone Tissue Engineering using Colloidal Gels and Native Extracellular Matrix Biomaterials

Committee Chair

_____

Dr. Cory J. Berkland, Committee Chair

February 3rd, 2015

Date approved

ABSTRACT

Self-assembling and shear-responsive biomaterials possess favorable rheological and viscoelastic properties to be injectable and facilitate minimally invasive surgery. The current thesis work describes the evaluation of malleable colloidal gel scaffolding technology for the regeneration of bone tissue in non-load bearing critical-sized defects. This represents the first attempt to form colloids exclusively from biomaterials found in the microenvironment of healing bone fractures including hyaluronic acid (HA), hydroxyapatite (HAP), bone and cartilage extracellular matrix (ECM). Work in the current thesis evaluated preliminary *in vitro* and *in vivo* efficacy of several injectable colloids. Specifically, HA-HAP colloids exhibiting desirable rheological, viscoelastic, and swelling properties for surgical placement and defect site retention were identified from an array of formulations. Subsequent formulation refinement incorporated micronized decellularized cartilage (DCC) and demineralized bone matrix (DBM) particles into HA-HAP colloids, which did not result in any significant decreases in measured fluid properties. Coupling ECM microparticles within a colloidal fluid carrier was hypothesized to enhance the regenerative capacity of HA-HAP colloidal formulations. *In vitro* studies demonstrated evidence of temporal chondrogenic, hypertrophic, and osteogenic gene expression in response to changes in colloidal composition. More specifically, the inclusion of DCC led to hypertrophic chondrogenesis while both HAP and demineralized bone matrix DBM colloidal formulations appeared to direct cell lineage down an osteogenic pathway in a temporal manner similar to expression profiles observed in native bone fracture healing. *In vivo* studies demonstrated the feasibility and efficacy of colloidal scaffolds in critical-sized rat calvarial defects. Although no significant differences in regenerated bone were observed in defects treated with colloidal formulations compared to negative control, the presence of endochondral (EC) derived ossification foci were only observed in HA-HAP and

HA-HAP-ECM treated defects. Thus, definite advantages of using colloidal gel technology were observed in these preliminary studies, but future iterations of the implant formulation design may yield enhanced bone tissue regeneration. Ultimately, the idea of colloidal-based tissue implants has been taken from concept to practice, produced promising results for the treatment of non-load bearing bone defects, and has given rise to numerous areas of tangential research to refine the technology.

ACKNOWLEDGEMENTS

I would like to express my sincere gratitude to my advisor, Dr. Cory Berkland, for his continued support over the course of my graduate studies. His advice and encouragement in my professional and personal life have been instrumental in the shaping of my scientific career. I will forever be in your debt for the opportunities and experiences you have given me, thank you. I would like to also acknowledge the other members of my dissertation committee, Dr. Michael Detamore, Dr. Sarah Kieweg, Dr. Stevin Gehrke, and Dr. Teruna Siahaan for their support with regard to the development of this thesis along with their continued guidance of my scientific research in the laboratory and in the classroom. I would also like to thank the faculty and staff of the Bioengineering Graduate Program for giving me the opportunity to pursue my passion for biomaterials, tissue engineering, and regenerative medicine.

This research would not have been possible without the generous funding from the National Institutes of Health (NIH RO1 DE022471) and the NIGMS Pre-doctoral Training Grant Program (NIH/NIGMS T32-GM08359), and the University Of Kansas School Of Engineering.

Special thanks are needed for all of my undergraduate research assistants who made my graduate experience more enlightening and rewarding: Jon Whitlow, Addison Schile, Austin Childress, Kathryn Scherich, Michael Holtz, Martin Wind, and Jake Hopkins. Their contributions in the laboratory were essential to the completion of this thesis. I would like to thank current and former graduate and post-doctorate collaborators for their scientific insight, persistent work ethic, and extraordinary kindness that have made my graduate studies rich in knowledge and friendship. I would especially like to thank Emily Beck, Amanda Sutherland, and Dr. Brad Sullivan for their assistance with *in vitro* characterization along with Dr. Ye Feng for his surgical work and management of *in vivo* studies and Dr. Prem Thapa and Heather Shinogle in the KU Microscopy

Lab for their assistance in SEM and TEM imaging. In addition, I would like to thank Chris Kuehl, Sharadvi Thati, Vineet Gupta, Amanda Renth, BanuPriya Sridharan, Cate Wisdom, Dr. Nathan Dormer, Dr. Amir Fakhari, Dr. Joshua Sestak, and Dr. Nashwa El-Gendy. I would also like to thank my industry mentors, Dr. Mark Menning and Sean Ritchie, as well as former KU alumni, Dr. Diana Davey and Dr. Eric Gorman, at Gilead Sciences Inc. for broadening my scientific experience.

There are two final groups of people that I need to acknowledge. The first are the inspirational mentors and teachers that have shaped my academic story. The University of Kansas in Lawrence has been my home throughout my undergraduate and graduate career, and special thanks are needed for the numerous educators that have opened my eyes and mind to the world. There truly is no place like home.

Lastly, I want to thank my family. I want to thank my parents, Jan and Steve, along with my step-parents, Chris and Melanie, for their unconditional love and support which has molded me into the person I am today and allowed me to pursue my academic dreams in science and engineering. Finally, I want to thank my wife, Elise. She is my muse, my confidant, and the mother of my beautiful child, Sloane. She challenges me to become the person I want to be in the world. Let this be another chapter, another memory in the book of our lives as we look forward to making new ones together. Adventure is out there!

TABLE OF CONTENTS

ACCEPTANCE PAGE..... ii

ABSTRACT..... iii

ACKNOWLEDGEMENTS v

TABLE OF CONTENTS vii

CHAPTER 1: Introduction to Thesis.....1

CHAPTER 2: Mapping Glycosaminoglycan-Hydroxyapatite Colloidal Gels as Potential Tissue Defect Fillers.....5

Abstract 6
Introduction 7
Experimental 10
Materials 10
Characterization of HAP nanoparticles 10
Preparation of colloidal gels 10
Swelling Characterization.....11
Rheological Characterization 11
Rheological Modeling 12
Statistical Analysis.....12
Results 13
Characterization of HAP nanoparticles 13
Swelling Characterization.....14
Rheological Characterization 15
Discussion 18
Conclusion 24
List of Abbreviations 25

CHAPTER 3: Endochondral Ossification for Enhancing Bone Regeneration: Converging Native ECM Biomaterials and Developmental Engineering *in vivo* 26

Abstract 27
Introduction 29
Overview of the natural bone healing process 33
Strategies to enhance EC ossification 34
Harnessing the potential of developmental engineering.....34
Coupling in vivo developmental engineering with native ECM biomaterials 35
Isolation, identifying and delivering native ECM for EC ossification 44
Incorporating SCBTs into the design 49
Discussion 55
List of Abbreviations 58

CHAPTER 4: Hyaluronic Acid-Hydroxyapatite Colloidal Gels Combined with Micronized Native ECM Biomaterials as Potential Bone Tissue Defect Fillers 60

Abstract 61
Introduction 62
Experimental 66
Colloidal materials 66
DBM and DCC procurement 66
Preparation of colloidal gels 68
Swelling characterization 69
Rheological and viscoelastic characterization 69
Statistical analysis 70
Results 71
Colloidal characterization 71
Swelling Characterization 71
Rheological and viscoelastic characterization 72
Discussion 75
Conclusion 81
List of Abbreviations 82

CHAPTER 5: Preliminary *in vitro* and *in vivo* Evaluation of Native ECM Colloidal Gels for Filling Bone Tissue Defects 83
Abstract 84
Introduction 85
Experimental 88
Colloidal materials 88
DBM and DCC procurement 88
Preparation of colloidal gels 89
BMSC harvest, expansion, and seeding 90
Cell viability and gene expression analysis 91
Surgical implantation of colloidal gels in cranial defects 92
Gross anatomy and MicroCT imaging 92
Histology 93
Statistical analysis 93
Results 93
Characterizing in vitro cell response to pure DCC 94
Characterizing in vitro cell response to HA-HAP and HA-HAP-DCC Colloids 94
Characterizing in vitro cell response to colloids with HAP, DCC, and DBM 95
Characterizing in vivo bone regeneration to colloids with HAP, DCC, and DBM 96
Discussion 98
Conclusion 103
List of Abbreviations 104

CHAPTER 6: Conclusion 106

APPENDIX A: Tables 110
APPENDIX B: Figures 124
APPENDIX D: References 155

CHAPTER 1: Introduction to Thesis

The overall objective of this thesis was to characterize a novel, native biomaterial based colloidal gel scaffold with self-assembling and shear-responsive rheological behavior for bone tissue regeneration. The overall progression was to first develop malleable colloidal gels to facilitate minimally invasive surgical repair, refine colloidal gel formulations to incorporate native extracellular matrix (ECM) biomaterials with potential to enhance bone regeneration via endochondral (EC) ossification, and finally evaluate preliminary *in vitro* and *in vivo* performance. Therefore, characterization of the colloidal gel scaffold design incorporated three specific aims: (1) synthesize and characterize novel colloidal gels with modulated rheological properties, (2) engineer and refine colloidal gels with incorporated native ECM substrates relevant to EC ossification, and (3) determine the efficacy of colloidal gel formulations *in vitro* and *in vivo*.

The first aim was designed to evaluate the importance of various rheological properties including yield stress, flow-behavior and consistency index as well as swelling and viscoelastic properties of glycosaminoglycan (GAG) and hydroxyapatite (HAP) colloidal gel composites for minimally invasive surgical delivery. The second aim elucidated the feasibility of incorporating native ECM biomaterials, including decellularized cartilage (DCC) and demineralized bone matrix (DBM), into refined colloidal gel formulations. This would facilitate the inclusion of both physically conductive and chemically inductive signaling moieties for bone regeneration into colloidal gel scaffolds. The third and final aim tested the performance of colloidal gels and ECM biomaterials *in vitro* and in rat calvarial defect models. The subsequent chapters reflect chronological progression of these aims, which provided essential information that directed later phases of the work. The organization of these chapters is as follows:

Chapter 2 gives historical context on the development of non-setting tissue fillers within the confines of tissue engineering and regenerative medicine and provides a framework for colloidal gel technology to impact and potentially obviate existing scaffolding paradigms in the field. This chapter additionally addresses the first aim and provides experimental evidence to suggest the use of these colloidal gel formulations in subsequent chapters involving *in vitro* and *in vivo* designs. Chapter 2 thus introduces the central motif for this thesis: colloidal gels for enhancing bone regeneration.

Chapter 3 addresses the other central motif for this thesis, which is the application of native ECM biomaterials to enhance EC ossification in bone regeneration. This chapter highlights the key differences that distinguish marginally successful bone tissue engineering strategies, which focus on mimicking the composition of late reparative stage ECM in bone fracture repair (i.e. 'hard' or 'bony' callus), with underexplored alternatives that focus on developmental engineering strategies and mimic the composition of early reparative phase ECM in natural bone repair (i.e., 'pro-' or 'soft' callus). Chapter 3 thus provides a framework for subsequent colloidal gel refinement, aim 2, with regard to bone regeneration applications.

Chapter 4 addresses the second aim by discussing subsequent iterations of colloidal gel formulations for the purpose of regenerating bone in non-load bearing defects. Initially, the effect of GAG polymer molecular weight on rheological performance of colloidal gels was evaluated. In addition, chapter 4 builds on engineering principles discussed in chapter 3 by incorporating native ECM biomaterials, specifically micronized DCC and DBM, into colloidal formulations and evaluating rheological performance. These studies suggested that the initial colloidal formulations discussed in chapter 2 could be adjusted and beneficially loaded with native ECM biomaterials without compromising rheological performance.

Chapter 5 addresses the third aim and final aim by investigating the efficacy of colloidal formulations *in vitro* and *in vivo*. Studies combined colloidal gels with isolated rat bone mesenchymal stem cells (rBMSCs) for up to 3 weeks. Preliminary cell viability and gene expression results suggested that the incorporation of DCC may be beneficial for eliciting EC ossification in tissue engineered constructs. Several pilot *in vivo* studies in 8-mm rat calvarial defect models were conducted to further investigate bone regenerative capacity of colloidal gel formulations. Micro computed tomography (MicroCT), histology, and gross anatomy of implants were evaluated 8 weeks following surgical placement. These studies suggested that the native ECM colloidal formulations discussed in chapter 4 could be retained in the defect space over the span of the study and more importantly could elicit bone regeneration in the defect space. Evidence of EC ossification foci were observed in animals treated with colloidal gels, but minimal differences in the extent of ossification were observed between treated animals and negative sham control. Future studies will aim to reformulate colloidal gels to improve retention of implant material and enhance bone regeneration in the defect space.

Chapter 6 addresses concluding remarks for this thesis. It provides a summary of key internal findings along with global perspective on the impact of colloidal gels in the field of bone tissue engineering and regenerative medicine. Recommendations for worthwhile future experimental directions are discussed, which attempt to address limitations in current colloidal gel designs.

Overall, the work conducted within this thesis proposes potential solutions for treating irregularly shaped, critical-sized bone defects. Current technologies in the non-setting bone paste market may inadequately meet the needs of minimally invasive surgery, which include limited injectability due to high viscosity and poor wound site retention due to poor viscoelastic recovery

following shear. Furthermore, current bone regeneration products focus primarily on mimicking the complex composition and signals present in late reparative stage fracture healing environment, or bony callus, which may be obviated by tissue engineered constructs that alternatively mimic the procallus ECM and native bone healing process.

Autologous bone grafting (ABG) remains the gold standard of treatment for bone regeneration in critical size defects due to its inherent osteoconductive, osteoinductive, and osteogenic capabilities; however, concerns remain regarding donor site pain and morbidity, increased risk of infection, and graft resorption.[1-3] Substantial efforts with synthetic (e.g. Ostim®; Heraeus Kulzer)[4] and allograft (e.g. DBX®; MTF-Synthes)[5] biomaterial products have attempted to replace ABG technology, yet they still rely on direct intramembranous (IM) ossification, which may limit bone regenerative capacity in critical-sized, avascular bone defects compared to the EC ossification pathway. The advantages of the colloidal gel technology proposed within this thesis center on improving delivery and retention of non-setting bone pastes while simultaneously stimulating the EC ossification pathway in critical-sized bone defects.

CHAPTER 2: Mapping Glycosaminoglycan-Hydroxyapatite Colloidal Gels as Potential Tissue Defect Fillers

S. Connor Dennis[1, 2], *Michael S. Detamore*[1 ,2], *Sarah L.Kieweg*[1, 3], *Cory J. Berkland*[1, 2, 4*]

[1]Bioengineering Program, [2]Chemical and Petroleum Engineering Department, [3]Mechanical Engineering Department, [4]Pharmaceutical Chemistry Department

University of Kansas, Lawrence, KS 66045

KEYWORDS: Hydroxyapatite; Glycosaminoglycan; Chondroitin Sulfate; Hyaluronic Acid; Colloidal Gel; Self-Assembling Fluid; Herschel-Bulkley Fluid; Tissue Defect Filler

*Corresponding author

ABSTRACT

Malleable biomaterials such as Herschel-Bulkley (H-B) fluids possess shear responsive rheological properties and are capable of self-assembly and viscoelastic recovery following mechanical disruption (e.g., surgical placement via injection or spreading). This study demonstrated that the addition of moderate molecular weight glycosaminoglycans (GAGs) such as chondroitin sulfate (CS) (M_w = 15-30 kDa) and hyaluronic acid (HA) (M_w = 20-41 kDa) can be used to modify several rheological properties including consistency index (K), flow-behavior index (n), and Yield Stress (τ_y) of sub-micron hydroxyapatite (HAP) particle ($D_{avg} \leq$ 200 nm) colloidal gels. GAG-HAP colloidal mixtures exhibited substantial polymer-particle synergism, likely due to 'bridging' flocculation, which led to a synergistic increase in consistency index ($K_{GAG\text{-}HAP} \geq K_{GAG} + K_{HAP}$) without compromising shear-thinning behavior ($n < 1$) of the gel. In addition, GAG-HAP colloids containing high concentrations of HAP (60-80% w/v) exhibited substantial yield stress ($\tau_y \geq$ 100 Pa) and viscoelastic recovery properties ($G'_{recovery} \geq$ 64%). While rheological differences were observed between CS-HAP and HA-HAP colloidal gels, both CS and HA represent feasible options for future studies involving bone defect filling. Overall, this study identified mixture regions where rheological properties in CS-HAP and HA-HAP colloidal gels aligned with desired properties to facilitate surgical placement in non-load bearing tissue filling applications such as calvarial defects.

1. INTRODUCTION

Developing malleable biomaterials for filling tissue defects is desirable for minimally invasive surgical repair and potential regeneration of bone defects.[6-8] Minimally invasive surgery reduces the risk of infection and scar formation while also decreasing patient discomfort and cost of treatment.[6-9] Malleable biomaterials with shear responsive rheological properties, such as Herschel-Bulkley (H-B) fluids which possess favorable yield stress and shear-thinning behavior, may be injected or extruded to fill irregular shaped bone defects. It may also be necessary for these materials to have sufficient viscoelastic recovery kinetics following placement to ensure retention at the defect site. An ideal H-B fluid biomaterial candidate would facilitate surgical placement and site retention with desirable shear responsive properties and viscoelastic properties, respectively.

Many injectable scaffolds exhibit thickening or stiffening after placement via *in situ* chemical crosslinking in the presence of water, heat, light, or other stimuli; however, concerns exist where unreacted reagents or catalysts may persist and impose localized cytotoxicity or adversely affect encapsulated biomolecules.[8, 10, 11] Alternatively, self-assembling biomaterials that rely on physical crosslinking may yield or flow in response to variation in external shear stress (i.e., extrusion or spreading) during placement.[8, 12] Upon removal of shear (i.e., after placement), such materials could potentially recover *in situ*, thus providing local structure and delivery of biological cues in non-load bearing tissue sites.

Colloids are a promising candidate for this application. The cohesive strength of these materials is dependent on electrostatic forces, van der Waals attraction, and steric hindrance. These forces in combination directly influence the macroscopic material properties.[8, 10-12] Of particular interest is the colloidal sol-gel transition, which is distinguished by a shift from dispersed solid particles at low concentrations to the formation of sample-spanning networks of particle

flocculations at higher solid concentrations.[13-15] On the macroscopic level, this transition is marked by an appreciable increase in the material yield stress and viscosity.[13-15] Previous investigations have explored leveraging these interactions in oppositely charged poly(lactic-co-glycolic) acid nanoparticles[10, 11], gelatin nanoparticles[16], and dextran microparticles[17, 18] to form cohesive colloidal gels capable of delivering a variety of therapeutic osteogenic proteins for bone tissue engineering. More recently, nanoparticle gelatin colloidal gels were shown to outperform microparticle gelatin gels with regard to malleability during injection and as drug delivery vehicles *in vitro* and *in vivo*.[19, 20] The current study aims to expand upon previous work leveraging nanoparticle colloidal interactions by using biomolecules found in native human bone including hydroxyapatite (HAP) and glycosaminoglycans (GAGs).

HAP [$Ca_{10}(PO_4)_6(OH)_2$] is a well-studied calcium orthophosphate bone substitute material similar to the mineral component of mammalian bones and is commonly referred to as 'biological apatite.'[21, 22] HAP has been studied extensively in bone regeneration, and results indicate HAP nanoparticles (e.g., Ostim® and Nanostim®) can be delivered as highly concentrated colloidal pastes in injectable bone filler applications.[4, 13, 14, 21-26] Phase separation has been observed in some HAP nanoparticle suspensions, leading to poor injectability or 'filter-pressing'[4, 27] and poor retention at the defect site[28] resulting in limited tissue regeneration. Such limitations could be improved by incorporating large biomolecular polymers into the suspending fluid phase.[12, 26, 29-36] Polymer solutions exhibit a significant increase in viscosity with concentration due to increased entanglements or associations between polymer chains in the solution.[37-40] Additionally, polyelectrolytes (i.e., charged polymers) may be leveraged in a charged colloidal system to improve particle-polymer interactions to induce cohesiveness in the colloidal gel.[41]

Naturally occurring polymeric GAGs such as hyaluronic acid (HA) and chondroitin sulfate

(CS) are found in extracellular matrix, cartilage, and skin. These GAGs exhibit desirable physicochemical properties as scaffolds in tissue engineering.[32, 38-40, 42, 43] HA is a linear, high-molar-mass polysaccharide composed of alternating (1→4)-β linked D-glucuronic acid and (1→3)-β linked *N*-acetyl-D-glucosamine residues. CS differs only in the *N*-acetyl-D-glucosamine residue, which is sulfonated at either the 4 or 6 carbon site.[39, 40, 43, 44] Due to repeating carboxyl or sulfonate moieties along the backbone, HA and CS occur as anionic macromolecules in aqueous environments at extracellular pH.[39, 40, 43, 44] As a result, these highly charged macromolecules possess desirable shear-thinning and viscoelastic properties[37-39, 42, 43] and have primarily been used as inert carrier fluids in bone tissue engineering applications.[5] Emerging efforts, however, aim to elicit 'bridging' connections within colloidal gels by using particles to act as anchoring points between multivalent, adsorbing polymers.[12, 26, 29-31, 33-35, 41, 45, 46]

In this study, polyanionic GAG polymers were combined with HAP nanoparticles in various concentrations and weight ratios to create cohesive 'bridging' colloidal gels as potential scaffolds for bone tissue regeneration in irregular bone defects. This study represents the first attempt to exclusively combine native tissue components in a particle-polymer colloidal gel mixture with the goal of creating H-B fluids. More specifically, this study aims to elucidate the relationship between bulk rheological properties as a function of relative HAP nanoparticle and GAG biopolymer content. The primary goal of this assessment is to identify GAG-HAP colloidal gel candidates with appropriate yield stress, consistency, flow behavior and recovery properties to explore surgical delivery in non-load bearing bone regeneration applications.

2. EXPERIMENTAL

2.1. Materials

Hydroxyapatite was purchased as a powder ($D_{avg} \leq 200$ nm (BET Analysis); Sigma-Aldrich). Chondroitin sulfate A from bovine trachea (M_w =15-30 kDa) (Sigma Aldrich; St. Louis, MO) and hyaluronic acid (M_w =20-41 kDa) (Lifecore Biomedical; Chaska, MN) were purchased as sodium salts.

2.2. Characterization of HAP Nanoparticles

Size, morphology, and elemental distribution analysis of HAP was observed using a combination of transmission and scanning electron microscopy (TEM and SEM) and energy dispersive x-ray spectrometry (EDS) (FEI Tecnai F20 XT Field Emission TEM-EDS and Carl Zeiss Leo 1550 Field Emission Scanning). Additional sizing and zeta-potential measurements of HAP were conducted using dynamic light scattering (Brookhaven; ZetaPALS).

Fourier transform infrared (FTIR) spectroscopy (PerkinElmer; Frontier FTIR) was used to confirm chemical identity. HAP samples were press formed into a thin disk with KBr crystals. The spectrum was collected in the 4000-400 cm^{-1} range with an average of 256 scans.

Crystallographic structural analysis of the sample was determined using X-ray diffraction (XRD) method (Bruker; D8 Advance). Monochromatic CuK_α radiation ($\lambda = 0.15406$ nm) was used over the 2θ range of 20-45° at a step size of 0.014° per 0.5 s. XRD data was compared with built-in Bruker software utilizing standard International Center for Diffraction Data (ICDD) for HAP. [21, 22]

2.3. Preparation of Colloidal Gels

HA or CS powders were combined with HAP nanoparticles and dispersed in PBS solution (pH = 7.4, 150 mM NaCl). CS and HA concentrations in the mixtures were varied between 0-80%

(w/v) and 0-40% (w/v), respectively. GAG:HAP weight ratio (w:w) was controlled by the incremental addition of HAP particles to GAG solutions at ratios of 2, 1, 0.5, 0.25, and 0.125. These mixtures were compared to pure component controls (GAG and HAP), respectively. Overall volume fraction of HAP ($\Phi = V_{HAP}/V_{Mixture}$) was calculated from particle density and resulting mixture volume measurements. Homogeneous colloid mixtures were prepared by manual stirring (5 min) at ambient conditions and stored at 4°C. Samples were allowed to equilibrate to ambient conditions (2 hr) before testing.

2.4. Swelling Characterization

Relative swelling ratios (*S*) of CS-HAP and HA-HAP colloidal gels were determined by placing 1.0 mL of PBS (pH = 7.4, 150 mM NaCl) on top of 0.5 mL of material contained in a 2 mL Eppendorf tube. Tubes were then constantly agitated (24 hr, 100 rpm, 37°C) in an incubator shaker (New Brunswick Scientific; Excella E24). Swelling ratio ($S = (M_{(swollen)}-M_{(before)})/M_{(before)}$) was determined from the initial ($M_{(before)}$) and final ($M_{(swollen)}$) mass of the material as described by Holland et al.[47] The final weight was determined by removing excess PBS from tube and drying the surface of gel with evaporative paper.

2.5. Rheological Characterization

The rheological properties of the colloidal gels were characterized using a controlled stress rheometer (TA Instrument; AR2000). All measurements were performed using a stainless steel plate geometry (20 mm diameter) at a gap distance of 500 μm. The shear stress profile of the colloidal gels was determined using a stepped flow test (1 min/step) with an increasing shear rate (1-1000 s^{-1}). All samples were tested at 37°C.

Recovery kinetics following temporary disruption of the colloidal gel network were determined by measuring viscoelastic properties as described by Ozbas et al.[48] Initially, an

oscillatory stress sweep (1-1000 Pa) was performed at a constant frequency (1 Hz) to determine the linear viscoelastic (LVE) region. Subsequently, the gel viscoelastic properties including storage modulus (G'), loss modulus (G''), and loss angle (δ) were determined in a three phase oscillatory time sweep at 37°C following pre-shear (1 min, 100 s^{-1}) and equilibration (5 min). Gels were oscillated (5 min, low stress in LVE regime, 1 Hz) before and after an intense disruption phase (30 s, 1000 Pa, 1 Hz).

2.6. Rheological Modeling

Rheological flow property estimations were determined with a three-parameter fit to the H-B fluid model (Equation 1):

$$\tau = \tau_y + K\dot{\gamma}^n \qquad \text{(Eq. 1)}$$

where τ was the measured shear stress [Pa] in the sample resulting from the fluid's yield stress, τ_y [Pa], consistency index, K [Pa•s^n], and flow behavior index, n [unitless], at a given shear rate, $\dot{\gamma}$ [s^{-1}]. Optimal fit was determined using curve fitting tool software in MATLAB (The Mathworks, Inc.) with a non-linear least squares method. Some GAG-HAP mixtures exhibited localized shear banding at low shear rates (< 10 s^{-1}) as described by Möller et al.[49] As a result, data points below the critical shear rate, determined from the point of minimum shear stress in the sample, were excluded from H-B modeling. 95% confidence intervals were reported from triplicate measurements for all three parameters in each tested colloidal mixture along with the overall root-mean-squared error (RMSE) of the fit.

2.7. Statistical Analysis

All measurements were performed in triplicate (n = 3) and depicted as average ± standard deviation (SD) unless stated otherwise. Statistical analyses of data were performed using one-way analysis of variance (ANOVA) and Tukey's HSD was used post-hoc to compare differences

between individual groups. A p-value ($p < 0.05$) was accepted as statistically significant.

3. RESULTS

3.1. Characterization of HAP Nanoparticles

TEM-EDS analysis of HAP (Figure 2.1) revealed spherical particle morphology with polydisperse diameters near the supplier's specified value ($D_{avg} \leq 200$ nm (BET); Sigma-Aldrich); however, a small fraction of particles were visually observed to exceed this specification. SEM analysis of HAP, CS-HAP, and HA-HAP (Figure 2.2A-C) likewise revealed spherical HAP particle morphology. Colloidal aggregation was also observed with SEM. However, negligible aggregation differences were observed between groups most likely due to the dehydrated state of the sample. Contrary to the supplier's elemental purity analysis (≥ 97% HAP (wt %) (XRF Assay); Sigma-Aldrich), elemental distribution analysis (EDS) indicated the presence of calcium deficient HAP (Figure 2.3). Atomic composition of HAP samples were (Average atomic % ± SD) Ca (24.58 ± 0.20 %), P (15.91 ± 0.15 %), and O (59.49 ± 0.30 %), yielding a Ca/P ratio of 1.54. Pure stoichiometric HAP yields a Ca/P ratio of 1.67, while CDHA has a Ca/P ratio around 1.50-1.67.[22] CDHA has been studied extensively in bone tissue regeneration due to its similar stoichiometry to that of 'biological apatite'.[4, 50-52]

Dynamic light scattering was used to measure HAP particle size (nm) and zeta potential (mV) (average ± SD; n = 10). Dilute suspensions (0.167 mg/mL) of pure HAP particles where combined with either HA or CS in GAG:HAP weight ratios of 1:1 or 10:1, and the changes in size and zeta potential were observed (Table 2.1). Only the 10:1 ratio of CS:HAP resulted in a significant increase in particle size ($p < 0.05$) compared to the pure HAP. The inclusion of CS or HA at both weight ratios resulted in a significant increase in HAP zeta potential ($p < 0.01$) compared to the

pure HAP suspensions.

FTIR spectra (Figure 2.4) of HAP revealed the presence of expected bonds in the crystal. Strong modes for stretching (1035 cm^{-1}) and bending (564, 604 $cm^{=1}$) indicated the presence of PO_4^{3-}.[53, 54] Characteristic stretching (3572 cm^{-1}) of the –OH group was also observed.[53, 54] Additionally, some bands indicating the weak presence of adsorbed water (1635 and 3000-3700 cm^{-1}) were observed.[53, 54]

The XRD pattern (Figure 2.5) revealed expected HAP diffraction peaks at 2θ regions of 26°, 29°, 32-34°, 40°, and 46-54°, indicating the crystalline nature of the HAP particles when compared with the International Center for Diffraction Data (ICDD) for HAP.[53, 54]

3.2. Swelling Characterization

Relative swelling of CS-HAP (Figure 2.6A) and HA-HAP (Figure 2.6B) gels increased with a clear dependence on HAP Φ. While sedimentation and swelling tolerances were initially set (-20% ≤ S ≤ 20%) in an attempt to identify suitable GAG-HAP candidates for retention of material at a bone defect surgical site, the most desirable colloidal mixtures exhibited the least amount of swelling or sedimentation (S ≈ 0%). Excessive sedimentation (S ≤ -20%) occurred in pure HAP mixtures below Φ = 0.25. The addition of CS or HA resulted in increased swelling at a given HAP Φ. Furthermore, swelling also exhibited dependence on GAG:HAP ratio (w:w), where mixtures with GAG in excess tended to show increased swelling, and mixtures with HAP in excess tended to demonstrate swelling behavior of pure HAP. As a result, excessive sedimentation only occurred below HAP Φ = 0.12 and Φ = 0.06 for CS-HAP and HA-HAP colloidal mixtures, respectively. Excessive swelling (S ≥ +20%) occurred in mixtures containing GAG:HAP ratios in equivalence or in GAG excess ([1:1] and [2:1]) above Φ = 0.18. The only mixtures exhibiting excessive swelling and favoring HAP content were [1:2] GAG:HAP colloids with HAP concentrations above

$\Phi = 0.37$.

3.3.Rheological Characterization

3.3.1. Consistency Index

Measuring shear stress in response to increasing external shear rate yielded flow behavior properties which were estimated from a three-parameter H-B Fluid model. An extensive array of CS-HAP (Table 2.2) and HA-HAP (Table 2.3) mixtures were tested and compared to pure HAP colloids (Table 2.4). Consistency index (K [Pa•s^n]) in CS-HAP and HA-HAP gels increased exponentially with increasing GAG content (% w/v) and increasing HAP content (% w/v) in the mixture, respectively. In addition, GAG-HAP mixtures containing HA had higher K values than respective CS mixtures. Plotting K values versus HAP Φ (Figure 2.7A and Figure 2.7B) for constant GAG:HAP weight ratios (w:w) yielded a noticeable shift in K values from predominantly GAG-like behavior when in polymer excess to HAP-like behavior when in particle excess.

All tested mixtures, except those exhibiting high yield stress ($\tau_y > 500$ Pa), exhibited higher K values than the addition ($K_{GAG\text{-}HAP} \geq K_{GAG} + K_{HAP}$) of their respective pure GAG and HAP components. Examples of this synergistic K value behavior are seen in shear stress versus shear rate plots (Figure 2.8A and Figure 2.8B), where the mixtures of 15% CS – 60% HAP and 15% HA – 60% HAP (% w/v) exhibited higher K values than predicted by the summation of their respective pure GAG 15% and pure HAP 60% components. Mixtures exhibiting high yield stress ($\tau_y \geq 500$ Pa) were the exception to this trend, where estimated K values were smaller than the addition of respective pure components. This likely reflects possible limitations attributed to how the H-B constitutive relationship captures τ_y and K behavior for some GAG-HAP mixtures. At high HAP concentrations, the increased apparent viscosity of the material is modeled more by an increase in τ_y and not captured by K (Table 2.2 and Table 2.3).

3.3.2. Flow Behavior Index

Flow behavior index (n [unitless]) of the pure aqueous PBS media was indicative of a Newtonian fluid ($n = 0.95 \pm 0.18$). In CS-HAP (Figure 2.7C) and HA-HAP (Figure 2.7D) mixtures, n values decreased from unity with the addition of HAP and GAG content, an indication of shear-thinning behavior ($n < 1$) in the gels. Further evidence of this was seen in plots containing n values versus HAP volume fraction (Φ) (Figure 2.7C and Figure 2.7D) for constant GAG:HAP weight ratios (w:w). There was no conclusive evidence to support shear-thinning dependence on the concentration of GAG or GAG:HAP ratio in colloidal mixtures.

Examples elucidating the extent of shear-thinning over the range of shear rates tested (1-1000s^{-1}) was observed in log-log plots of viscosity versus shear rate for 15% CS – 60% HAP and 15% HA – 60% HAP (Figure 2.4C and Figure 2.4D), respectively. While apparent viscosity was nearly independent of $\dot{\gamma}$ in pure GAG solutions such that n values were near unity ($n \approx 1$), GAG-HAP colloidal mixture viscosities decreased at least an order of magnitude over the tested shear rate range. These GAG-HAP mixtures exhibited high viscosities ($\mu > 100$ Pa•s) at lower shear rates and relatively low viscosities ($\mu < 10$ Pa•s) at higher shear rates.

3.3.3. Yield Stress

Yield stress (τ_y [Pa]) estimation from rheological data appeared to only be dependent on HAP particle concentration (Figure 2.7E and Figure 2.7F), and an exponential increase in τ_y was seen across the entire range of tested HAP concentrations, 0%-80% (w/v) or $0.00 \leq \Phi \leq 0.49$. For some GAG-HAP mixtures H-B fluid modeling resulted in large confidence intervals and negative τ_y values (Table 2.2 and Table 2.3). This likely reflects possible limitations attributed to how the H-B constitutive relationship captures τ_y and K behavior for some GAG-HAP mixtures, favoring an increase in τ_y instead of K at high HAP concentrations. Fluids with negative yield values were

interpreted to possess no yield. Colloidal mixtures exhibited appreciable τ_y ($\geq$ 10 Pa) only at the highest HAP concentrations 60-80% (w/v), which translated to a volume fraction of Φ = 0.37-0.49. CS-HAP colloidal mixtures exhibited yield stress across all tested CS concentrations, while HA-HAP mixtures only exhibited τ_y below 20% HA (w/v).

3.3.4. Rheological and Swelling Summary

Tested CS-HAP (Figure 2.9A) and HA-HAP (Figure 2.9B) colloidal mixtures were mapped on ternary diagrams (weight %). Based off of both swelling (S) and rheological properties (τ_y, K, and n) exhibited by each tested mixture, regions of desirable properties for facilitating surgical delivery were identified. Explicitly, a desirable mixture contained swelling or sedimentation within tolerance (-20% $\leq S \leq$ +20%), identifiable yield stress ($\tau_y \geq$ 100 Pa), and shear responsive flow properties (n < 1). From these criteria, 15% GAG – 60% HAP mixtures were selected due to overlapping regions of desirable swelling and flow properties between CS and HA colloidal gels (Figure 2.6).

3.3.5. Viscoelastic Recovery

Selected colloidal gels were initially subjected to an oscillatory shear stress sweep (1-1000 Pa) at a constant frequency (1 Hz) to determine the linear viscoelastic (LVE) regime of the fluid. This was determined to be less than 100 Pa for all mixtures. Subsequent viscoelastic time sweeps were therefore conducted at an oscillatory shear stress selected to be sufficiently within the LVE regime for all samples (10-25 Pa). Viscoelastic properties including storage modulus (G'), loss modulus (G''), and phase angle (δ) of GAG-HAP mixtures were measured before, during, and after an intense temporary disruption period, which involved a large increase in external oscillatory shear stress on the material.

Based on previous swelling and flow behavior results, 15% GAG – 60% HAP mixtures

were selected as desirable candidates for viscoelastic recovery studies (Figure 2.10A and Figure 2.10B) and then compared to their respective pure components at the same concentration. Recovery was assessed 5 minutes after disruption and expressed as a percentage ($G'_{\text{recovery}} = G'_{(\text{Final})}/G'_{(\text{Initial})} \bullet 100\%$) compared to initial G' in the mixture. Both the CS-HAP and HA-HAP mixtures recovered a large portion of their initial viscoelastic behavior within the brief recovery period, 64% and 85% respectively. HA-HAP appeared to recover its initial G' within seconds of disruption while the CS-HAP mixture and pure HAP took several minutes. This may favor HA-HAP mixtures in a surgical application, since rapid self-assembly may improve retention in the tissue defect site. Pure HAP recovered a higher percentage, 92%, and pure CS and pure HA both recovered 100% of their initial viscoelastic properties almost instantaneously following disruption. Furthermore, G', G'' and δ values measured from GAG-HAP mixtures appeared to exhibit intermediate values between pure GAG and pure HAP components. Pure GAG exhibited primarily viscous behavior and pure HAP exhibited predominately elastic behavior during periods of low oscillatory stress. CS-HAP, HA-HAP, and pure HAP displayed primarily elastic behavior ($\delta \leq 14°$) during the initial low oscillatory stress phase, transitioned to predominately viscous behavior during the temporary disruption phase ($\delta \geq 84°$), and rapidly (< 5 min) returned to primarily elastic behavior ($\delta \leq 16°$) while recovering from disruption at low oscillatory stress (Figure 2.10C and Figure 2.10D). HA-HAP exhibited larger G' and G'' values than CS-HAP at the given GAG-HAP ratio.

4. DISCUSSION

Colloidal sols are suspensions of submicron particles undergoing Brownian motion.[8, 12] Stabilization of these sols relies on the balance of particle-particle interactions such as electrostatic

forces, Van der Waals attraction, and steric hindrance.[8, 10-12] Stable HAP sols have been created with the use of adsorbed polyelectrolytes that act as dispersing agents by forming steric barriers around particles.[55] However, these stable HAP sols generally possess a small consistency index and lack yield stress, which limit their application as bone tissue fillers.

Destabilized colloidal sols exhibit widespread flocculation across the colloidal mixture. When concentrations of particles are high enough, sample-spanning networks of flocculated particles are formed creating a colloidal gel.[13, 56] In this study, pure HAP particles with spherical morphology and sub-micron diameter suspended in PBS media formed destabilized flocculations above 40% w/v as evidenced by significant sedimentation ($S \leq$ -20%) over 24 hrs (Figure 2.6A and Figure 2.6B). Inclusion of polyelectrolytes can also induce substantial destabilization in colloids, where non-adsorbing polymers can induce depletion flocculation[57-59] and adsorbing polymers can induce flocculation by bridging.[57, 60, 61] In the latter case, particles act as cross-linkers between polymer molecules or vice versa. CS and HA contain repeat carboxylic acid moieties similar to polyacrylic acid and were hypothesized in this study to adsorb to the surface of the HAP particles via a similar mechanism.[55, 56] The inclusion of either CS or HA at dilute HAP concentrations significantly increased overall zeta potential of HAP particles (Table 2.1), supporting the hypothesis that CS and HA adsorb to the particle surface. Although GAGs act to increase electrostatic stability at dilute concentrations, it is hypothesized that at high concentrations, similar to those tested in rheological experiments, bridging flocculation occurs due to multivalent GAG polymers adsorbing simultaneously to multiple HAP particles in close proximity.

The formation of sample spanning networks was observed macroscopically in swelling studies with the addition of CS and HA to suspensions of HAP, and the onset of these networks

appeared at lower total HAP Φ compared to pure HAP suspensions (Figure 2.6A and Figure 2.6B). Swelling of the GAG-HAP mixtures were dependent on absolute GAG and HAP concentrations as well as relative GAG:HAP ratio, where mixtures favoring GAG content exhibited higher swelling compared to mixtures with HAP in excess. High concentrations of CS and HA exhibited undesirable swelling ($S \geq 20\%$), which may have been due to sodium salt associated with GAGs causing an osmotic pressure difference between the mixture and swelling media. The most desirable colloidal mixtures exhibited the least amount of swelling or sedimentation ($S \approx 0\%$), and were identified as suitable GAG-HAP candidates for enhancing retention of material at a tissue defect surgical site (Figure 2.9). This occurred only in mixtures containing both high concentrations of HAP ($\Phi \geq 0.36$) and GAG:HAP ratios favoring HAP ([1:4] and [1:8]).

More importantly, this study aimed to associate colloidal microstructure dynamics with observed synergistic rheological properties including τ_y, K, n, and G'_{recovery}. Critical boundaries of GAG-HAP colloidal mixtures were mapped with regard to potential tissue defect filling (Figure 2.9). Presence of τ_y was desired to improve chances of retention at a bone defect wound site, and therefore, a lack of τ_y (e.g., a liquid or phase-separated suspension) was considered the minimum fail point in colloidal mixtures. Although a maximum τ_y limit was not defined, it was observed that mixtures containing more than 80% (w/v) HAP particles failed to reconstitute completely in PBS media. Therefore, this practical limit served as the basis for defining a maximum obtainable τ_y. Yield appeared to only be dependent on HAP (Figure 2.7E and Figure 2.7F) within the tested concentration range, $0 \leq \Phi \leq 0.49$ (v/v). Furthermore, τ_y increased exponentially with increasing HAP Φ, where appreciable τ_y (> 10 Pa) was observed only at the highest HAP concentrations 60-80% (w/v) or $\Phi = 0.37\text{-}0.49$, respectively. This observed transition corresponded with computer simulations and experiments on monodisperse colloidal hard-spheres.[57, 62] Below $\Phi < 0.49$

suspensions were reported to be disordered fluids exhibiting random local order; however, these networks can be sample-spanning and exhibit small amounts of τ_y.[57, 62] Above $\Phi > 0.49$, suspensions became a mixture of colloidal fluid and colloidal crystals, where particles began ordering in macrocrystalline structure of either face-centered cubic or hexagonally close packed orientation.[57, 62] CS-HAP colloidal mixtures exhibited appreciable τ_y across all tested CS concentrations, but HA-HAP mixtures above 20% HA (w/v) possessed no yield regardless of HAP concentration. Since τ_y in these GAG-HAP mixtures was solely the result of HAP particle flocculation, the observed τ_y differences between CS and HA colloidal gels may have been caused by differences in the ability of the two GAGs to sterically hinder particle flocculation.

In addition to τ_y, GAG-HAP colloidal mixtures also exhibited significant viscosity changes over the range of shear rates tested (1-1000 s^{-1}), and were described by *K* and *n* in H-B fluid models. *K* and *n* behavior in high solid content HAP particle gels has been described previously[13, 15, 55, 56] and were in agreement with tested pure HAP colloids. As particle concentrations become large enough to form sample-spanning flocculation networks, *K* undergoes a rapid increase due to the significant increase in attractive particle interactions.[13, 15, 55, 56] Likewise, the *K* and *n* behavior of pure HA solutions at various molecular weights and concentrations have been observed[37, 38, 42] and appeared to be in agreement with pure HA solutions tested here. As polymer concentrations became larger, *K* values in the solution increased exponentially (Figure 2.7A and Figure 2.7B). Previous work has attributed this exponential increase in polymer consistency to increased amounts of intermolecular entanglements.[37, 38, 42]

GAG-HAP mixtures tested here exhibited a synergistic increase in *K* compared to respective pure GAG and pure HAP components (Figure 2.7A and Figure 2.7B), and this increase was seen clearly in the shear stress versus shear rate profiles for GAG 15% - HAP 60% colloidal

gels (Figure 2.8A and Figure 2.8B). The nature of this observed synergistic increase was most likely due to the GAG polymer chains inducing bridging flocculation between HAP particles.[8, 12, 31, 33, 57, 60, 61, 63] Furthermore, the differences in *K* values exhibited by CS-HAP and HA-HAP gels were most likely a result of inherent *K* value differences in the respective GAG polymers combined with the nature of the particle flocculation induced by the addition of GAG polymer.[8, 12, 31, 33, 57, 63]

Meanwhile, shear-thinning ($n < 1$) in colloidal gels occurs when the applied shear rate is high enough to disrupt the particle-particle spacing away from equilibrium.[57] Pure HAP and pure GAG mixtures exhibited shear-thinning behavior within the tested shear rate range (1-1000 s^{-s}) which was concentration dependent (Figure 2.7C and Figure 2.7D). The addition of HAP into GAG-HAP mixtures enhanced shear-thinning behavior compared to pure GAG mixtures. Previous work with polymer-particle composites has also shown enhanced shear-thinning in these materials because shear rates experienced locally by a polymer confined between particles can be much larger than the overall external shear rate.[57]

Specific tolerance values for *K* and *n* were not pre-defined with regards to surgical application; however, these properties were shown to be highly tunable with respect to GAG and HAP concentrations. In general, higher consistency values were considered favorable since they coincided with enhanced shear responsive behavior including enhanced shear-thinning ($n < 1$) and viscoelastic recovery. Flow behavior results indicated a mutually beneficial relationship between *K* and *n*, where *K* values increased exponentially while shear-thinning behavior was enhanced with respective increase in GAG or HAP concentration. Additionally, it was shown that *K* was highly dependent on the polymer-particle ratio (w:w) in the GAG-HAP mixtures (Figure 2.7A and Figure 2.7B). At high ratios where GAG was in excess, mixture properties were dominated by the polymer component. Likewise, at low ratios where HAP was in excess, mixture properties reflected those

of pure HAP particles. Overall, flow experiments revealed that GAG-HAP colloidal mixtures could be tuned to exhibit large and synergistic *K* values without compromising shear-thinning behavior, a result that proves promising for surgical delivery purposes.

While the aforementioned rheological flow properties defined colloidal mixture behavior during shear induced disruption (Figure 2.11; Phase 1 → 2), oscillatory shear experiments attempted to elucidate GAG-HAP rheological recovery behavior following disruptive shear conditions. In these experiments, the colloidal mixture was allowed to recover initial viscoelastic properties following temporary microstructure breakdown (Figure 2.11; Phase 2 → Phase 3). A malleable material desirable for non-load bearing surgical application would possess a G' and G'' conducive to retention when no external force was present (e.g., primarily elastic behavior; $\delta < 45°$) and flow when exposed to an external shear (e.g., primarily viscous behavior; $\delta > 45°$). Additionally, a material with rapid recovery kinetics on the order of seconds to minutes following disruption (e.g., injection) may be desired. Utilizing results from swelling and rheological flow studies, colloidal mixtures containing 15% GAG – 60% HAP exhibited the most desirable behavior among tested mixtures. Thus, dynamic viscoelastic recoveries of 15% GAG – 60% HAP colloidal gels were compared to their pure GAG and HAP components, respectively (Figure 2.10A and Figure 2.10B). In terms of $G'_{recovery}$ magnitude, 15% GAG – 60% HAP mixtures recovered less extensively compared to pure 60% HAP. This result was expected since return to particle spacing equilibrium following microstructure disruption is dependent on the particle diffusivity in the suspending fluid.[57, 64] However, HA-HAP appeared to recover its initial G' within seconds of disruption while the CS-HAP mixture and pure HAP took several minutes. This may be due to the rapid and extensive self-association of HA polymers in the mixture compared to CS.[37-39] This may favor HA-HAP mixtures in a tissue filler application, since rapid self-assembly may improve

retention in the defect site. Overall, the rapid (< 5 min) and extensive ($G'_{recovery} \geq 64\%$) recovery of viscoelastic properties in 15% GAG – 60% HAP colloidal mixtures was encouraging with regard to potential surgical applications.

5. CONCLUSION

Malleable polymer-colloidal gels represent a desirable approach for minimally invasive filling of tissue defects and may ultimately facilitate regeneration of non-load bearing bone defects. This study demonstrated that the addition of moderate molecular weight GAGs such as CS (M_w = 15-30 kDa) and HA (M_w = 20-41 kDa) can be used successfully to modify the rheological properties of sub-micron HAP ($D_{avg} \leq 200$ nm) colloidal gels. GAG-HAP colloidal mixtures appeared to exhibit substantial polymer-particle interactions, leading to a synergistic increase in consistency index (K) without compromising shear-thinning behavior ($n < 1$) of the gel. In addition, GAG-HAP colloids containing high concentrations of HAP exhibited substantial yield stress (τ_y) and viscoelastic recovery properties ($G'_{recovery}$) which may be desirable for retention of these materials at surgical sites. While rheological differences were observed between CS-HAP and HA-HAP colloidal gels, both CS and HA represent feasible options for future studies investigating bone defect filling. HA is available across a large range of molecular weights (10-1000s kDa) compared to CS, which may ultimately yield additional rheological advantages. Overall, this study mapped and identified desirable mixture regions (Figure 2.9A and Figure 2.9B) where rheological properties of certain CS-HAP and HA-HAP colloidal gels aligned with desired properties to facilitate surgical delivery of fillers in non-load bearing bone regeneration applications.

6. LIST OF ABBREVIATIONS

CS, Chondroitin Sulfate; GAG, Glycosaminoglycan; HA, Hyaluronic Acid; HAP, Hydroxyapatite; H-B, Herschel-Bulkley Fluid; LVE, Linear Viscoelastic Region

CHAPTER 3: Endochondral Ossification for Enhancing Bone Regeneration:

Converging Native ECM Biomaterials and Developmental Engineering *in vivo*

S. Connor Dennis[1, 2], *Cory J. Berkland*[1, 2, 3], *Lynda F. Bonewald*[4], *Michael S. Detamore*[1 ,2*]
[1]Bioengineering Program, University of Kansas, Lawrence, KS 66047
[2]Chemical and Petroleum Engineering Department, University of Kansas, Lawrence, KS 66047
[3]Pharmaceutical Chemistry Department, University of Kansas, Lawrence, KS 66047
[4]Oral Biology, University of Missouri-Kansas City, Kansas City, MO 64108

KEYWORDS
Bone Regeneration, Developmental Engineering, Stem Cell Based Therapeutics, Native Biomaterials, Endochondral Ossification, Decellularized ECM

*Corresponding Author:
Professor, Department of Chemical and Petroleum Engineering
The University of Kansas
4163 Learned Hall, 1530 W. 15th Street, Lawrence, KS 66045-7618
Phone: (785) 864-4943
FAX: (785) 864-4967
detamore@ku.edu

ABSTRACT

Autologous bone grafting (ABG) remains entrenched as the gold standard of treatment in bone regenerative surgery. Consequently, many marginally successful bone tissue engineering strategies have focused on mimicking portions of ABG's 'ideal' osteoconductive, osteoinductive, and osteogenic composition resembling the late reparative stage extracellular matrix (ECM) in bone fracture repair, also known as the 'hard' or 'bony' callus. An alternative, less common approach that has emerged in the last decade harnesses endochondral (EC) ossification through developmental engineering principles, which acknowledges that the molecular and cellular mechanisms involved in developmental skeletogenesis, specifically EC ossification, are closely paralleled during native bone healing. EC ossification naturally occurs during the majority of bone fractures[65-73] and thus can potentially be utilized to enhance bone regeneration for nearly any orthopedic indication, especially in avascular critical-sized defects where hypoxic conditions favor initial chondrogenesis instead of direct intramembranous (IM) ossification. The body's native EC ossification response, however, is not capable of regenerating critical-sized defects without intervention. We propose that an underexplored potential exists to regenerate bone through the native EC ossification response by utilizing strategies that mimic the initial inflammatory or fibrocartilaginous ECM (i.e., 'pro-' or 'soft' callus) observed in the early reparative stage of bone fracture repair. To date, the majority of strategies utilizing this approach rely on clinically burdensome *in vitro* cell expansion protocols. This review will focus on the confluence of two evolving areas, (i) native ECM biomaterials and (ii) developmental engineering, which will attempt to overcome the technical, business and regulatory challenges that persist in the area of bone regeneration. Significant attention will be given to native 'raw' materials and ECM-based designs that provide necessary osteo- and chondro- conductive and inductive features for

enhancing EC ossification. Additionally, critical perspectives on existing stem cell based therapeutic (SCBT) strategies will be discussed with a focus on their use as an extension of the acellular ECM based designs for specific clinical indications. Within this framework, a novel realm of unexplored design strategies for bone tissue engineering will be introduced into the collective consciousness of the regenerative medicine field.

1. Introduction

The human body has an extensive capacity to regenerate bone tissue following trauma. Disruption of the surrounding vasculature and bone marrow resulting from a bone fracture initially facilitates a cascade of coagulation and inflammatory events within the fracture space (Figure 3.1).[65-70, 72, 73] The subsequent bone healing process overlaps with this inflammatory phase spatially and temporally via both bone developmental pathways: intramembranous (IM) and endochondral (EC) ossification.[65-70, 72, 73] Large defects above a 'critical-size', however, cannot be restored without intervention and often lead to non-union.[71, 74] Although current surgical intervention strategies, most notably autologous bone grafting (ABG), have yielded favorable bone healing outcomes in these situations, it is clear from the past decade's surge in clinically available tissue engineered bone implants, some coupled with stem cell based therapeutics (SCBTs), that alternative bone regenerative strategies have gained a significant market share.[75]

Clinically, however, ABG remains the gold standard of treatment due to its inherent osteoconductivity, osteoinductivity, and thus osteogenic capabilities.[1-3, 70] Despite these advantages, ABG has key clinical limitations including donor site morbidity and pain, increased risk of infection, limited handling capacity, graft resorption problems, and restricted tissue availability.[1-3, 70] Nearly three decades of bone tissue engineering research have been aimed at overcoming these limitations by finding performance competitive alternatives to ABG. As a result, many bone regeneration strategies have focused on mimicking portions of the complex composition and bioactive signals present in ABG, such as demineralized bone matrix (DBM), which resembles the late reparative stage extracellular matrix (ECM) in bone fracture repair (i.e., 'hard' or 'bony' callus).[65-70, 72, 73] These efforts have yielded dozens of clinical products including

synthetic scaffolds, allografts, and xenografts[4, 5], yet the majority of orthopedic procedures continue to utilize ABG.[1-3, 70]

To date, acellular biomaterial-based products have dominated the alternative bone implant market at the commercial level.[4, 5, 75] A major characteristic of these products is the ability to mimic the biological ECM environment specific for bone regeneration. These materials possess both conductive scaffold moieties and inductive signaling molecules that have been difficult to match with synthetic designs.[76-80] Within the realm of bone biomimetics, native ECM based biomaterials (e.g., DBM) have been a key protagonist.[5] However, there may be underexplored potential to enhance the bone regenerative response with native ECM biomaterials that instead mimic the initial inflammatory or fibrocartilaginous ECM (i.e., 'pro-' or 'soft' callus) observed in the early reparative stage of the native bone fracture healing process.

Addressing this avenue of research is the emerging paradigm of "developmental engineering" first introduced in 2009 in two reviews by Lenas *et al.*[81, 82], which offers an innovative approach to enhance the regenerative capacity of tissue engineered implants, including bone tissue applications, by focusing on path-dependent precursor tissue formation. This new strategy involves engineering developmental 'processes' *in vitro* in addition to 'tissues', and recognizes that the molecular and cellular mechanisms involved in developmental skeletogenesis, specifically EC ossification, are closely paralleled during native bone healing.[65-70, 72, 73] Primarily, these strategies have involved *in vitro* chondrogenic priming of various adult and embryonic stem cells for subsequent implantation and EC ossification *in vivo*. To date, however, no review has critically analyzed these *in vitro* priming approaches across various stem cell sources as a collective endeavor for the purpose of advancing bone regenerative medicine. While these priming strategies

have successfully produced EC ossification in several animal models, their clinical translation remains tethered to burdensome donor cell expansion protocols.

The incorporation of donor cells via stem cell based therapeutic (SCBT) strategies may provide advantageous osteo- and chondrogenic capabilities to acellular bone implants, which rely solely on recruited cells from the peripheral host tissue. These benefits are likely the reason behind the increasing saturation of product pipelines (i.e., preclinical and clinical level) with SCBTs across the areas of tissue engineering and regenerative medicine.[75] As a result, the bone regeneration market is likely to see an influx of SCBT products, either as exclusive therapies or combined with biomaterial implants, within the next decade. The clinical acceptance of these products will primarily depend on achieving (i) improved patient outcomes while at the same time reducing procedural (ii) complications and (iii) expenses compared to current standards of treatment.[75, 83, 84] Key to the success of SCBTs will be the reduction in time and cost consuming manufacturing practices (multiple days to weeks) associated with traditional *in vitro* cell expansion. Critical-sized bone defects often require surgical intervention within hours as opposed to weeks because delayed bone healing leads to higher risk of non-union.[71] Therefore, traditional cell expansion procedures represent a non-feasible clinical option in most critical-sized defect indications. Advances in intraoperative SCBT strategies offer innovative solutions to overcome this challenge by combining cell harvest, isolation, and implantation in one surgical setting without compromising progenitor cell and signal efficacy, thus eliminating the prolonged cell expansion phase.[84] Although SCBT strategies could revolutionize the orthopedic market, basic biomaterial designs incorporating the appropriate native ECM components to accompany these SCBTs will be crucial in the advancement of bone regenerative medicine.

An alternative strategy to reduce or remove the cell expansion step may reside in extending developmental engineering principles to *in vivo* designs (i.e., within the graft or implant), thus removing *in vitro* chondrogenic priming requirements altogether. Inspiration for *in vivo* developmental designs already exists with native ECM biomaterials, specifically acellular DBM grafts, which have already been shown to elicit some EC ossification in addition to the IM pathway.[85-91] However, as mentioned previously, DBM composition reflects the physicochemical properties of the late bone reparative stage ECM (Figure 3.1)[70, 71, 92, 93] and suggests that designs aimed at mimicking the composition of bone ECM may insufficiently elicit an EC ossification response inside healing fractures.

This review will highlight essential design criteria involved in the underexplored regenerative area of developmentally engineering bone *in vivo* (Figure 3.2). Traditional strategies have approached tissue-engineered construction through a combination of factors described in the tissue engineering triad: cells, signals, and scaffolds. However, the use of 'raw' ECM biomaterials may serve to bridge the gap between the latter two components of this triad by recognizing their integrated contribution to the local ECM[79], potentially obviating the need for additional incorporation of cells and signaling molecules. Crucial to developmentally engineering the process of EC ossification inside an implant will not only be the selection of native biomaterials that mimic the relevant tissue's ECM composition, but also materials that serve to modulate the developmental process. The primary focus will be on acellular ECM strategies, where the physicochemical cues that native ECM biomaterials possess may sufficiently elicit a bone regenerative response. Within this framework, the advantages of incorporating SCBT strategies will be discussed along with design criteria relating to specific bone defect indications.

2. Overview of the Natural Bone Healing Process

As mentioned before, the human body has an extensive capacity to regenerate bone tissue following trauma and fracture. The cellular and molecular processes involved in developmental skeletogenesis are closely paralleled during native bone healing.[65-73] Characterization of the complex mechanisms involved in bone healing has been the focus of several extensive reviews[65, 66, 71, 92], and readers interested in further details surrounding this cascade of events should direct their attention to these recommended citations.

In general, the fracture healing process is most often described in three overlapping phases: Inflammatory, Reparative, and Remodeling (Figure 3.1), where each phase represents a complex spatiotemporal distribution of cells, ECM, and bioactive signals.[65-73] Initially, disrupted vasculature and bone marrow during the inflammatory phase facilitates a coagulation cascade along with an influx of progenitor cells, including bone mesenchymal stem cells (BMSCs), into the fracture space forming a hematoma. Without permanent vasculature, however, the fracture space becomes hypoxic, and it remains unclear whether enough of these stem cells survive the initial inflammatory phase to play an active role in subsequent tissue regeneration.[65-73] Established bioactive signaling from the inflammatory phase ECM subsequently recruits progenitor cells from both the exposed periosteum and bone marrow that migrate into the fracture space initiating both bone developmental pathways: IM and EC ossification.[65-70, 72, 73] Primary differences in these pathways reside in precursor requirements. While IM requires condensation and proliferation of progenitor BMSCs for ossification, EC requires cartilage and fibrous intermediate tissue formation before ossification.[65-73] EC ossification therefore can further be divided into three generalized steps: 1) chondrogenesis, 2) cartilage hypertrophy, and 3) ossification.[65-73] Regardless of the pathway, however, neo-vascularization and angiogenesis are necessary before ossification can

proceed.[69, 70, 94-97] In contrast, chondrogenesis predominately occurs in avascular environments where oxygen tension is low.[98-102] The main consequence of this difference is that IM and EC ossification manifest in physiologically distinct regions of the fracture space, where the former primarily occurs adjacent to the fracture ends and the latter occurs primarily in the avascular bulk of the fracture space.[66, 69, 70] Collectively, this early reparative stage climaxes in the formation of a spanning fibrocartilaginous callus (i.e., 'pro-' or 'soft' callus) in the majority of the fracture space developing from EC ossification. The procallus serves both a chemical and mechanical function and acts as a primed template for subsequent osteoblast infiltration, woven bone ossification (i.e., 'hard' or 'bony' callus), and finally bone remodeling to restore healthy lamellar bone architecture.[65-73]

While the aforementioned process describes successful bone regeneration within the body, it is well understood that large defects above a 'critical-size' are incapable of completely restoring native bone structure without intervention and often lead to non-union.[71, 74] It is important to note that critical-sized defects are inherently large, avascular spaces that present favorable conditions for EC ossification as opposed to IM. This review will outline several studies (Tables 2-4) that have leveraged EC ossification and developmental engineering strategies within critical-sized defects in various animal models. Collectively, this evidence suggests that enhancing EC ossification may be a viable, underexplored strategy for improving bone regeneration.

3. Strategies to Enhance EC Ossification

3.1 Harnessing the Potential of Developmental Engineering

Developmental engineering, a term first introduced into the tissue engineering community with two reviews in 2009 by Lenas *et al.*[81, 82], involves the engineering of developmental 'processes'

and ‘tissues’ *in vitro*, and recognizes that the embryonic and morphological paradigms involved in developmental skeletogenesis are closely paralleled during native bone healing.[65-70, 72, 73] This approach attempts to recapitulate aspects bone regeneration by leveraging several concepts in developmental biology including.[81, 82]

1) Path-dependence: successive developmental tissue relies on previous tissue formation
2) Robustness: tissue developmental process resistant to unintended external perturbation
3) Semi-autonomy: partially self-governed tissue development

EC ossification is a feasible route to utilize these guiding principles of developmental engineering, and the current review will cover advances made over the past decade in engineering EC ossification for bone regeneration (Table 3.2-3.4).

While the Lenas reviews only covered replicating *in vivo* developmental processes in an *in vitro* environment[81, 82], the current review aims to expand their previous concept further to include reproduction of developmental processes in an *in vivo* environment (i.e., within implanted grafts/scaffolds). If evidenced to produce similar regenerative outcomes compared to their *in vitro* counterparts, *in vivo* developmental designs would obviate the need for cost and time-consuming cell expansion protocols, which remain a critical challenge in the translation of SCBTs.[75, 83, 84]. However, there remains a deficiency in both fundamental research and translatable products within the expansive framework of *in vivo* developmental designs.

3.2 Coupling *In Vivo* Developmental Engineering with Native ECM Biomaterials

3.2.1 Characterizing the Influence of DBM on Ossification Pathway

Inspiration for *in vivo* developmental designs already exists in the form of native ECM biomaterials. There is significant evidence that EC ossification occurs in acellular DBM grafts[85-88], which inherently resemble the composition of late reparative stage bone healing ECM.[5, 65-70, 72,

[73] In a critical-sized rat femoral defect model, Oakes *et al.*[85] observed histological evidence of increased EC ossification foci in human DBM implants suspended in a hyaluronic acid carrier fluid compared to similar DBM implants suspended in a glycerol solution. However, radiographic scoring 16 weeks post implantation revealed no significant difference in their mineral content.[85] Although the authors did not further pursue developmental differences between groups, this evidence suggests that both EC and IM pathways were utilized within DBM implants. This could have been due to differences in carrier fluid. Hyaluronic acid is known to be a major component of cartilage ECM[68] and therefore could play a regulatory role in both chondrogenesis and EC ossification.[73]

Regardless, the DBM composition containing conductive and inductive biological agents likely influences developmental pathways during bone healing.[85-88] DBM composition, however, is not uniform throughout the body. There exist compositional differences in bone ECM originating from IM sources during fetal development (e.g., cranium) and EC sources (e.g., femur).[103] Furthermore, DBM originating from IM and EC bone have been shown in a series of studies by Rabie *et al.*[87, 89-91] to elicit different healing pathways during regeneration of parietal bone defects in New Zealand White Rabbits. The parietal bone is formed by IM ossification during fetal development[103], suggesting that only implants directed toward IM ossification will possess regenerative potential. However, evidence from Rabie *et al.* [87, 89, 90] showed that IM and EC ossification pathways can be utilized, exclusively or in combination, to regenerate parietal defects based entirely on the source of DBM. In addition, the amount of bone regeneration was shown to be source dependent, where grafts favoring IM ossification displayed a significantly higher degree of newly formed bone observed by serial histological sectioning.[91] While these studies collectively support the ‘same for same’ surgical practice in bone regeneration[91], where DBM from IM and EC

sources is matched on a developmental basis to the respective bone defect site, the major limitation of these studies was the short timeframe of healing (14 days) observed following implantation. Since Oakes *et al.*[85] observed no evidence of a difference in bone regeneration 16 weeks post implantation, similar longitudinal studies are necessary to determine whether DBM implants from EC or IM sources display significant regenerative capacities.

The differences in regenerative potential and developmental pathways seen in the Rabie studies were attributed to varying inductive and conductive ECM factors within DBM.[87, 89-91] Inductive factors such as bone morphogenic proteins (BMPs) have been implicated in bone morphogenesis dating back to their initial isolation from DBM, reviewed in chronological detail by Gruskin *et al.*[5] Consequently, BMP-2 content, release, and bioactivity has become an important guideline in determining efficacy and quality control of commercially available DBM products.[5] BMPs, however, represent only a fraction of the growth factors in the spatiotemporal cascade of inductive molecules involved during bone healing, reviewed extensively by Mehta *et al.*[71] Inductive signaling alone could have been responsible for the regenerative effect seen in DBM as well as account for differences seen between DBM from IM and EC sources. However, the conductive proteins present in DBM may also provide key regulatory control since it has become increasingly evident that structural components of native ECM along with mechanical forces acting on the tissue have significant influence on cellular and molecular bioactivity.[80, 104]

Collectively, there is significant evidence to suggest that EC ossification can occur within native ECM biomaterials in the form of acellular DBM implants. While there has been extensive research into the bone regenerative capacity of DBM, an underexplored avenue of research is the focus on the developmental pathway's effect on regenerative capacity of these implants. The characterization of DBM's influence, and perhaps limitation, in stimulating EC ossification should

be elucidated in the future to advance the understanding of the bone healing process and potentially enhance bone regenerative designs.

3.2.2 Exploring EC Ossification Potential in ECM Biomaterials

In general, native ECM refers to both soluble and insoluble biomolecules that may be utilized as cell scaffolding and bioactive signaling. Additionally, the effectiveness of autologous, allogeneic and xenogeneic ECM biomaterials can be assessed in terms of physical, chemical, and mechanical properties of the tissue. While it remains debatable whether native ECM represents nature's ideal biological scaffold, particularly because resident cells exhibit physiologically relevant synthesis and maintenance within it, these materials have received significant attention for their potential efficacy in the regenerative tissue market.[76, 77, 79, 80]

3.2.2.1 Traditional Bone ECM Strategies

ABG intrinsically involves the grafting of native bone ECM tissue with associated autologous cells into bone defects, and it remains the gold standard of treatment in bone regeneration due to its inherent osteoconductivity, osteoinductivity, and osteogenic capacity.[1-3, 70] It intuitively followed that designs mimicking the native bone ECM (Figure 3.1) held potential for bone regeneration, and as a result, many alternative bone regeneration strategies focused on mimicking portions of the complex composition and bioactive signals present in ABG, which resembles the late reparative stage ECM in bone fracture repair (i.e., 'hard' or 'bony' callus).[65-70, 72, 73] Some of these strategies were discussed in the previous DBM characterization section where allogeneic tissue was used to elicit bone regeneration. Subsequently, efforts in the bone ECM biomimetic area have yielded dozens of commercially available products.[4, 5] Two reviews by Gruskin *et al*.[5] and Bohner[4] compare an extensive number of these products which can be divided into two broad categories: 1) organic scaffolds (e.g., allografts, and xenografts) and 2) inorganic

scaffolds (e.g., calcium phosphate cements), yet the majority of orthopedic procedures continue to utilize ABG.[1-3, 70] This is likely due to the fact that bone ECM biomimetic strategies fail to sufficiently mimic the complex 3D physical, chemical, and cellular composition of healthy autologous bone.[1-3, 70]

It is important to note, however, that the functional and structural properties of ECM during the bone healing process are spatially and temporally dynamic and do not resemble healthy native bone until well into the reparative and remodeling stages of healing (Figure 3.1).[70, 71, 92, 93] This delay in resemblance suggests that designs aimed at mimicking the composition of bone ECM may insufficiently elicit a regenerative response inside healing fractures and could be a worthwhile focus of future investigation in bone regeneration.

3.2.2.2 Alternative ECM Biomaterial Strategies for EC Ossification

By instead leveraging the concepts of both developmental engineering and the spatiotemporal dynamics of ECM in bone healing, there may be potential to enhance the extent and quality of EC ossification. Specifically, native ECM biomaterials that mimic the initial inflammatory stage ECM or fibrocartilaginous ECM (i.e., 'pro-' or 'soft' callus) in the early reparative stage of bone fracture healing may be selected instead of materials that mimic the composition of bone ECM. These scaffolds or grafts based on inflammatory or fibrocartilaginous ECM may harness the path-dependent, robust, and semi-autonomous nature of EC ossification, potentially leading to extensive bone regeneration.

Characterization of the complex cascade of signaling events and ECM changes involved in bone healing and EC ossification has been the focus of several recent reviews[70, 71, 92, 93], and readers interested in further multifaceted details surrounding relevant biomolecules should direct their attention to these recommended citations. While the characterization of the spatiotemporal

distribution of these molecules may be of value for developmental engineering, few efforts have been made to mimic the appropriate array of bioactive scaffolding and signaling molecules with native ECM biomaterials that correspond to the early and intermediate stages of native bone healing.

Native ECM biomaterials possess both conductive and inductive potential that are difficult to match with synthetic designs (e.g., non-native polymers).[76-79] Additionally, it is increasingly evident that the structural components of native ECM also provide a regulatory role for key processes in cellular development and tissue regeneration.[80, 104] These processes include cell adhesion, proliferation, differentiation, migration, and survival along with modulating signaling activity of soluble bioactive molecules.[80, 104] Furthermore, the native ECM's integrated approach to combine the traditional signaling and scaffolding components of the tissue engineering triad suggests that acellular designs may obviate the need for burdensome cell expansion protocols and additional bioactive signal incorporation which introduce major challenges that threaten commercial success in bone regeneration.[83, 84]

To date, few studies have attempted to coordinate developmental bone engineering strategies with acellular native ECM biomaterials (Figure 3.1 and Figure 3.2). Subsequent sections will address key features of existing technology and more importantly focus on worthwhile areas of future investigation for the purpose of enhancing EC ossification and bone regeneration.

3.2.2.3 Inflammatory Stage ECM Strategies for EC Ossification

Since most tissues primarily rely on broken vasculature to supply damaged areas with inflammatory signals and cells, modulating the body's initial inflammatory response following any tissue trauma has been well studied.[105, 106] As a result, many regenerative design strategies have focused on isolating and concentrating portions of human blood such as platelets and plasma

(e.g., platelet rich plasma or PRP) or pro-coagulation molecules (e.g., fibrin sealants) to enhance endogenous healing responses.[107-113] It remains to be seen whether a scaffold with only inflammation-related chemical and mechanical cues can elicit enough of an EC ossification response to heal critical-sized bone defects. Pure fibrin scaffolds and PRP alone do not appear to exhibit sufficient cartilage[107-109, 111] and bone[110, 112, 113] regeneration in critical-sized defects, which suggests that additional regenerative stimuli such as bioactive molecules and progenitor stem cells may be required.

One strategy to enhance the regenerative response in inflammatory stage ECM strategies has been to supply the fracture space with stem cells from bone marrow aspirate since fractured bone is supplied with bone marrow intrusion when the inner marrow space is disrupted.[65-73] This intrusion of marrow allows supplementary signaling molecules and progenitor cells, including BMSCs, to infiltrate the fracture space. However, hypoxic conditions within the mechanically unstable fracture lead to significant cell mortality, and it remains unclear whether enough of these stem cells survive the initial inflammatory phase to actively participate in subsequent tissue regeneration.[65-73] Jakob *et al.*[84] reviewed some bone engineering strategies that included isolated and concentrated bone marrow aspirate to enhance regeneration, but concluded that the fraction of BMSCs present in bone marrow (1 in 10,000 nucleated cells) limited the regenerative capacity of these designs. Extensive work has also been conducted to additionally isolate, differentiate, and expand the BMSCs within bone marrow to enhance the regenerative capacity of engineered bone implants, discussed in subsequent sections on SCBT strategies (Tables 2-4). However, the expansion of BMSCs requires financially burdensome and time consuming protocols that limit the commercial application of these strategies.[83, 84] Therefore, cell expansion should likely be considered as a contingent reserve to cell recruitment strategies.

Coupling the evidence of low progenitor count with poor cell survival rate observed in hypoxic bone defects suggests the importance of spatiotemporal cellular recruitment strategies for bone regeneration. As the native bone healing process continues into the reparative stages of healing, the exposed periosteum and bone marrow continue to serve as reservoirs of progenitor cells that subsequently migrate into the fracture space.[70, 71, 92, 93] Several important reviews have focused on physical (e.g., osmotic gradients and hydrodynamic forces) and chemical (e.g., chemokines) cellular recruitment strategies for tissue regeneration.[114, 115] Within the realm of developmental engineering and native ECM biomaterials, the subsequent differentiation pathway should also be emphasized with regard to overall cellular recruitment strategy. Since critical-sized defects are primarily avascular and hypoxic[66, 69, 70], initial chondrogenesis involved in EC ossification may be a more favorable condition to exploit in this lower oxygen tension environment compared to direct osteogenesis in IM ossification.[98-102]

Collectively, the evidence surrounding the use of inflammatory stage ECM scaffolds, signals, and recruited cells indicates that current designs remain insufficient in regenerating bone in critical-sized defects. To date, no studies have focused on controlling the recruitment and differentiation of BMSCs down the EC ossification pathway within the realm of inflammatory stage ECM strategies. This underexplored area may be an advantageous condition to exploit in future bone regeneration strategies.

3.2.2.4 Procallus Stage ECM Strategies for EC Ossification

An intuitive source for enhancing stimulation of EC ossification is the procallus ECM since natural bone healing progresses to this stage early in the regenerative process.[65-73] Insight into the conductive and inductive biomolecules that control EC ossification have been essential to tissue engineering strategies focusing on cartilage formation[116, 117], osteochondral defects[118, 119], and

more recently bone regeneration (Table 3.2-3.4).[86, 102, 116, 117, 120-135] While cartilage tissue engineering strategies have focused on inducing and maintaining chondrogenic phenotypes, the induction and modulation of cartilage hypertrophy is critical to the progression of EC ossification in bone regeneration designs.[71, 92, 93, 96-102, 131, 136-144] Whereas the key transcription factor involved in initial chondrogenesis is SOX9, the primary hypertrophy associated factors are runt-related transcription factor 2 (Runx2) and myocyte enhancer factor 2C (MEF2C).[92, 93, 100, 137] In this critical maturation stage of EC ossification, chondrocytes experience a large increase in volume (~5 to 10 fold), and downstream proteins activated by Runx2 and MEF2C transcription factors begin to remodel the surrounding ECM.[92, 93, 100, 137] These targets include MMPs that degrade cartilaginous ECM[65-70, 72, 73], Indian Hedgehog (Ihh) that induces proliferation of non-hypertrophic chondrocytes[92, 93, 100, 137], angiogenic factors like vascular endothelial growth factor (VEGF) to promote neo-vascularization[93, 94, 131, 136, 137] along with collagen type X, alkaline phosphatase (ALP), and matrix vesicles for ECM mineralization.[145-147] While several *in vitro* studies have shown that external chemical[71, 92, 97, 100, 132, 139-144, 148, 149], physical[98-101] and mechanical cues[100, 104] stimulated BMSCs to stay locked in a stable cartilage state or progress into a hypertrophic phenotype (Table 3.1), it remains to be seen whether acellular procallus ECM designs have the potential to elicit similar responses from incorporated or recruited stem cells.

In summary, the success of *in vivo* developmental engineering designs for EC ossification will likely depend on the incorporation of physiologically relevant bioactive chemical mediators along with physical and mechanical cues drawn from these important *in vitro* studies. Coupling these results with the previously discussed evidence regarding DBM's influence on EC ossification[85-91] provides a potent array of strategies for future bone regeneration designs. Furthermore, it is evident that the selection of appropriate native ECM components is essential for

exploiting the advantages of EC ossification. However, strategies to efficiently and feasibly incorporate these biomolecules into bone regenerative implant designs require consideration and thus will be further discussed below.

3.3 Isolating, Identifying and Delivering Native ECM for EC Ossification

3.3.1 Utilizing Step-Wise ECM Strategies

Strategies to design scaffolds with incorporated native ECM components can be divided into two main categories: 1) Bottom-up approach or 2) Top-down approach (i.e., step-wise designs) (Figure 3.3). While the former aims to mimic native ECM with complex biomaterial re-synthesis strategies (e.g., collagen polymerization), the latter step-wise approach attempts to process native ECM from autologous, allogeneic, or xenogeneic sources without completely compromising tissue structure and function (e.g., decellularization and demineralization). Two extensive reviews by Badylak[76] and Renth *et al.*[79] provided detailed experimental outcomes and current clinical products utilizing 'raw' native ECM biomaterials for tissue regeneration, which include both bottom-up and step-wise strategies. In general, nearly all step-wise design approaches described in these reviews, with the exception of autologous tissue harvesting, require some form of processing to avoid immunogenicity with host (i.e., recipient) tissue since allogeneic and xenogeneic cellular antigens are recognized as foreign.[76-78, 150] To address this immunogenicity, a variety of physical, chemical, and enzymatic processing methods have demonstrated the possibility of sufficiently devitalizing or decellularizing these tissues to suppress host rejection without compromising the conductive, inductive and mechanical components of the ECM.[76-78, 150]

In a comprehensive review of current tissue and whole organ decellularization methods by Crapo *et al.*[150], it was recognized that all current techniques cause some degree of ECM disruption. As manufacturing requirements increase, the complex physical and chemical components of the

native ECM tissue decrease along with corresponding mechanical structures and functions.[76-80, 150] At the extreme end of this spectrum, where individual 'raw' ECM components are isolated (e.g., collagen, glycosaminoglycans, and soluble growth factors)[79], designs necessarily require some form of bottom-up re-synthesis to regain a portion of the physiologically relevant ECM structure and functionality, yet it poorly resembles the initial native ECM tissue (Figure 3.3).[76] The main advantage of using 'raw' biomaterial re-synthesis, however, is that designs can be modular, which means that separate elements of the design can be tested independently. As a result, each component can be characterized for its contribution to the process as a whole in a full-factorial experimental design (e.g., scaffolding protein vs. soluble factor vs. scaffolding protein + soluble factor). Nevertheless, the problem with modular re-synthesis based designs is that mimicking complex environments, such as the complex cascade of signaling events involved in bone healing[70, 71, 92, 93], is nearly impossible in addition to being economically infeasible.[151] This is compounded by the fact that the characterization of the complex 3D structures and functions of native ECM remains incomplete.[76, 150] A modular design coupling both conductive and inductive biomolecules present in native bone ECM yields nearly infinite permutations, yet this has remained entrenched as the primary philosophy of bone tissue engineering over the past three decades.[151] Even with current sophisticated manufacturing technology, including 3D printing, complex polymerization and chemical conjugation techniques, artificial re-synthesis of this biological material remains physiologically dissimilar compared to its native tissue counterpart in terms of relevant physicochemical composition.[76-80] Although future technological advances may someday improve bottom-up re-synthesis designs, the main consequence is that step-wise design strategies may currently represent the more favorable option when attempting to mimic native ECM.[150]

Step-wise designs from both allogeneic and xenogeneic tissue sources have been utilized clinically for cartilage and bone tissue engineering along with dermal, vascular, nerve, and urogenital tissue.[5, 76, 77, 79, 152] Furthermore, previous evidence was presented linking step-wise derived DBM to extensive bone regeneration via IM and EC ossification,[85-91] attributes which likely contribute to its role as a key protagonist in the bone graft substitute market.[5] If alternative ECM biomaterials are to be used to enhance bone regeneration as proposed in the current review, then key technical, regulatory, and commercial features surrounding the use and approval of DBM should be utilized as a guiding template for potential success.

3.3.2 Decellularized Cartilage for Enhancing EC Ossification

Intuitively, it follows that designs mimicking the native bone or cartilage ECM hold vast potential for eliciting ossification and chondrogenesis, respectively. Therefore, it is understandable that for many years, bone and cartilage tissue engineering strategies have focused primarily on treating these two tissues as separate regenerative endeavors. Although a pivotal review by Singh *et al.*[114] established chemical and mechanical based spatial gradients as an advantageous design approach in osteochondral interfacial tissue regeneration, these strategies still involve a binary differentiation pathway, where the transition zone is only a spatial gradient formed by a gradual change in either chondrogenic or osteogenic cues. EC ossification, however, is a spatial and temporal transition process where cartilage precursor gradually transitions to bone over extended periods of time.[65, 66, 71, 92] Thus, the chondrogenic signaling cues initially present in a scaffold may be required to transition over time to influence hypertrophy and osteogenesis.

Previously mentioned in this review was emerging evidence that has shown the potential of DBM to prompt EC ossification *in vivo*[85-91], and subsequent sections will discuss evidence that *in vitro* primed cartilage constructs may also prompt EC ossification *in vivo* (Table 3.2-3.4).

Coupling this evidence with motifs in developmental engineering including path-dependence, robustness, and semi-autonomy suggests that decellularized cartilage (DCC), which mimics portions of the native procallus ECM, may provide extensive potential in prompting EC ossification within an implant and could be a worthwhile focus of future investigation in bone regeneration.

DCC, from both allogeneic and xenogeneic sources, is a poorly explored native ECM biomaterial. Recently, it has emerged as a source rich in both chondroinductive and chondroconductive potential.[77, 79, 80, 152-154] Current commercially available products utilizing articular cartilage and/or DCC include Biocartilage® (Arthrex), De Novo NT® and ET® Live Graft (Zimmer), and Chondrofix® (Zimmer). However, all of these products use cartilage ECM for the purpose of regenerating only cartilage tissue. In the framework of developmental engineering, DCC provides a source for modulating and enhancing EC ossification, yet there remains an extreme deficiency in both fundamental research and translatable products incorporating this material. Hyaline cartilage is avascular in nature, which may be advantageous to pursue for critical-sized bone defects since chondrocytes are better suited for hypoxic environments compared to osteoblasts. Moreover, an avascular tissue may minimize potential developmental disturbance from unintended external perturbations.[65-73, 81, 82] An additional consequence of this isolation is that the progression of cartilage to bone during EC ossification is primarily dictated within the tissue by intercellular signaling, incorporating semi-autonomous control into the process.[65-73, 81, 82] Furthermore, many forms of cartilage exist in the body including hyaline cartilage (e.g., femoral condyles and tibial plateau), fibrocartilage (e.g., temporomandibular joint disc and knee meniscus), elastic cartilage (e.g., nose and ear), and even hypertrophic cartilage (e.g., fetal bones and growth plates).[68] Fibrocartilage may provide an even better procallus mimetic tissue than hyaline cartilage

since the procallus is fibrocartilaginous in nature. Additionally, fetal bones undergoing EC ossification during skeletogenesis may provide primed hypertrophic cartilage that could facilitate rapid ossification in a bone defect. Thus, there exists a range of DCC-derived tissues that may be explored in relation to EC ossification.

3.3.3 Delivery Strategies for Decellularized Tissues

Crucial to the future success of these ECM materials will be the strategies used to incorporate and deliver them within engineered implants. If maximum retention of native inductive, conductive, and mechanical potential of ECM is desired, then minimal required processing is preferred to keep the microarchitecture of the native tissue intact.[76-80] However, this severely limits native ECM's potential to be incorporated within an engineered implant or delivered surgically to a defect site. Large sections of native ECM tissue have been broken down by various morselization and solubilization strategies, which can be used to enhance decellularization efficiency.[5, 77-79] However, the effect of particle size on regenerative capacity of these materials remains unclear. A recent review of DBM clinical products and procurement by Gruskin *et al.*[5], indicated that larger particles of DBM (420-840 μm) might be more osteoinductive than smaller particles (<250 μm) but warned readers that the majority of preclinical data regarding particle size effects are inconsistent due to varying animal models and subjective outcome measures. Furthermore, the authors of the current review are not aware of any studies that analyze chondrogenesis as a function of DCC particle size or EC ossification as a function of ECM particle size.

While morselization strategies most often include some form of mechanical breakdown (e.g., pulverization or cyrogrinding), solubilization uses chemical and enzymatic methods (e.g., demineralization and collagenase) to breakdown ECM.[77, 78] The primary advantage of breaking

down native ECM into micron or sub-micron sized particles is an increased relative surface area per volume of material. This can be exploited to improve decellularization efficiency, but it may also be essential in exposing cellular adhesion proteins, modulating growth factor release, and uncovering potential crosslinking moieties to facilitate synthetic reconstruction strategies (e.g., polymerization).

In summary, the extent of native ECM processing required to enhance the regenerative capacity of a bone implant will be application specific. These specifications will include issues like load-bearing requirements, defect geometry (e.g., irregular vs. machined defects), bone architecture (e.g., cortical vs. cancellous), and vulnerable surrounding tissues (e.g., the spinal cord in vertebral fusion or brain tissue in calvarial repair). Existing design paradigms already used to support DBM particles, such as solid scaffolding or chemically crosslinked hydrogels[5] along with emerging design paradigms such as shear-responsive and self-assembling colloidal gels[8, 10-12, 155], will likely yield an extensive array of application specific bone regenerative scaffolds with EC ossification potential.

3.4 Incorporating SCBTs into the Design

3.4.1 Priming Chondrogenesis *in vitro* for EC Ossification

While acellular ECM design strategies possess great conductive and inductive potential for eliciting *in vivo* EC ossification, SCBTs may provide advantageous osteo- and chondrogenic capacity within bone implants. Without the incorporation of donor cells, acellular implants such as allografts, xenografts, or synthetic scaffolds must rely solely on recruited cells from the peripheral host tissue. Recruitment strategies often involve biochemical agents (e.g., chemokines) or induced physical migration (e.g., osmotic gradients or hydrodynamic forces), which may be insufficient for some indications with limited access to progenitor cell reservoirs in the bone

marrow and periosteum. BMSC recruitment also involves successful cellular migration into the scaffold, which may be limited by physical constraints within the implant (e.g., small pore size, limited pore connectivity).[156] By incorporating a donor stem cell population within an implant instead, these cellular recruitment challenges may be overcome.

The bone regeneration community has attempted to harness the advantages of SCBT strategies, either as exclusive therapies or combined and encapsulated within biomaterial implants, to overcome cell recruitment limitations and to obviate ABG as the standard of treatment for bone fractures.[157] Gamie *et al*.[157] provided a comprehensive review of various sources of stem cells in combination with bone graft substitutes for bone tissue engineering through osteogenic differentiation. Sources of these cells range from embryonic stem cells (ESCs) to an array of cells from adult mesenchymal origin including umbilical cord stem cells (UMSCs), bone marrow and periosteum derived stem cells, adipose derived stem cells (ADSCs), synovium derived stem cells (SDSCs), and more recently induced pluripotent stem cells (iPSCs) were shown to lead to osteogenesis *in vitro* and *in vivo*.[100, 157] Cells from these sources possess some degree of pluripotency, where differentiation can lead to a number of distinct cell types including osteoblasts and chondrocytes.

Within the realm of SCBTs for bone regeneration, a majority of strategies have focused on stimulating cell populations to undergo direct osteogenesis rather than chondrogenesis. However, as previously mentioned, the EC ossification pathway holds key advantages over IM ossification. This is especially true in critical-sized defects which are inherently large avascular spaces and favor intermediate chondrogenesis of tissue rather than direct ossification.[65-73] An emerging group of successful research efforts have focused on exploiting this condition over the past decade. These recent publications (Table 3.2-3.4) have demonstrated the capacity of cartilage tissue constructs to

promote EC ossification *in vivo* following *in vitro* priming with seeded BMSCs[119, 122, 123, 125, 126, 131-135, 158-162], ESCs[86, 121, 126, 135], ADSCs[163], iPSCs[164], and articular chondrocytes (ACs)[120, 126, 129, 130, 134]. Most of these studies utilized a heterotopic bone formation model in immunocompromised animals to provide evidence of osteo- and chondro- conductivity, and inductivity. However, more recent studies by Bahney *et al.*,[165] van der Stok *et al.*,[161] Harada *et al.*,[160] and Shoji *et al.*[163] (Table 3.2) showed critical-size defect regeneration in rat femurs and mice tibias via EC ossification. Likewise, studies by Montufar-Solis *et al.*[86] and Doan *et al.*[121] (Table 3.3) showed critical-sized defect regeneration in murine calvaria. Collectively, these studies indicated that primed cartilage constructs can regenerate bone through EC ossification regardless of fetal developmental origin.

While the majority of the tissue priming research aimed to establish feasibility from a particular cell population (Table 3.2-3.3), several studies compared various cell sources to elucidate differences in their capacity to stimulate EC ossification (Table 3.4).[126, 134, 135] Most of these comparative studies concluded that only certain cell sources, most often ESCs or BMSCs were capable of inducing EC ossification in animal models,[126, 134-136, 166] yet other studies clearly showed significant EC ossification with ADSCs,[163] iPSCs,[164] and even ACs *in vivo*.[120, 129, 130] The only stem cell population that did not exhibit EC ossification were SDSCs, which instead went through fibrous degradation and resorption *in vivo*.[134, 136] This contradicting evidence highlights the fact that the spatiotemporal control of cell culture priming conditions are essential in determining implant fate *in vivo*. A review by Gawlitta *et al.*[100] focused on the modulation of these conditions to optimize the *in vitro* priming of BMSCs for EC ossification. However, a comprehensive overview of modulating EC priming conditions between comparative sources of stem cells has not been addressed and could be a worthwhile focus of future investigation in enhancing EC ossification and bone regeneration designs.

Regardless of the cell source used for priming EC ossification, several generalized conclusions from the reviewed primed *in vitro* stem cell studies (Table 3.2-3.4) can be summarized as follows:

1) Chondrogenic cell priming *in vitro* was required to elicit EC ossification *in vivo.*
2) Cartilage templates were necessary, but not sufficient to elicit EC ossification *in vivo*
    a. Stable or permanent AC templates did progress through EC ossification.
3) Osteogenic priming alternatively favored IM over EC ossification
4) Hypertrophic chondrocyte priming elicited the most extensive EC ossification.

While the collective evidence from these studies suggested that EC ossification remains necessarily tethered to the burden of *in vitro* cell priming and expansion, previous evidence was already presented linking EC ossification to acellular DBM grafts.[85-91] This evidence directly contradicts the notion that priming is necessary to elicit an EC response (Tables 2-4) and instead only represents a sufficient condition that can also be addressed by acellular native ECM biomaterials.

Consequently, this contradictory evidence suggests that an intermediate and underexplored strategy for bone regeneration may exist that incorporates advantages exhibited by both DBM biomaterials and primed cartilage constructs, such as the enhancement of EC ossification, and possibly minimizes their limitations, for example the extensive costs, risks, and time consuming manufacturing practices associated with *in vitro* cell expansion. Extensive supporting evidence has been presented previously in this review to suggest that native, acellular ECM biomaterials (e.g., DCC) mimicking the procallus healing microenvironment may be a worthwhile focus for future investigation in this underexplored design space for bone regeneration.

3.4.2 Intraoperative SCBT Strategies with Native ECM Biomaterials

An emerging strategy to streamline SCBTs is to consolidate necessary cell protocols, including the harvesting, isolation, stimulation, and implantation of autologous cells, into one surgical (i.e., intraoperative) setting. Intraoperative SCBTs usually involve the use of multiple surgical sites (e.g., a bone defect site and a bone marrow aspiration site) but obviates the need for cell expansion protocols. By definition, ABG falls under the description of an intraoperative SCBT since autologous stem cells are harvested and implanted within one surgical setting. Recent intraoperative strategies aim at minimizing the limitations associated with traditional stem cell expansion protocols and ABG while also maximizing stem cell efficacy.

To date, however, no intraoperative SCBT approaches using either BMSCs or ADSCs derived from the stromal vascular fraction (SVF) have been able to regenerate bone in critical-sized defects without the inclusion of additional stimulatory factors.[84] In a study by Helder *et al.*,[167] isolated SVF cells failed to generate bone when implanted in a goat intervertebral model. Likewise, Follmar *et al.*[168] saw limited angiogenesis and no evidence of ossification in ADSCs loaded fibrin glues implanted subcutaneously in rabbits. Muller *et al.*[169] did observe some evidence of combined angiogenesis and osteoid structures, identified with histology and immunostaining for bone sialoprotein and osteocalcin, in human ADSC loaded fibrin glues combined with beta-tricalcium phosphate, hydroxyapatite, and acellular bone xenografts implanted subcutaneously in nude mice. However, the authors found no evidence of murine derived bone structures in the implants, indicating a lack of osteoinductivity.[169] More recent data from the same group indicated that SVF combined with 250 ng of BMP-2 and encapsulated in a fibrin and porous calcium phosphate composite gel could form heterotropic bone when injected subcutaneously in nude mice.[170]

Overall, this combined evidence suggests that additional inductive stimulation of stem cells within the brief surgical time frame may be crucial in improving efficacy of intraoperative designs.

Emerging evidence in this area suggests that quick stimulation of isolated stem cells (e.g., minutes to hours) may improve differentiation and gene expression outcomes compared to untreated cells.[84, 105, 106, 171] Some strategies for stimulating isolated stem cells include the use of inductive and conductive signaling molecules, either in purified form (e.g., BMP-2)[169, 170] or from extracted endogenous tissue and fluids (e.g., PRP).[172] Kitamura *et al.*[172] showed histological and mechanical evidence that BMSCs loaded with PRP regenerated bone in a dog mandible defect model comparable to autologous bone controls.

Meanwhile, it should be reiterated and emphasized that native ECM biomaterials from allogeneic and xenogeneic sources possess both conductive and inductive biomolecules.[76, 77, 79, 80] These biomaterials alone may have the potential to stimulate stem cells in an intraoperative setting. As discussed previously, native ECM representing both the early and late stages of bone repair have the ability to induce both chondro- and osteogenesis by seeded stem cells.[85-88, 152] A critical area of future investigation, therefore, should be devoted to examining the capacity of these biomaterials to stimulate stem cell differentiation and gene expression within the time constrained intraoperative setting for the purpose of enhancing bone regeneration.

In summary, establishing the regenerative potential of acellular ECM biomaterial designs will help elucidate the additional benefits of incorporating either SCBTs or other purified inductive and conductive biomolecules into intraoperative manufacturing strategies for bone tissue engineering. Regardless of these future outcomes, it is critical for these intraoperative designs to maximize implant efficacy while at the same time reducing cost, time, and complexity of the surgical procedure compared to current standards of treatment.

4. DISCUSSION : Converging Framework of EC Ossification in the Future of Bone Regeneration

EC ossification, a process which naturally occurs in almost all bone healing events[65-73], can be utilized to enhance bone regeneration for nearly any orthopedic indication, especially in avascular critical-sized defects where hypoxic conditions favor chondrogenesis instead of direct IM ossification. The native EC ossification response, however, remains insufficient in regenerating critical-sized defects without intervention but can potentially be enhanced by combining *in vivo* developmental engineering strategies with biomimetic ECM biomaterials. Evidence to support this claim of utility reside in two evolving arenas of bone tissue engineering: 1) *in vitro* primed chondrogenic constructs (Tables 2-4) and 2) native DBM allografts and xenografts.[85-91] Both strategies have been shown to elicit EC ossification in heterotopic animal models and more importantly regenerate critical-sized defects in bone which originated during fetal development from EC ossification (e.g., femur) and IM ossification (e.g., cranium). This latter evidence gives credence to the potential versatility of strategies enhancing EC ossification for a vast array of clinical orthopedic indications.

Currently, however, both *in vitro* priming and DBM strategies face formidable technical, business, and regulatory challenges that limit their feasibility as commercially competitive alternatives to the standard of treatment, ABG. While the former approach remains tethered to burdensome, costly, and commercially inhibitive *in vitro* cell expansion protocols, the latter may elicit an insufficient EC ossification response due to its primarily osteoinductive and osteoconductive ECM cues, which instead favor IM ossification.

Additionally, regulatory challenges exist for both strategies.[173] The *in* vitro expansion of autologous stem cells inherently involves a high level of manufacturing risk that must meet stringent quality assurance and control for approval by the U.S. Food and Drug Association (FDA)[173], potentially resulting in an expensive pre-market approval (PMA) process for each orthopedic indication. Furthermore, off-site facilities may be required to expand cells, which add to the associated risks involved in maintaining viability and preventing contamination of cells. Meanwhile, native ECM biomaterials also face regulatory approval challenges outlined by the FDA and American Association of Tissue Banks (AATB).[5] Allogeneic tissue (e.g., DBM or DCC) by itself is not considered a medical device by the FDA unless it is combined with a carrier material, such as hyaluronic acid (e.g., DBX®; MTF/Synthes), in which case it must go through 510(k) approval. Instead, these materials (e.g., Puros® DBM; Zimmer) are categorized under the heading of human cells, tissues, and cellular and tissue based products (HCT/P). However, the majority of orthopedic DBM products have undergone 510(k) approval by the FDA.[5] Based on this knowledge of the regulatory landscape surrounding these strategies, it is evident that acellular ECM biomaterials face fewer challenges than SBCT strategies for approval and therefore may represent the more favorable route to clinical translation.

An alternative, and underexplored, developmental engineering strategy integrates the advantages of these two EC ossification approaches with a new class of ECM biomaterials that instead resemble the early fibrocartilaginous bone healing microenvironment and may enhance the EC ossification response from damaged host tissue. The primary native ECM candidates proposed to potentially elicit such a response are decellularized biomaterials originating from articular, fibrocartilaginous, or hypertrophic cartilage sources. These tissues inherently possess relevant chondroconductive and chondroinductive biomolecules that may potentially modulate EC

ossification within an implant. Additionally, decellularized ECM constructs may reduce or remove the need for time and cost consuming *in vitro* cell expansion protocols, expanding the developmental engineering paradigm[81, 82] to include *in vivo* design strategies. Likewise, the FDA regulatory approval associated with this new class of ECM biomaterials may possibly avoid the more costly and time consuming PMA process and instead follow a less stringent 510(k) approval process due to its similarity to existing commercially available DBM products.

Although significant focus was given to acellular ECM strategies, critical perspectives on SCBTs were also discussed. While the reviewed chondrogenic priming studies collectively concluded that *in vitro* stimulation was a necessary step to elicit EC ossification, contradicting evidence with acellular DBM implants suggests that the inclusion and priming of stem cells is not a requirement and may be obviated with the proper inclusion of native ECM components.[85-91] Regardless of this contradiction, SCBT strategies provided evidence that modulating hypertrophic signals in bone regenerative implants may lead to a significant enhancement of EC ossification (Table 3.2-3.4). Furthermore, SCBTs provide additional chondrogenic and osteogenic potential within implants compared to acellular ECM biomaterials that alternatively rely upon stem cell recruitment from surrounding host tissue. It is not clear if current orthopedic products in the pre-clinical and clinical development phase utilize *in vitro* expansion strategies, but according to Jaklenec *et al.*[75], a majority of SCBTs across the entire area of tissue engineering and regenerative medicine favor autologous cells (59%) compared to allogeneic (39%) and xenogeneic (2%) cell sources. This indicates the industry's growing interest in developing SCBTs, but it should be emphasized that regulatory approval is not a guarantee of commercial success. Intraoperative SCBT strategies may address these concerns by reducing or removing the burden of *in vitro* cell expansion without compromising the chondrogenic and osteogenic potential of incorporated stem

cells, thus furthering the bone regenerative potential of ECM implants along with overall commercial feasibility.

In summary, native ECM biomaterials inherently possessing ideal conductive, inductive, and mechanical properties have yet to be considered with respect to EC ossification and developmental engineering principles in general. A variety of ECM biomaterial criteria have been reviewed here, which are promising for regenerative investigations spanning bone, cartilage, and osteochondral defects. In the future, *in vivo* comparisons will be necessary to provide substantial evidence that native ECM biomaterials mimicking aspects of the reparative procallus microenvironment will provide superior performance compared to traditional tissue engineering strategies and current standards of treatment.

5. LIST OF ABBREVIATIONS

AATB – American Association of Tissue Banks; ABG – Autologous Bone Grafting

AC – Articular Chondrocyte; ADSC – Adipose Derived Stem Cell; ALP – Alkaline Phosphatase; BCP – Biphasic Calcium Phosphate; BMSC – Bone Mesenchymal Stem Cell; BMP – Bone Morphogenic Protein; β-TCP – Beta Tricalcium Phosphate; DBM – Demineralized Bone Matrix; DCC – Decellularized Cartilage; ECM – Extracellular Matrix; EC – Endochondral Ossification; ESC – Embryonic Stem Cell; FDA – Food and Drug Association; HAP – Hydroxyapatite; HCT/P – Human cells, tissue and cellular and tissue based products; IM – Intramembranous Ossification; iPSC – Induced Pluripotent Stem Cell; MEF2C – Myocyte Enhancer Factor 2C; MMP – Matrix Metalloproteinase; PMA – Pre Market Approval; PRP – Platelet Rich Plasma; Runx2 – Runt Related Transcription Factor 2; SCBT – Stem Cell Based Therapeutic; SDSC –

Synovium Derived Stem Cell; SVF – Stromal Vascular Fraction; UMSC – Umbilical Cord Stem Cell; VEGF – Vascular Endothelial Growth Factor

CHAPTER 4: Hyaluronic Acid-Hydroxyapatite Colloidal Gels Combined with Micronized Native ECM Biomaterials as Potential Bone Tissue Defect Fillers

S. Connor Dennis[1, 2], Katheryn Scherich[2], Austin Childress[2], Jon Whitlow[2], Michael S. Detamore[1 ,2], Sarah L.Kieweg[1, 3], Cory J. Berkland[1, 2, 4]*

[1]Bioengineering Program, [2]Chemical and Petroleum Engineering Department, [3]Mechanical Engineering Department, [4]Pharmaceutical Chemistry Department
University of Kansas, Lawrence, KS 66047

KEYWORDS: Hydroxyapatite; Hyaluronic Acid; Colloidal Gel; Native ECM Biomaterials, Demineralized Bone Matrix; Decellularized Cartilage; Herschel-Bulkley Fluid; Tissue Defect Filler

*Corresponding author

ABSTRACT

Malleable and injectable colloidal gels can be designed to exhibit self-assembling and shear-response behavior that may facilitate minimally invasive bone tissue filling. This study demonstrated that native extracellular matrix (ECM) microparticles, specifically demineralized bone matrix (DBM) and decellularized cartilage (DCC), could be formulated as injectable viscoelastic colloidal fluids when combined with hyaluronic acid (HA) and hydroxyapatite (HAP). An array of HA-ECM microparticle suspensions and HA-HAP-ECM colloidal gels exhibited either equivalent or substantially higher storage modulus ($G' \approx$ 100-10,000 Pa), yield stress ($\tau_y \approx$ 100-1000 Pa), and viscoelastic recovery ($G'_{Recovery} \geq 87\%$) kinetics compared to control fluids. Some rheological differences were observed between respective DBM and DCC formulations, especially in HA-HAP-DBM colloids, where both G' and τ_y were significantly higher ($p < 0.01$) than corresponding DCC mixtures. However, both DBM and DCC loaded suspensions and colloidal gels represent worthwhile options for future studies involving osteo- and chondro-regeneration. To date, this represents the first attempt to form composite colloidal gels with native ECM microparticles. Overall, this study identified notable HA-ECM and HA-HAP-ECM formulations to facilitate surgical placement and implant retention in non-load bearing tissue defect applications ranging from cranial and maxillofacial reconstruction to pelvic and posterolateral spine augmentation.

1. INTRODUCTION

Self-assembling and shear-responsive biomaterials possess favorable rheological and viscoelastic properties for filling bone tissue defects.[7, 8, 63] Such materials may be designed to be injectable to facilitate minimally invasive surgery that reduces risk of infection, scar formation, patient discomfort, and possibly cost of treatment.[7, 8, 63] In addition, these malleable biomaterials may also be designed to possess viscoelastic recovery following surgical placement to ensure sufficient retention of material at the defect site. Although numerous non-setting bone pastes already exist in the orthopedic market including DBX® (MTF/Synthes), Dynagraft II (Integra Orthobiologics), Grafton® Gel (Osteotech), Puros® DBM (Zimmer), and TricOS (Baxter)[5], the majority of these products contain suspended microparticles within a viscous carrier fluid. These microparticle formulations can be prone to exhibit undesirable phase-separation upon injection (e.g., filter-pressing) and following placement in the tissue defect (e.g., sedimentation)[4, 27], leading to poor retention at the defect site.[28] In addition, some ceramic microparticles have also displayed poor resorption kinetics *in vivo*, leading to their undesired persistence in the defect and delaying bone healing.[174]

Meanwhile, malleable colloidal gels comprised exclusively of nanoparticles have been identified as promising viscoelastic fluids for facilitating both surgical placement and wound site retention (Chapter 2).[10, 11, 175] The macroscopic rheological properties of these materials rely on the cohesive strength of physical crosslinking, which depend on electrostatic forces, van der Waals attraction, and steric hindrance in the microstructure.[8, 11, 12, 175] As a result, self-assembling and shear-responsive colloidal fluids may be designed to yield or flow in response to variations in external stress (i.e., injection) and rapidly recover these properties following placement. Previous investigations have explored leveraging these interactions in nanoparticles composed of

poly(lactic-co-glycolic) acid[10, 11], gelatin[16, 19, 20], dextran[17, 18], and hydroxyapatite (HAP)[175, 176] to form cohesive colloidal gels. While colloidal nanoparticles may exhibit advantageous physical properties for implantation, their higher surface area-to-volume ratio compared to respective microparticles can also be exploited to expedite material resorption and to modulate the release of incorporated bioactive signals. Recently, nanoparticle gelatin colloids were shown to enhance rheological properties and prolong delivery of bioactive molecules compared to corresponding microparticle gels both *in vitro* and *in vivo*.[19, 20] While loading and release of bioactive growth factors has been a major focus of colloidal technology, a less explored area of research has focused on utilizing the bone regenerative potential of colloidal components themselves.

Shear-responsive HAP formulations represent an intriguing sub-category within colloidal fluid designs since this biomolecule closely resembles biological apatite nanoparticles found in native bone extracellular matrix (ECM).[21, 22] Recently, it was shown that the rheology of pure HAP colloidal gels could be modulated with the addition of native glycosaminoglycan (GAG) polymers, including hyaluronic acid (HA), to elicit varying degrees of consistency, flow behavior, and viscoelastic recovery without compromising the material's inherent yield stress (Chapter 2).[175] These polymer-particle colloidal gels exhibited synergistic bulk fluid properties likely due to physical crosslinking and bridging flocculation, where multivalent GAG polyanions adsorbed simultaneously to multiple HAP particles in close proximity. Furthermore, these GAG-HAP composites represented the first attempt to exclusively combine native biomolecules in a colloidal system for tissue defect filling.

Native ECM biomaterials have been a key protagonist in the area of bone regeneration since they possess both conductive and inductive signaling moieties that are difficult to match with synthetic scaffold designs.[76-80] Demineralized bone matrix (DBM) from allogeneic sources

remains one of the most utilized native ECM biomaterials for bone regeneration[5] since it resembles portions of the complex composition and structure of healthy bone.[65-67, 69, 70] DBM's osteogenic potential has previously been correlated to the relevant concentration of bone morphogenic proteins (BMPs).[5, 71] However, recent evidence has shown that the structural components of native ECM also provide regulatory control on signaling activity of soluble growth factors and modulate cell adhesion, proliferation, differentiation, and migration.[80, 104] Therefore, the coupling of DBM microparticles within a colloidal fluid carrier, such as GAG-HAP, may act to enhance both the physical (e.g., rheological) and chemical (e.g., osteoinductive) properties of traditional bone pastes.

An alternative native ECM biomaterial strategy has also recently emerged which relies upon mimicking the processes of developmental skeletogenesis involved in native bone healing (Chapter 3).[177] While traditional ECM biomaterials such as DBM implants aim to mimic the composition of healthy bone, it is well understood that the fracture space undergoes extensive spatiotemporal ECM changes before bone can be formed.[65-67, 69, 70] More specifically, a fibrocartilaginous ECM is generated primarily through the process of endochondral (EC) ossification, where cartilage precursor tissue is formed prior to bone, as opposed to direct bone formation by intramembranous (IM) ossification.[65-67, 69, 70] While DBM has been shown to elicit both EC and IM ossification in critical-sized defect models[85-88], DBM implants may elicit a limited bone regenerative response compared to ECM biomaterials mimicking the early inflammatory and intermediate fibrocartilaginous ECM observed of fracture repair, commonly referred to as the procallus or soft callus.[65-67, 69, 70]

To address this underexplored area of bone regeneration, decellularized cartilage (DCC) has been proposed as a possible procallus ECM biomimetic.[177] DCC has emerged as an ECM

biomaterial rich in both chondroinductive and chondroconductive potential.[77, 79, 80] Current commercially available products utilizing articular cartilage and/or DCC include Biocartilage® (Arthrex), De Novo NT® and ET® Live Graft (Zimmer), and Chondrofix® (Zimmer). However, all of these products use cartilage ECM for the sole purpose of regenerating cartilage tissue. Exploring DCC's potential for modulating and enhancing EC ossification remains underexplored. However, recent evidence from our group suggests that DCC may stimulate bone mesenchymal stem cells (BMSCs) to differentiate into hypertrophic chondrocytes [unpublished], a necessary intermediate step in the EC ossification pathway. Thus, the incorporation of DCC microparticles with existing H-B fluid formulations may be a worthwhile scaffolding strategy to address bone regeneration in critical-sized non-load bearing defects.

In the current study, rheological and viscoelastic performance was assessed in HA-HAP colloidal gels combined with micronized native ECM biomaterials. This builds upon previous work that mapped and identified GAG-HAP colloidal gel candidates with promising yield stress, consistency, flow behavior and recovery properties to explore surgical delivery into non-load bearing bone defects (Chapter 2).[175] However, the HA used in these previous studies only consisted of relatively small molecular weight polymers (20-41 kDa). Since HA is available across a large range of molecular weights (MW = 10-1000s kDa), there may be rheological advantages of using higher MW polymers in colloidal gels. Initial results in the current study highlighted the effect of HA polymer molecular weight (35-1500 kDa) on the resulting fluid parameters in HA-HAP colloidal formulations. It was hypothesized that at a given concentration higher molecular weight HA formulations could produce superior rheological and viscoelastic performance compared to lower molecular weight HA.

Additionally, this study represents the first attempt to form colloidal gel composites with incorporated native ECM microparticles. More specifically, this study aims to elucidate the relationship between bulk fluid properties and relative HA polymer, HAP nanoparticle, and ECM microparticle composition. While the addition of ECM microparticles may in the future prove to enhance the osteo-regenerative capability of HA-HAP colloids, it was hypothesized that the addition of ECM microparticles would disrupt the existing colloidal interactions between HA and HAP, leading to inferior rheological and viscoelastic performance. Despite this potential weakening of the colloidal network, the primary goal of this assessment was to identify worthwhile colloidal ECM composites for future investigation in bone defect regeneration applications.

2. EXPERIMENTAL

2.1.Colloidal Materials

Hydroxyapatite was purchased as a powder ($D_{avg} \leq 200$ nm (BET Analysis); Sigma-Aldrich). Hyaluronic acid at various molecular weights (M_w = 21-40 kDa, M_w = 351-600 kDa, M_w = 1200-1800 kDa) (Lifecore Biomedical; Chaska, MN) was purchased as a sodium salt.

2.2.Demineralized Bone Matrix and Decellularized Cartilage Procurement

Human demineralized bone matrix was procured as a course ground powder (Biomet, Irvine, CA). DBM particles were cryo-ground into a fine powder with a freezer-mill (SPEX, SamplePrep, Metuchen, NJ), and particles were sieved (Spectra/Mesh Woven Filters, Spectrum Laboratories, Inc., Rancho Dominguez, CA) to exclude particles measuring above 350 μm to facilitate subsequent rheometer experiments.

Decellularized cartilage procured from porcine knee and hip joints was purchased from a local abattoir following sacrifice (120 kg, mixed breed, mixed gender) (Bichelmeyer Meats, Kansas

City, KS). Articular cartilage from both the knee and hip joints was carefully removed and collected using scalpels. The cartilage was rinsed in phosphate buffered saline (PBS) and stored at -20°C. Following freezing, the cartilage was coarsely ground using a cryogenic tissue grinder (BioSpec Products, Bartlesville, OK). The coarsely ground tissue was packaged into dialysis tubing (3500 MWCO) packets for decellularization.

An adapted version of our previously established cartilage decellularization method was used which included reciprocating osmotic shock, detergent, and enzymatic washes.[178] Reagents were purchased from Sigma-Aldrich (St. Louis, MO) unless otherwise noted. All steps of decellularization were carried out under agitation (200 rpm) at 21°C unless otherwise noted. First, the cartilage packets were placed in hypertonic salt solution (HSS) overnight to disrupt membranes and lyse the cells. Following HSS treatment, the tissue was subjected to 2 cycles of reciprocating triton-X 100 (0.05% v/v) and HSS treatments to further breakdown cellular membranes. The tissue was then treated with benzonase (0.0625 KU ml^{-1}) overnight at 37°C to fragment nucleic acids. Sodium-lauroyl sarcosine (NLS, 1% v/v) was then used overnight to further solubilize and remove cells. Next, the tissue was washed with 40% ethanol, followed with organic exchange resins to remove all organic solvents. Lastly, the tissue was removed from the dialysis tubing packages and rinsed with deionized water before freezing.

After decellularization, the tissue was lyophilized for 48 hours and cryo-ground into a fine powder with a freezer-mill (SPEX SamplePrep, Metuchen, NJ). Particles were sieved (Spectra/Mesh Woven Filters, Spectrum Laboratories, Inc., Rancho Dominguez, CA) to exclude particles measuring above 350 μm. Size measurements of micronized DCC and DBM particles were taken via scanning electron microscopy (Carl Zeiss Leo 1550 Field Emission SEM).

2.3.Preparation of Colloidal Gels

HA polymers were combined with HAP nanoparticles according to our previously published protocols in PBS solution (pH = 7.4, 150 mM NaCl).[175] HA concentrations were varied between 0-15%, 0-5%, and 0-2% (w/v) in colloidal mixtures containing 35 kDa, 350 kDa and 1500 kDa HA polymers, respectively. HA:HAP weight ratio (w:w) was controlled by the incremental addition of HAP particles to HA solutions. These mixtures were compared to pure component controls (HA and HAP), respectively. Overall volume fraction of HAP ($\Phi_{HAP} = V_{HAP}/V_{TOTAL}$) was calculated from particle density and resulting mixture volume measurements. Additional sizing and zeta-potential measurements of HAP nanoparticles in the presence of HA polymers at various molecular weights (35, 350, and 1500 kDa) were conducted using dynamic light scattering (Brookhaven; ZetaPALS) to analyze colloidal particle-polymer interactions.

Lyophilized DBM and DCC microparticles were formulated as HA-ECM suspensions and HA-HAP-ECM colloids to elucidate the effect of ECM on rheological and viscoelastic properties (Table 4.1 and Table 4.2). This was achieved by maintaining constant media volume (1 ml), HA concentration (1-2% w/v) and HAP volume fraction (Φ_{HAP} = 30-32%) in the tested fluids. The incremental incorporation of ECM was varied in terms of dry mass fraction (w_{DCC} = 3-9% and w_{DBM} = 3-28%) and in terms of volume fraction (Φ_{DCC} = 15-45% and Φ_{DBM} = 5-45%). ECM volume fraction was estimated from measured water content and density of respective particles following hydration. ECM hydration was assumed to be 100% in all formulations. In reality, the incorporated HA polymers likely exhibit some amount of osmotic pressure on nearby ECM particles, leading to a hydration equilibrium state slightly below 100%. Although the dynamics of this equilibrium were not characterized in this study, the amount of incorporated media was well above the hydration limit of DCC and DBM. At this limit, it could be assumed that all available

media in the formulation would reside within ECM particles, leaving no free media to solubilize the carrier fluid. Homogeneous suspensions and colloid mixtures were prepared by manual stirring (5 min) at ambient conditions and stored at 4°C. Samples were allowed to equilibrate to ambient conditions (2 hr) before testing.

2.4.Swelling Characterization

Relative swelling ratios (*S*) of colloidal gels were determined by placing 1.0 mL of PBS (pH = 7.4, 150 mM NaCl) on top of 0.5 mL of material contained in a 2 mL Eppendorf tube. Tubes were then constantly agitated (24 hr, 100 rpm, 37°C) in an incubator shaker (New Brunswick Scientific; Excella E24). Swelling ratio ($S = (M_{(swollen)}-M_{(before)})/M_{(before)}$) was determined from the initial ($M_{(before)}$) and final ($M_{(swollen)}$) mass of the material as described by Holland et al.[47] The final weight was determined by removing excess PBS from tube and drying the surface of gel with evaporative paper.

2.5.Rheological and Viscoelastic Characterization

The rheological and viscoelastic properties of HA-HAP colloidal formulations (Table 4.1) consisting of 35, 350, and 1500 kDa HA were characterized using a controlled stress rheometer (TA Instrument; AR2000) and compared to an HAP colloidal control group. In addition, HA-ECM microparticle suspensions and HA-HAP-ECM colloidal gel formulations (Table 4.2) were tested for rheological and viscoelastic performance compared to respective HA (1500 kDa), HAP, and HA-HAP controls. All measurements were performed at a gap distance of 500 μm using a roughened stainless steel plate geometry (20 mm diameter) and roughened base plate to minimize slip conditions. All samples were tested at 37°C.

Viscoelastic properties and recovery kinetics following temporary disruption of the colloidal gel network were determined by measuring viscoelastic properties as described by Ozbas et al.[48]

Initially, an oscillatory stress sweep (1-10,000 Pa) was performed at a constant frequency (1 Hz) to determine several fluid properties, including storage modulus (G'), loss modulus (G''), loss angle (δ), and yield stress (τ_y) within the linear viscoelastic (LVE) region of each fluid, which is characterized by G' and G'' behaving independent of external stress or strain at a given oscillatory frequency.[57] Within the LVE, strain measured during small external oscillatory stress is controlled by rates of spontaneous rearrangements or relaxations in the fluid, and thus can be assumed to represent the resting, or quiescent, state of the fluid.[57] The upper boundary limit of the LVE region was used to approximate the yield stress, τ_y [Pa], in the material.[179, 180] To ensure internal consistency in estimating this boundary limit, τ_y was calculated from the external oscillatory stress corresponding to a 10% reduction in G' averaged within the fluid's LVE region. Above the LVE, stress induced deformations cause temporarily disruptions in the fluid microstructure. Subsequent gel recovery time sweeps were conducted as four alternating rounds of intense oscillatory disruption above the LVE region (30 s, 1000 Pa, 1 Hz) and recovery within the LVE region (5 min, 10-25 Pa, 1 Hz) at 37°C following pre-shear (1 min, 100 s^{-1}) and equilibration (5 min). Recovery was assessed 5 minutes after disruption and expressed as a percentage ($G'_{\text{recovery}} = G'_{(\text{Final})}/G'_{(\text{Initial})} \bullet 100\%$) compared to initial G' in the mixture.

2.6. Statistical Analysis

All measurements were performed in triplicate (n = 3) and depicted as average ± standard deviation (SD) unless stated otherwise. Statistical analyses of data were performed using one-way analysis of variance (ANOVA) and Tukey's HSD was used post-hoc to compare differences between individual groups. A p-value ($p < 0.05$) was accepted as statistically significant.

3. RESULTS

3.1. Colloidal Characterization

3.1.1. DCC, DBM, and HAP Sizing

SEM was used to verify particle size of DCC, DBM, and HAP (Figure 4.1A-C). Both DCC and DBM dry powders exhibited polydisperse size (D_{avg} ≈ 10-100s μm) and heterogeneous morphology. All imaged particles appeared to be below the mesh screen size (< 350 μm), verifying effectiveness in sieving particles. HAP nanoparticles appeared to be of spherical particle morphology with polydisperse diameters near the supplier's specified value ($D_{avg} \leq 200$ nm (BET); Sigma-Aldrich); however, a small fraction of particles were observed to exceed this specification.

3.1.2. Effective Diameter and Zeta Potential

Dynamic light scattering was used to measure HAP particle size (nm) and zeta potential (mV) in the presence of solubilized 35, 350, and 1500 kDa HA. Dilute suspensions (0.167 mg/ml) of pure HAP particles were combined with HA at a 1:1 weight ratio. Both the effective diameter and zeta potential magnitude increased with HA molecular weight (Table 4.3). However, only 350 and 1500 kDa HA resulted in a significant increase in measured particle size and zeta potential ($p < 0.01$) compared to pure HAP suspensions.

3.2. Swelling Characterization

Relative swelling of HA-HAP colloidal formulations (Figure 4.2) composed of 35, 350, and 1500 kDa HA increased with a clear dependence on Φ_{HAP}. While sedimentation and swelling tolerances were initially set ($-20\% \leq S \leq 20\%$) in an attempt to identify suitable HA-HAP candidates for retention of material at a bone defect surgical site, the most desirable colloidal mixtures exhibited the least amount of swelling or sedimentation ($S \approx 0\%$). Swelling increased with increasing HA molecular weight but could be maintained within the swelling tolerances by

decreasing polymer concentration. HA-HAP formulations at all tested molecular weights appeared to minimize swelling and sedimentation at $\Phi_{HAP} \approx 0.30$. Therefore, this value was targeted in subsequent rheological and viscoelastic characterization studies.

Pure DCC and DBM water content and density upon hydration was also measured with the swelling protocol. Water content in hydrated particles was determined to be 80.5 ± 1.0% (w/w) and 39.5 ± 2.1% for DCC and DBM, respectively. The corresponding densities of hydrated DCC and DBM were 1.09 and 1.06 g/ml.

3.3. Rheological and Viscoelastic Characterization

3.3.1. HA Molecular Weight Studies

3.3.1.1. Storage Modulus (G') and Loss Angle (δ)

Measuring shear strain in response to an increasing external oscillatory shear stress allowed for quantification of relevant viscoelastic properties, including G', G'', δ, and τ_y, within and above the LVE region of tested HA-HAP fluids with varying HA molecular weight (Table 4.1). The presence of either HA or HAP resulted in measurable G' and G'', indicating that all tested fluids resided within the viscoelastic spectrum (Figure 4.3). A significant increase in G' was observed when HAP was added to pure HA solutions, regardless of polymer molecular weight, to form HA-HAP colloidal gels. Furthermore, there was a significant increase ($p < 0.01$) in G' for HA(350)-HAP and HA(1500)-HAP colloids compared to the pure HAP control fluid. This increase in G' appeared to be combinatorial for these colloids, where $G'_{HA\text{-}HAP} >> G'_{HA} + G'_{HAP}$. The measured δ in HA-HAP colloids was 18°, 12°, and 13° for HA 35, 350, and 1500 kDa formulations, respectively. These values were more similar to the loss angle of pure HAP ($\delta = 7°$) than respective pure HA solutions, 89°, 78° and 37°.

3.3.1.2. Yield Stress (τ_y)

Yield stress (Figure 4.3) in each tested fluid was approximated at the upper boundary limit of the LVE region obtained from the stress sweep profile. Measureable τ_y amongst pure HA solutions was only observed in 1500 kDa HA at 1% w/v. All tested formulations with HAP had a measureable τ_y. In the 1500 kDa HA-HAP colloid where both pure HA and pure HAP controls possessed independent τ_y values, the resulting colloidal τ_y appeared to be an additive property of the fluid, such that $\tau_{y\,(\text{HA-HAP})} \approx \tau_{y\,(\text{HA})} + \tau_{y\,(\text{HAP})}$.

3.3.1.3. Viscoelastic Recovery ($G'_{Recovery}$ and $\delta_{Recovery}$)

Following intense oscillatory disruption of the fluid microstructure, all tested colloids exhibited near complete recovery of G' ($\geq$ 98%) within 5 minutes (Figure 4.4C). Repeated disruption did not affect the ability of these colloids to recover their resting viscoelastic properties (Figure 4.4A). All tested colloidal formulations displayed a shift toward more viscous behavior during disruption ($\delta_{Disruption} \rightarrow 90°$), and likewise exhibited a shift toward more elastic behavior during recovery ($\delta_{Recovery} \rightarrow 0°$) (Figure 4.4B).

3.3.2. HA-ECM and HA-HAP-ECM Viscoelastic Studies

3.3.2.1. Storage Modulus (G') and Loss Angle (δ)

Based on the HA molecular weight rheological results in HA-HAP colloids, 1500 kDa HA was chosen for subsequent use in HA-ECM and HA-HAP-ECM studies (Table 4.2). A significant increase in G' was observed ($p < 0.01$) upon addition of DCC and DBM in HA-ECM microparticle suspensions (Figure 4.5). G' increased with increasing ECM concentration in the suspension. While there was no significant difference between HA-DCC and HA-DBM formulations with regard to ECM mass fraction, HA-DBM exhibited significantly higher G' than corresponding HA-DCC ($p < 0.01$) at $\Phi_{ECM} = 0.30$ and 0.45. No ECM concentration trend was observed in G' of HA-

HAP-ECM colloids. However, all HA-HAP-DBM formulations exhibited significantly higher G' values than both HAP ($p < 0.01$) and HA-HAP ($p < 0.05$) controls as well as corresponding HA-HAP-DCC formulations ($p < 0.05$). HA-HAP-DCC colloids did not have significantly different G' values compared to HA-HAP, but they did exhibit significantly higher G' than the HAP control. Above $\Phi_{DBM} = 0.30$, HA-HAP-DBM colloids appeared to incompletely hydrate during reconstitution and fractured upon mixing. Consequently, these samples could not be tested on the rheometer.

While the addition of DCC microparticles to HA suspensions and HA-HAP colloids did not significantly change δ values, DBM microparticles exhibited significantly more elastic behavior than respective HA ($p < 0.01$) control. DBM formulations also resulted in more elastic behavior than corresponding DCC suspensions ($p < 0.01$) and colloids ($p < 0.01$) at a given mass and volume fraction. However, both HAP and HA-HAP were observed to have similar elastic behavior to HA-HAP-DBM formulations.

3.3.2.2. Yield Stress (τ_y)

While measureable τ_y was observed in all formulations tested (Figure 4.5), no significant differences were observed when DCC or DBM was added to HA suspensions, except at $\Phi_{DBM} = 0.45$ ($p < 0.01$). HA-HAP-DCC colloids only showed a significant increase in τ_y at the highest tested volume fraction of DCC ($\Phi_{DCC} = 0.45$) compared to HA, HAP, and HA-HAP controls ($p < 0.01$). Furthermore, increasing DCC concentration in the colloid appeared to result in an increased τ_y. This trend was not observed in HA-HAP-DBM colloids, where increasing DBM concentration in the colloid resulted in a decreased τ_y. However, all tested HA-HAP-DBM colloids exhibited significantly higher τ_y than HA, HAP, and HA-HAP controls ($p < 0.01$).

3.3.2.3. Viscoelastic Recovery ($G'_{Recovery}$ and $\delta_{Recovery}$)

All tested HA-ECM and HA-HAP-ECM fluids and corresponding controls exhibited near complete recovery of G' ($\geq$ 87%) within 5 minutes (Figure 4.6C). Recovery experiments with DCC and DBM were only run at an equivalent volume fractions (Φ_{ECM} = 0.15) since few differences were observed in previous ECM viscoelastic stress sweep profiles. Similar to HA-HAP molecular weight studies, repeated disruption of HA-ECM and HA-HAP-ECM did not affect the ability of these fluids to recover their resting viscoelastic properties (Figure 4.6A). All tested colloidal formulations displayed a shift toward more viscous behavior during disruption ($\delta_{Disruption} \rightarrow 90°$), and likewise exhibited a shift toward more elastic behavior during recovery ($\delta_{Recovery} \rightarrow 0°$) (Figure 4.6B).

3.3.2.4. Needle and Syringe Fluid Extrusion Study

All tested formulations from the viscoelastic recovery study above were subsequently tested for injectability. All fluids were successfully loaded into 1 ml syringes and readily extruded through attached 18-gauge needles (Figure 4.7A). Qualitatively, only HA-HAP and HA-HAP-ECM colloids appeared to exhibit substantial shape retention following extrusion, while HA, HAP, and HA-ECM suspensions appeared to exhibit primarily viscous behavior (Figure 4.7A). Furthermore, only HA-HAP and HA-HAP-ECM could be subsequently molded into shapes following extrusion (Figure 4.7B) and maintain shape in ambient conditions following handling (Figure 4.7C).

4. DISCUSSION

The effects of molecular weight on polymer solution rheology and viscoelasticity has been thoroughly characterized. [37-40] At non-dilute concentrations, these solutions exhibit complex, non-

Newtonian behavior due to increased intermolecular entanglements and self-associations of polymer chains in the solution.[37-40] Highly viscous and shear-thinning HA solutions of varying molecular weight and concentration have been studied for biomedical applications such as synovial fluid supplements and as inert carrier fluids in tissue engineered scaffolds.[5, 181, 182] More recently, our group studied the effects of HA (35 kDa) in HAP colloidal gels for tissue defect filling.[175] Rheological and light scattering data from these studies supported the hypothesis that multivalent HA polymers adsorbed to surrounding HAP nanoparticles forming 'bridging' flocculations within the polymer-particle colloidal network. This interaction led to a combinatorial increase in corresponding bulk fluid rheology, which was mapped across an extensive array of concentrations and particle-polymer ratios to fit potential tissue filling parameters.[175]

Initial light scattering experiments in the current study showed similar polymer-particle colloidal interactions exist with higher molecular weight HA (350 and 1500 kDa) formulations. The inclusion of HA (350 and 1500 kDa) at dilute HAP concentrations significantly increased overall effective diameter and zeta potential ($p < 0.01$) of HAP particles (Table 4.3) compared to HA 35 kDa and pure HAP control. While increased zeta potential at dilute concentrations may translate to increased attractive strength of bridging flocculations at high colloidal concentrations, the resultant increase in particle diameter may act to inhibit particle flocculation via steric repulsion[183, 184] and compromise beneficial particle-polymer interactions seen with higher molecular weight HA. While strengthening inter-particle attraction would hypothetically lead to increased elastic behavior in tested viscoelastic colloidal fluids, characterized by a higher G' and τ_y along with lower δ, increasing steric repulsion between particles would likely lead to an opposing viscous shift.

Evidence from swelling (Figure 4.2) revealed that even at lower HA concentrations, the higher molecular weight HA polymers (350 and 1500 kDa) in HA-HAP formulations exhibited similar sample spanning flocculation networks compared to HA(35 kDa)-HAP. Furthermore, corresponding viscoelastic studies (Figure 4.3 and 4.4) with these gels showed that higher molecular weight HA formulations led to a significant increase in elastic behavior compared to HA(35 kDa)-HAP. Collectively, this evidence supports the hypothesis that higher molecular weight HA strengthens the resulting bridging flocculations in HA-HAP colloids. While some steric repulsive effects may have been present, their contribution to the resulting bulk rheological properties was not observed and may have been outweighed by attractive polymer-particle interactions.

Ultimately, these molecular weight studies showed that less HA was needed at 350 and 1500 kDa to achieve equivalent rheological properties in HA-HAP colloids relevant for surgical delivery. The advantages of using 350 and 1500 kDa HA compared to lower molecular weight formulations are (i) the potential to achieve wider ranges of rheological properties for surgical applications and (ii) lower material requirements, which lead to smaller increases in osmolality of the colloid due to the addition of HA polyelectrolytes and associated sodium ions in solution. Because of these advantages, HA 1500 kDa was chosen for subsequent studies with ECM suspensions and colloids.

Micronized DBM particles have been used extensively in bone tissue engineering applications.[5] While DBM has often been formulated with inert polymer carrier fluids such as HA and glycerol, combining these particles with colloidal fluids has to date remained underexplored. Microparticles suspended in viscous media do not remain in suspension like colloidal nanoparticles undergoing Brownian motion.[8, 12] This leads to phase separation and heterogeneity

over time. As a result, microparticle suspensions must be formulated near or above a critical concentration, the percolation threshold (Φ_p), such that particles are suppressed by the crowding or caging effect of neighboring particles and exhibit a randomly packed continuous network that spans the sample volume.[185] While pure spheres have a geometric Φ_p threshold around 0.29, ellipsoids of various aspect ratios have lower thresholds. SEM images of micronized DCC and DBM (Figure 4.1) revealed slight ellipsoid morphology that could be approximated as having aspect ratios between 1/3 and 3. The corresponding Φ_p values for these morphologies were reported to be around 0.22.[185]

HA-ECM suspensions and HA-HAP-ECM colloids were formulated to elucidate the effect of ECM, near Φ_P, on rheological and viscoelastic properties during rest and during microstructure disruption. Because DCC and DBM exhibit different water contents and densities upon hydration, the effect of ECM on bulk fluid properties could be directly compared in terms of both mass and volume fraction (Table 4.1 and Table 4.2). It was hypothesized that the addition of ECM microparticles would effectively disrupt the continuity of the respective carrier fluid because shear stress experienced locally by a polymer confined between particles can be much larger than the bulk external shear stress[57, 186], leading to inferior viscoelastic properties compared to HA, HAP, and HA-HAP controls. The evidence collected in these viscoelastic studies, however, did not support this phenomenon. Almost all tested HA-ECM and HA-HAP-ECM fluids exhibited equivalent or increased G' and τ_y values compared to respective HA, HAP, and HA-HAP controls (Figure 4.5).

A potential explanation of this result might be related to the hydration of the incorporated ECM microparticles. As these particles hydrate in the suspending HA solution or HA-HAP colloid, available aqueous media becomes scarcer and carrier fluid concentration increases. This

concentrating effect may counteract and outweigh the overall destabilizing contributions caused by stress localization of ECM microparticles. Although carrier fluid thickening may have occurred in both the microparticle suspensions and the colloidal gel formulations, the only identifiable trend was observed in the HA-ECM microparticle suspensions, where G' increased with increasing ECM concentration (Figure 4.5). ECM concentration dependency was not observed in HA-HAP colloidal formulations, suggesting that competing fluid phenomenon could be occurring in these gels. This could be due to the fact that the total volume fraction ($\Phi_{Total} = \Phi_{HAP} + \Phi_{ECM}$) of these colloids resided well above (Φ_{Total} = 0.36-0.75) the estimated percolation threshold ($\Phi_p \approx$ 0.22-0.29). At these high concentrations, localized stress experienced the colloidal fluid may become significant compared to the concentrating effect of the ECM microparticles, leading to complex viscoelastic behavior.

In general, it was also observed that DBM suspensions and colloids exhibited higher G' and τ_y values than corresponding DCC formulations on both a mass and volume fraction basis (Figures 5 and 6). Not all differences were shown to be significant, especially in HA-ECM suspensions where a significant increase in both G' and τ_y was only observed at the highest ECM volume fraction (Φ_{ECM} = 0.45) ($p < 0.01$). However, HA-HAP-DBM colloids exhibited significantly higher G' and τ_y than all mass fraction equivalent DCC colloidal formulations ($p < 0.01$). Some of these observed viscoelastic differences between DBM and DCC formulations could have been attributed to deviations in sample preparation, including fluid component heterogeneity and shear-history. During mixing and reconstitution, samples could have experienced a broad range of shear stresses, and strongly flocculated colloids have been shown to be extremely dependent on shear-history.[187, 188] Subsequent recovery studies, however, highlighted the fact that these gels recover viscoelastic properties very rapidly following microstructure breakdown. Allowing these samples to

equilibrate for multiple hours before testing ensured that shear-history effects were minimized. Heterogeneity of suspensions and colloids was also minimized by thoroughly mixing formulations as dry powders prior to reconstitution.

Because the effect of both mass fraction and volume fraction of respective ECM components was controlled in these formulations, differences in water content and density of hydrated DBM versus DCC were accounted for in viscoelastic studies. However, differences in ECM intra-particle properties could have affected overall viscoelastic trends. Pure DBM would likely exhibit significantly higher elastic modulus compared to DCC under compression. Although these measurements were not directly collected in the current study, referenced values for elastic modulus of DBM (130-230 MPa)[189] were several orders of magnitude higher than respective DCC values (1.9 MPa).[153] Since both HA-ECM suspensions and HA-HAP-ECM colloids were formulated near or above Φ_p, ECM particles formed a continuous disordered network throughout the sample volume, meaning differences in intra-particle elastic modulus could have played a significant role in overall bulk viscoelastic properties.

Inter-particle interactions between HAP and ECM particles may also have attributed to the differences between DBM and DCC formulations. It is possible that HAP interacted differently with DBM upon reconstitution compared to DCC since significant increases in G' and τ_y were predominately observed in colloidal gels instead of microparticle suspensions. During demineralization, DBM is stripped of biological apatite, which has dimensions on the order of several nanometers.[21, 22] The intimate association of apatite nanoparticles in healthy bone with the organic osteoid matrix, primarily collagen type 1, lead to a significant increase in the overall elastic modulus of the tissue (16-23 GPa).[189] It may be possible that HAP nanoparticles present in tested colloidal formulations associated with DBM and subsequently increased G' and τ_y. The mechanism

of this interaction may be similar to direct mineralization observed in collagen and DBM scaffolds.[68]

5. CONCLUSION

Overall, the rheological and viscoelastic properties of tested HA-ECM suspensions and HA-HAP-ECM colloids were observed to be primarily dependent on the fluid properties of the respective carrier fluid, either HA or HA-HAP. However, the addition of DCC and DBM resulted in equivalent or higher G', τ_y and $G'_{Recovery}$ values compared to control fluids, which directly contradicted our initial hypothesis. While some differences were observed between DCC loaded suspensions and colloids compared to DBM counterparts, the main finding of these studies was that HA-ECM and HA-HAP-ECM fluids could be readily formulated for potential surgical injection into tissue defects. To date, this represents the first attempt to combine native ECM microparticles with colloidal gel fluid carriers. The future work in this space will explore the osteo- and chondro- regeneration potential of both HA-ECM suspensions and HA-HAP-ECM colloids.

Furthermore, the highest HA-DBM suspension explored in this study (Φ_{DBM} = 0.45; W_{DBM} = 0.28) possessed a similar microparticle concentration compared to DBX® Paste and Putty commercial products (DBM 26% and 31% w/w) as reported by the supplier MTF/Synthes. This could be used as an external reference point for tested colloidal formulations, where significantly higher G' values were observed in HA-HAP-ECM colloids (Figure 4.5). Although higher τ_y values were observed in the HA-DBM (Φ_{DBM} = 0.45) suspension compared to tested colloidal formulations, it is possible for HA-HAP-ECM gels to be further refined by decreasing the relative amount of suspending media, leading to increases in both G' and τ_y. As such, these studies were not designed to cover a comprehensive array of all possible HA, HAP, and ECM fluid

combinations. Instead, this study served to highlight the viscoelastic contribution of ECM filled HA suspensions and HA-HAP colloidal gels. Future refining work in this space may lead to enhanced rheological and viscoelastic features that may suit a wider variety of bone defect indications including but not limited to use in cranial, oral/maxillofacial, mandibular, pelvic and posterolateral spine reconstruction.

6. LIST OF ABBREVIATIONS

BMSC – Bone Mesenchymal Stem Cell; BMP – Bone Morphogenic Protein; DBM – Demineralized Bone Matrix; DCC – Decellularized Cartilage; ECM – Extracellular Matrix; EC – Endochondral Ossification; GAG – glycosaminoglycan; HA – hyaluronic acid; HAP – Hydroxyapatite; HHS – hypertonic salt solution; IM – Intramembranous Ossification; LVE – linear viscoelastic region; PBS – phosphate buffered saline

CHAPTER 5: Preliminary *in vitro* and *in vivo* Evaluation of Native ECM Colloidal Gels for Filling Bone Tissue Defects

S. Connor Dennis[1, 2], *Michael S. Detamore*[1 ,2], *Cory J. Berkland*[1,2,3*]

[1]Bioengineering Program, [2]Chemical and Petroleum Engineering Department,
[3]Pharmaceutical Chemistry Department
University of Kansas, Lawrence, KS 66047

KEYWORDS: Hydroxyapatite; Hyaluronic Acid; Colloidal Gel; Native ECM Biomaterials, Demineralized Bone Matrix; Decellularized Cartilage; Bone Tissue Defect Filler

*Corresponding author

ABSTRACT

In vitro and *in vivo* performance of self-assembling and shear-responsive colloidal gels combined with micronized native extracellular matrix (ECM) biomaterials, specifically demineralized bone matrix (DBM) and decellularized cartilage (DCC), was assessed for potential bone regenerative properties. This builds upon previous work that characterized injectable colloidal formulations comprised of hyaluronic acid (HA), hydroxyapatite (HAP) nanoparticles, and ECM microparticles. A series of *in vitro* studies with rat mesenchymal stem cells (rBMSCs) tested cell viability and gene expression in an array of colloids combining HA, HAP, DCC, and DBM. While the incorporation of DCC in colloids resulted in a temporal gene expression profile that resembled the early stages of the endochondral (EC) ossification cascade in native bone fracture healing, the inclusion of HAP and DBM into formulations appeared to direct rBMSC differentiation down an osteogenic pathway. Colloidal formulations were then implanted in critical-sized rat calvarial defects and analyzed 8 weeks post-operation with MicroCT and histology. Despite supportive *in vitro* evidence that colloidal gels could significantly influence gene expression associated with EC ossification, incomplete regeneration of critical-sized defects was observed. Furthermore, no significant differences were observed in defects treated with colloidal gel formulations compared to the sham control. Evidence of EC ossification foci in the central region of the defect space, however, were only observed when animals were treated with colloidal gels. This may have been evidence of an enhanced EC ossification response, though notably not sufficient enough to regenerate the entire defect after 8 weeks. Overall, this study represented the first attempt to evaluate the efficacy of HA-ECM and HA-HAP-ECM colloid formulations *in vitro* and *in* vivo toward bone regeneration. Future studies will aim to reformulate colloidal gels to improve retention of implant material and enhance bone regeneration in the defect space.

1. INTRODUCTION

Addressing treatment strategies for non-load bearing bone applications is important to victims requiring cranial and maxillofacial reconstruction to pelvic and posterolateral spine augmentation. Recently, self-assembling and shear-responsive colloidal gels were formulated into complex viscoelastic fluids which possessed favorable rheological properties for filling bone tissue defects and retaining implanted material at the defect site following surgical placement (Chapter 2).[175] Furthermore, these colloidal gels were formulated exclusively from native extracellular matrix (ECM) biomaterials involved in the bone healing process including hyaluronic acid (HA), hydroxyapatite (HAP), demineralized bone matrix (DBM), and decellularized cartilage (DCC). While native ECM biomaterials have played an essential role in the area of bone regeneration[76-80], the efficacy of native ECM combined with colloidal gels remains to be determined in both *in vitro* and *in vivo* bone models.

Native ECM biomaterials have been implicated in bone regeneration strategies because they possess both conductive and inductive bioactive molecules that are difficult to reproduce with synthetic tissue engineered designs.[76-80] Historically, autologous bone grafting (ABG) has remained the gold standard of treatment in bone repair due to autologous bone tissue inherently resembling healthy and native bone ECM, which attributes to its osteoconductive, osteoinductive, and osteogenic properties.[1-3] However, concerns about ABG's associated donor site morbidity, increased risk of infection, graft resorption problems, limited handling capacity and restricted tissue availability have led to the emergence of an entire market of alternative bone grafts and tissue engineered implants.[1-3] Amongst these alternatives, allogeneic bone grafts and DBM have remained one of the most utilized native ECM biomaterials for bone regeneration since they resemble portions of the complex composition and structure of healthy bone.[5] Several non-setting

DBM paste formulations are currently commercially available for regenerating bone tissue including DBX® (MTF/Synthes), Dynagraft II (Integra Orthobiologics), Grafton® Gel (Osteotech), and Puros® DBM (Zimmer).[5] Although these formulations incorporate micronized DBM particles in a viscous carrier fluid to aid surgical delivery and retention in the defect, they can be prone to exhibit undesirable phase-separation upon injection (e.g., filter-pressing) and following placement in the tissue defect (e.g., sedimentation).[4, 27] Recent studies combining DBM in HA-HAP colloidal gels showed that rheological and viscoelastic properties of non-setting microparticle pastes could be enhanced to improve surgical delivery and material retention in a tissue defect. Prolonged retention of bioactive ECM materials in a bone defect may potentially lead to an enhanced regenerative response in the host.

Although some of DBM's osteogenic potential has been attributed its relevant concentration of inductive bone morphogenic proteins (BMPs)[5, 71], it has become increasingly evident that the structural components of native ECM also provide regulatory control on signaling activity of soluble growth factors and modulate key processes in tissue regeneration including cell adhesion, proliferation, differentiation, and migration.[80, 104] While traditional ECM biomaterials such as DBM implants aim to mimic the composition of healthy bone, it is well understood that the fracture space undergoes extensive spatiotemporal ECM changes before bone can be formed.[66, 67, 69-71] An alternative native ECM biomaterial strategy has recently emerged which relies upon mimicking the processes of developmental skeletogenesis involved in native bone healing (Chapter 3).[177] More specifically, a fibrocartilaginous ECM is generated primarily through the process of endochondral (EC) ossification, where cartilage precursor tissue is formed prior to bone, as opposed to direct bone formation by intramembranous (IM) ossification.[66, 67, 69, 70] While DBM has been shown to elicit both EC and IM ossification in critical-sized defect models[85-88], DBM

implants may elicit a limited bone regenerative response compared to ECM biomaterials mimicking the early inflammatory and intermediate fibrocartilaginous ECM observed of fracture repair, commonly referred to as the procallus or soft callus. To address this underexplored area of bone regeneration, decellularized cartilage (DCC) has been proposed as a possible procallus ECM biomimetic.[177] DCC has emerged as an ECM biomaterial rich in both chondroinductive and chondroconductive potential.[77, 79, 80] Current commercially available products utilizing articular cartilage and/or DCC include Biocartilage® (Arthrex), De Novo NT® and ET® Live Graft (Zimmer), and Chondrofix® (Zimmer). However, all of these products use cartilage ECM for the sole purpose of regenerating cartilage tissue. Exploring DCC's potential for modulating and enhancing EC ossification remains underexplored.

In the current study, the *in vitro* and *in vivo* performance of HA-HAP colloidal gels combined with micronized native ECM biomaterials was assessed for potential bone regenerative properties. This builds upon previous work that identified injectable HA-HAP-ECM colloidal gel formulations possessing similar or superior viscoelastic properties, including storage modulus (G'), yield stress (τ_y), and gel recovery ($G'_{Recovery}$), to HAP and HA-HAP control formulations. It was hypothesized that enhanced viscoelastic properties would lead to improved retention of implanted material at the defect site, possibly translating to enhanced bone regeneration. In addition to rheological enhancement, it was hypothesized that both DCC and DBM loaded colloidal gels would lead to improved bone regeneration at the defect site compared to control formulations. The primary goal of this assessment was to determine whether micronized DBM and DCC particles loaded into HA-HAP colloidal gel formulations could significantly direct bone mesenchymal stem cell (BMSC) proliferation and differentiation toward bone phenotypes *in vitro* and facilitate *in* vivo bone regeneration in rat calvaria.

2. EXPERIMENTAL

2.1. Colloidal Materials

Hydroxyapatite was purchased as a powder ($D_{avg} \leq 200$ nm (BET Analysis); Sigma-Aldrich). Hyaluronic acid at various molecular weights (M_w = 21-40 kDa, M_w = 351-600 kDa, M_w = 1200-1800 kDa) (Lifecore Biomedical; Chaska, MN) was purchased as a sodium salt.

2.2. Demineralized Bone Matrix and Decellularized Cartilage Procurement

Human demineralized bone matrix was procured as a course ground powder (Biomet, Irvine, CA). DBM particles were cryo-ground into a fine powder with a freezer-mill (SPEX, SamplePrep, Metuchen, NJ), and particles were sieved (Spectra/Mesh Woven Filters, Spectrum Laboratories, Inc., Rancho Dominguez, CA) to exclude particles measuring above 350 μm.

Decellularized cartilage procured from porcine knee and hip joints was purchased from a local abattoir following sacrifice (120 kg, mixed breed, mixed gender) (Bichelmeyer Meats, Kansas City, KS). Articular cartilage from both the knee and hip joints was carefully removed and collected using scalpels. The cartilage was rinsed in phosphate buffered saline (PBS) and stored at -20°C. Following freezing, the cartilage was coarsely ground using a cryogenic tissue grinder (BioSpec Products, Bartlesville, OK). Following this step, tissue was considered to be devitalized cartilage (DVC). The coarsely ground tissue was packaged into dialysis tubing (3500 MWCO) packets for decellularization.

An adapted version of our previously established cartilage decellularization method was used which included reciprocating osmotic shock, detergent, and enzymatic washes.[178] Reagents were purchased from Sigma-Aldrich (St. Louis, MO) unless otherwise noted. All steps of decellularization were carried out under agitation (200 rpm) at 21°C unless otherwise noted. First, the cartilage packets were placed in hypertonic salt solution (HSS) overnight to disrupt membranes

and lyse the cells. Following HSS treatment, the tissue was subjected to 2 cycles of reciprocating triton-X 100 (0.05% v/v) and HSS treatments to further breakdown cellular membranes. The tissue was then treated with benzonase (0.0625 KU ml^{-1}) overnight at 37°C to fragment nucleic acids. Sodium-lauroyl sarcosine (1% v/v) was then used overnight to further solubilize and remove cells. Next, the tissue was washed with 40% ethanol, followed with organic exchange resins to remove all organic solvents. Lastly, the tissue was removed from the dialysis tubing packages and rinsed with deionized water before freezing.

After decellularization, the tissue was lyophilized for 48 hours and cryo-ground into a fine powder with a freezer-mill (SPEX SamplePrep, Metuchen, NJ). Resulting DCC particles were sieved (Spectra/Mesh Woven Filters, Spectrum Laboratories, Inc., Rancho Dominguez, CA) to exclude particles measuring above 350 μm. Course DVC particles were also micronized with cryogrinding, which served as a positive control group for cell viability and gene expression studies.

2.3. Preparation of Colloidal Gels

HA polymers were combined with HAP nanoparticles according to our previously published protocols in PBS solution (pH = 7.4, 150 mM NaCl).[175] HA concentrations from 35, 350, and 1500 kDa batches were varied between 0-15%, 0-5%, and 0-2% (w/v) in colloidal mixtures, respectively. HA:HAP weight ratio (w:w) was controlled by the incremental addition of HAP particles to HA solutions. These mixtures were compared to pure component controls (HA and HAP), respectively. Overall volume fraction of HAP ($\Phi = V_{HAP}/V_{Mixture}$) was calculated from particle density and resulting mixture volume measurements.

Lyophilized DBM and DCC microparticles were combined with dry HA-HAP colloidal gel formulations before suspension in PBS. DCC and DBM concentrations were varied between 0-

40% (w/w) in colloidal mixtures. Homogeneous colloid mixtures were prepared by manual stirring (5 min) at ambient conditions and stored at 4°C. Samples were allowed to equilibrate to ambient conditions (2 hr) before testing.

2.4. BMSC Harvest, Expansion, and Seeding

Rat bone marrow mesenchymal stem cells (rBMSC) were harvested from the femurs of male Sprague-Dawley rats (200-250 g) following a University of Kansas approved IACUC protocol. The BMSCs were cultured in minimum essential medium (MEM) α culture medium with 10% fetal bovine serum (FBS) and 1% antibiotic-antimycotic (anti-anti) during expansion. At passage 4, the cells were suspended in MEM α culture media. In all studies, the medium was changed every 48 hours.

Initial studies identifying the effects of pure DCC on cell viability and gene expression seeded $1x10^6$ cells on 25 mg of non-sieved DCC or DVC microparticles. Results were compared to cells seeded with control expansion media (MEM α) and chondrogenic differentiation media composed of 10 ng/mL human recombinant transforming growth factor beta-3 (TGF-β_3) (PeproTech, Rocky Hill, NJ), 50 µg/mL ascorbic acid, 1% Penicillin Streptomycin, 40 µg/mL L-proline, 100 µmol sodium pyruvate, 0.1 µm dexamethasone, 1% insulin-transferrin-selenium 100X, and 1% non-essential amino acids. Cells were suspended in respective wells and centrifuged down (10,000 RPM, 5 min) to form a pellet culture.

The initial colloidal *in vitro* study aimed to identify the effects of HA, HAP, and DCC on cell viability over one week. Approximately 250 µL of reconstituted HA, HAP, HA-HAP, HA-DCC and HA-HAP-DCC fluid was placed in each well and then centrifuged (2,000 rpm, 1 min) to form a thin layer of material on the bottom of each well in 24-well non-treated culture plates. Cells were

seeded at $1x10^5$ cells/well, and samples were analyzed for attachment (Day 1) and viability (Day 7).

The subsequent three week colloidal *in vitro* study compared the effects of DCC, DBM, and HAP on cell viability and gene expression in HA-ECM and HA-HAP-ECM fluid formulations. Thin layers of fluid material were deposited into wells with the same protocol used in the initial colloidal study. Treated 24-well plates were used to ensure that control groups exhibited sufficient cell viability for RNA isolation and gene expression experiments. Cells were seeded at $1x10^6$ - cells/well, and samples were analyzed for attachment (Day 1) and viability (Day 7, 14, and 21) along with gene expression at each time point.

2.5. Cell Viability and Gene Expression Analysis

Overall cell count was determined for each group (n = 6) using previously established protocols[190] with a high sensitivity double-stranded DNA assay kit (Molecular Probes, Eugene, OR). A conversion factor of 8.5 pg DNA/cell may be used to convert DNA mass to cell number.[190] Subsequent gene expression profiles for each group (n = 5) were obtained following RNA isolation and purification from cells using the Qiagen RNeasy mini kit (Valencia, CA). All RNA samples were reverse transcribed using a high capacity cDNA reverse transcription kit (Invitrogen, Carlsbad, CA). Real-time quantitative polymerase chain reaction (RT-qPCR) was performed using a RealPlex MasterCycler (Eppendorf, Hauppauge, NY) and TaqMan gene expression assays normalizing for equal concentrations of cDNA in each sample. Rat specific commercial primers (Invitrogen, Carlsbad, CA) were used to analyze potential progression of cells through the EC ossification pathway. Collagen II (*Col2A1*), *Sox9*, and Aggrecan (*Acan*) were used as chondrogenic markers. *Runx2* and Collagen X (*Col10A1*) were used as hypertrophic cartilage markers. Collagen I (*Col1A1*) and Bone Sialoprotein (*BSP*) were used to identify bone lineage.

The $2^{-\Delta\Delta Ct}$ method was used to determine the relative expression of each gene with GAPDH used as an endogenous control.[191, 192]

2.6. Surgical Implantation of Colloidal Gels in Cranial Defects

Full thickness, critical-sized cranial defects (Diameter = 8 mm) in 7-8 week old Sprague-Dawley rats were used as the non-load bearing bone defect model in this study. The use of animals and the surgical procedures used in this study were approved by the Animal Care and Use Committee at the University of Kansas Medical Center (Kansas City, KS). All surgical procedures were performed under general anesthesia and sterile conditions. Two intersecting incisions were made centered over the mid-sagittal suture of the skull. Following removal of the cranial periosteum, a full thickness defect was produced in the parietal bone using a dental burr. The wound was carefully rinsed with normal saline to remove any bone debris in the defect, which was an important step in this procedure for evaluating the formation of new bone within the cranial bone defect. The cranial defects were filled with injectable colloidal gel formulations containing HAP, HA-HAP, HA-HAP-DCC, HA-HAP-DBM, or left untreated (sham). The wound was closed with a 5-0 nylon suture. The day of surgery was designated as day "0". Animals were sacrificed 8 weeks after surgery and operated calvarial bones were harvested for gross anatomical imaging, micro-computed tomography (MicroXCT-200, Xradia Inc., Concord, CA) and histological analysis.

2.7. Gross Anatomy and MicroCT Imaging

After 8 weeks, cranial biopsies of treated rats were dissected for imaging by careful removal of dermal tissue (superior to defect) and brain tissue (inferior to defect) near the defect space. Gross anatomical images were taken from an inferior view of the calvaria to visualize any signs of inflammation and tissue regeneration. Following dissection, MicroCT images of calvaria were

taken to assess extent of mineralization and retention of implant material in and around the defect space. Images were superior views of the defect space and were virtually rendered using two visualization modes to highlight tissue deposits in the defect: shaded surface display (SSD) and volume rendering technique (VRT). In SSD, virtual surfaces were generated from a threshold density value that was held constant across all samples. Likewise, color and transparency mapping of virtual surfaces in VRT was controlled with a density transfer function in the software (TXM3DViewer, Xradia), which was held constant across all samples.

2.8. Histology

To evaluate the cellular and ECM responses to the implants, implanted materials were retrieved with the surrounding host bone, residual periosteum, and underlying brain tissue. Tissue samples were fixed in neutral buffered 10% formalin solution (Sigma-Aldrich), decalcified in Cal-rite^{TM} solution (Thermo Scientific), embedded in paraffin, sectioned at 10 μm, and stained with either hematoxylin and eosin (H&E) or Safranin-O/Fast-green (Saf-O).

2.9. Statistical Analysis

All measurements were performed in triplicate ($n = 3$) and depicted as averages ± 95% confidence intervals unless stated otherwise. Statistical analyses of data were performed using one-way analysis of variance (ANOVA) and Tukey's HSD was used post-hoc to compare differences between individual groups. A p-value ($p < 0.05$) was accepted as statistically significant.

3. RESULTS

3.1. Characterizing *in vitro* Cell Response to Pure DCC

3.1.1. Cell Viability

A one week cell attachment (Day 1) and viability (Day 7) study comparing DCC treated cells to control media, chondrogenic media (TGF-β), and DVC showed that DCC exhibited significantly higher cell attachment than DVC ($p < 0.01$) and viability compared to control media ($p < 0.05$) and DVC ($p < 0.01$) (Figure 5.1). No significant differences were observed between DCC and TGF-β control. Overall DNA mass significantly increased ($p < 0.01$) for all treatment groups from Day 1 to Day 7 including control media ($p < 0.05$).

3.1.2. Gene Expression

Corresponding endochondral gene expression profiles of BMSCs treated with DCC were compared to control media, TGF-β control, and DVC. RT-qPCR data from Day 1, 3, and 7 was averaged ($n = 15$) for analysis (Figure 5.2). DCC exhibited significantly higher gene expression for all tested genes compared control media ($p < 0.01$) and DVC ($p < 0.01$). In addition, DCC exhibited significantly higher expression for *Acan* ($p < 0.05$), *Sox9* ($p < 0.01$), *Col2A1* ($p < 0.01$), *RunX2* ($p < 0.01$) and *Col10A1* ($p < 0.01$) compared to TGF-β with the exception being *Col1A1*. DCC, DVC, and TGF-β all exhibited significantly higher *Sox9* expression relative to *RunX2* ($p < 0.01$).

3.2. Characterizing *in vitro* Cell Response to HA-HAP and HA-HAP-DCC Colloids

3.2.1. Cell Viability

A one week cell attachment (Day 1) and viability (Day 7) study comparing the effects of HA, HAP, and DCC on rat BMSCs showed that DCC treated groups (HA-DCC and HA-HAP-DCC) exhibited significantly higher cell attachment compared to control media ($p < 0.01$), HA ($p < 0.01$),

HAP ($p < 0.01$), and HA-HAP ($p < 0.01$) (Figure 5.3). In addition, DCC treated groups exhibited significantly higher DNA mass (Day 7) compared to control media ($p < 0.05$) and HAP ($p < 0.01$). Only HA and HA-HAP treated cells exhibited significantly higher DNA mass from Day 1 to Day 7 ($p < 0.01$). All other groups exhibited statistically equivalent DNA mass over the span of the study.

3.3. Characterizing *in vitro* Cell Response to Colloids with HAP, DCC, and DBM

3.3.1. Cell Viability

A three week cell attachment (Day 1) and viability (Day 7, 14, and 21) study comparing the effects of HAP, DCC, and DBM on rat BMSCs showed that only DBM treated groups (HA-DBM and HA-HAP-DBM) exhibited DNA mass increase over the span of the study (Figure 5.4). HA-DBM treated cells exhibited a significant increase in DNA mass at Day 14 and Day 21 ($p < 0.01$) compared to initial DNA mass on Day 1. Meanwhile, DCC treated groups exhibited a significant decrease ($p < 0.01$) in DNA content over 21 days, which contradicted previous evidence of proliferation (Figure 5.3). All groups exhibited significantly DNA mass compared to cells in control media on a treated culture plate ($p < 0.01$) except for HA-DBM at Day 21 which exhibited significantly higher DNA mass ($p < 0.01$).

3.3.2. Gene Expression

Corresponding endochondral gene expression profiles of BMSCs treated with HAP, DCC, and DBM were compared to control media. Poor viability and RNA isolation from various groups over the span of the study prevented RT-qPCR data from being obtained on days 1, 7, and 21. However, sufficient data was obtained on Day 14 to compare treatment groups. HA-DCC exhibited significantly higher expression of *Sox9* and *Runx2* and significantly lower *Acan* expression compared to control media ($p < 0.01$), suggesting that cells may be undergoing intermediate

hypertrophic changes. HA-DBM exhibited significantly higher *Col1A1* ($p < 0.05$) and *BSP* ($p < 0.01$) expression compared to control media, indicating that cells might be osteogenic. The presence of HAP in both HA-HAP-DCC and HA-HAP-DBM also appeared to direct cells toward an osteogenic lineage compared to control as suggested by significantly higher *BSP* expression ($p < 0.05$) and ($p < 0.01$), respectively.

3.4. Characterizing *in vivo* Bone Regeneration to Colloids with HAP, DCC, and DBM

3.4.1. Gross Anatomy

During 8 weeks of post-operative treatment, no rats were reported to exhibit signs of inflammation at or near the calvarial defect site. After 8 weeks, gross anatomical images (Figure 5.6) of cranial biopsies were taken to visualize signs of tissue response. Proximal brain tissue appeared morphologically healthy and undisturbed by the implant materials in all treatment groups, and no accumulation of interstitial fluid was observed in or around defect site. In HAP, HA-HAP, and HA-HAP-ECM treated animals, small aggregates of white material, presumed to be HAP, were observed in and around the defect space on the superior side of the rat calvaria. Visualizing the defect space from an inferior view with backlit illumination (Figure 5.6) revealed varying levels of opacity in the defect space. While HA-HAP and HA-HAP-ECM groups appeared to exhibit less opacity than respective HA and HAP controls, variability in opacity within each treatment group was observed. The type of tissue spanning the defect space was indiscernible via gross anatomical imaging.

3.4.2. MicroCT Imaging

MicroCT images of rat calvaria were obtained to visualize retention of implant material and extent of mineralization in the defect (Figure 5.7 and Figure 5.8). An estimate of the initial defect location (dotted lines, Diameter = 8 mm) was made to aid qualitative assessment of the tissue

response. Mineralized tissue was observed growing radially inward from the defect borders in all tested groups including sham. In addition, bony spicules dispersed through the defect were observed more in HA-HAP and HA-HAP-ECM colloids than HAP and sham controls. Retention of colloidal material in the defect could be tracked with HAP, which appeared pink in MicroCT images using VRT visualization (Figure 5.8). More HAP was retained in the colloidal treatment groups containing HA compared to pure HAP. Migration of HAP outside the defect space was observed in some cases, which corresponded to the appearance of small white aggregates observed in gross anatomical imaging.

Relative differences in mineralization were assessed (Table 5.1) through scoring of MicroCT images (n = 3), as defined by Spicer *et al*.[193] HA-HAP exhibited the highest mineralization score (average ± SD) (2.67 ± 0.58) followed by HA-HAP and sham (2.33 ± 0.58). HAP and HA-HAP-DBM exhibited the lowest mineralization score (1.67 ± 0.58), but no significant differences were found between the tested groups. The presence of HAP from implanted material was not factored into defect scoring.

3.4.3. Histology

H&E and Saf-O/Fast Green histological images of rat calvarial defects revealed most bone formation directly appositional to native bone regions, but bony spicules were observed in the middle of the defect space (Figure 5.9). This corresponded to previous MicroCT observations of regionalized mineralization in the healing defect. All treatment groups including sham exhibited areas of newly ossified bone, but no relative comparisons were made with histological analysis. No evidence of cartilaginous regions, hypertrophic cartilage, or ongoing EC ossification was observed across all tested groups. However, retention of colloidal material in the defect was observed in all implant groups. In some cases, active ossification was observed directly adjacent

to implanted colloidal material. Images were sagittal cross-sections of the border between the defect space and the native bone tissue with left-to-right orientation representing inferior-to-superior direction (Figure AD). Fibrous connective tissue was observed spanning the defect space interspersed with colloidal implant material. Blood vessels were also identified in the defect space. Loose connective tissue was observed anterior to the defect space.

4. DISCUSSION

The current study utilized colloidal technology to make HA-HAP gels loaded with ECM microparticles. This was the first study to evaluate the *in vitro* cellular and genetic response of rBMSCs to various components of HA-HAP-ECM colloidal gels. In addition, this was the first study to assess potential *in vivo* bone regeneration of HA-HAP-ECM colloids in critical-sized rat calvarial defects. While micronized DBM has previously been shown to elicit bone regeneration in critical-sized defects[85-88], DCC has remained underexplored as a potential ECM biomaterial for regenerating bone despite its physical and chemical resemblance to the intermediate procallus microstructure involved in native bone fracture healing.[66, 67, 69, 70]

Initial *in vitro* studies revealed that pure DCC microparticles significantly increased rBMSC viability over one week compared to negative control ($p < 0.05$) and DVC microparticles ($p < 0.01$). Coupling this result with significant up-regulation ($p < 0.01$) of chondrogenic genes *Acan*, *Sox9*, and *Col2A1* in response to DCC treatment suggests that the novel decellularization method utilized in this study may be worthwhile for future cartilage tissue engineering endeavors. However, a significant increase in both hypertrophic cartilage markers *Runx2* and *Col10A1* was also observed in DCC treated rBMSCs compared to negative control media ($p < 0.01$), DVC ($p <$

0.01), and TGF-β positive chondrogenic media ($p < 0.01$). This result suggests that DCC may be better suited for tissue engineering applications requiring EC ossification for bone regeneration.

The relative expression of *Sox*9:*Runx2* can be used as an indicator of cartilage progression toward a hypertrophic phenotype.[93] While the former key transcription factor is involved in initial chondrogenesis, the latter is associated primarily with cartilage hypertrophy.[92, 93, 100, 137] Furthermore, a study by Hattori *et al*.[138] showed that murine *Sox9* was a major antagonistic regulator of cartilage vascularization, bone marrow formation, and EC ossification. In their study, newborn transgenic mice misexpressing *Sox9* exhibited an extreme lack of bone marrow due to retardation of vascular invasion into hypertrophic cartilage and delayed cartilage ECM remodeling. Cartilage hypertrophy is a critical maturation stage of EC ossification. Chondrocytes experience a large increase in volume (~5 to 10 fold), and downstream proteins activated by Runx2 transcription factor begin to remodel the surrounding ECM.[92, 93, 100, 137] These targets include matrix metalloproteinases (MMPs) that degrade cartilaginous ECM[65-70, 72, 73], Indian Hedgehog (Ihh) that induces proliferation of non-hypertrophic chondrocytes[92, 93, 100, 137], angiogenic factors like vascular endothelial growth factor (VEGF) to promote neo-vascularization[93, 94, 131, 136, 137] along with collagen type X, alkaline phosphatase (ALP), and matrix vesicles for ECM mineralization.[145-147]

In the current study, rBMSCs treated with DCC microparticles exhibited significantly higher expression levels of *Sox9* compared to *Runx2* ($p < 0.01$) over the first week (Figure 5.2). This ratio was reversed during the subsequent gene expression study (Day 14) where DCC was formulated as an HA-DCC suspension and HA-HAP-DCC colloid (Figure 5.5). In these studies, *Runx2* expression was significantly higher than *Sox9* when DCC was present, ($p < 0.05$) and ($p < 0.01$) respectively. This temporal shift in expression levels corresponds well with previous observations

of the spatiotemporal change in growth factors and ECM molecules involved in EC ossification and native bone healing.[66, 71] The presence of DBM in HA-DBM and HA-HAP-DBM formulations also resulted in elevated, albeit insignificant, *Runx2* expression relative to *Sox9*. Meanwhile HA-DBM and HA-HAP-DBM exhibited significantly higher *BSP* levels compared to control ($p < 0.01$), which may be an indication of osteogenic differentiation. This result corresponds with previous evidence showing that DBM can elicit both IM and EC ossification in critical-sized bone defects.[85-88] Furthermore, the temporal expression of *BSP* at Day 14 corresponds well with previous observations of the spatiotemporal change in *BSP* expression involved in native bone healing.[66, 71] A similar significant increase in *BSP* expression was observed in HA-HAP-DCC treated cells compared to control media ($p < 0.05$) and HA-DCC ($p < 0.05$) groups. Taken together, these results suggest that the presence of DCC may have directed cell differentiation down the EC ossification pathway while the presence of DBM or HAP may have directed cell differentiation down an osteogenic pathway or accelerated EC ossification into an osteogenic phase.

Meanwhile, the two cell attachment and viability studies with various HA-HAP-ECM colloids provided contradicting evidence on the suitability of DCC and nanocrystalline HAP as a compatible biomaterial with rBMSCs in the proposed application. While the preliminary one week study (Figure 5.3) provided evidence of elevated cell attachment and sustained viability in DCC and HAP treated groups, the subsequent 21-day viability study showed significant depletion of cell population in similar treated DCC and HAP groups over the course of study. The latter result was hypothesized to be attributed to the presence of undesirable excipients in HAP powder, which were introduced during the manufacturer's crystallization protocol of HAP nanoparticles, and the residual presence of decellularization reagents in the batch of DCC used for the 21-day study, which may have caused cytotoxicity in seeded rBMSCs. As a result, subsequent *in vivo* cranial

defect studies incorporated an additional dialysis step before colloids were formulated. This involved dialyzing HAP nanoparticles and DCC microparticles in PBS solution (pH = 7.4, 150 mM NaCl) for 72 hours followed by lyophilization. No evidence of necrosis or prolonged inflammation was observed *in vivo* when colloids incorporated dialyzed HAP and DCC particles. Collectively, these preliminary *in vitro* cell viability results provided limited evidence to support or reject the use of HAP or DCC in colloidal formulations. However, coupling these results with the corresponding gene expression studies showing positive signs of chondrogenic, hypertrophic, and osteogenic differentiation did provide evidence to support the hypothesis that HA-HAP-ECM colloidal formulations could influence EC ossification and potentially facilitate bone regeneration.

The rat calvarial critical-sized defect model used in the current study was chosen because its non-load bearing nature was suitable for colloidal gel implantation. In fetal development, the calvaria is formed by IM ossification rather than EC ossification[103], suggesting that only implants directed toward IM ossification will possess regenerative potential. However, evidence from Rabie *et al.* [87, 89, 90] showed that IM and EC ossification pathways can be utilized, exclusively or in combination, to regenerate critical-sized calvarial defects with DBM implants. This was supported by evidence that both IM and EC ossification occur in the native process of bone fracture healing.[66, 67, 69-71] In the current study, implantation of various colloidal gel formulations (Table 5.1) into critical-sized rat calvarial defects yielded MicroCT and histological evidence of both IM and EC ossification in the defect space (Figure 5.7, Figure 5.8, and Figure 5.9).

A primary aim of the current *in vivo* study was to assess 1) the retention of colloidal implant material and 2) the extent of bone regeneration at the defect site. With regard to the first aim, retention was qualitatively assessed by observing gross anatomy, MicroCT, and histological sections. The collective evidence from these analyses confirmed that delivered colloidal material

was retained in all tested animals to varying extents. MicroCT imaging (Figure 5.7 and Figure 5.8) especially highlighted the presence of HAP material in and around the defect site. It was clear that the presence of HA in colloidal formulations increased the retention of HAP material within the defect. However, it was also evident from these images that some colloidal material in all treatment groups was displaced around the defect in a superior orientation to the calvaria. This undesirable migration from the defect site may have been due to various operative and post-operative conditions including unintentional disruption of the material by the surgeon during wound closure, wound-site mechanical disruption by the animal during recovery, or even swelling of the exposed inferior brain tissue. Regardless, a favorable colloidal material in the future should be designed to resist migration from these external mechanical perturbations. This could possibly be accomplished by increasing concentration of colloidal components which would increase yield stress and storage modulus of the colloidal implant.

The extent of ossification in the defect space was also qualitatively assessed by observing gross anatomy, MicroCT, and histological sections. All tested animals, including the negative control sham groups, exhibited some evidence of ossification at the border of the defect. Both H&E and Saf-O/Fast-green stains revealed bone morphology at these sites without the presence of nearby cartilage tissue (Figure 5.9). This likely meant that bone formation observed at the borders of the defect were formed via IM ossification. IM ossification has previous been observed in defect spaces occurring adjacent to existing healthy bone because this pathway requires angiogenesis and permanent vasculature to occur before bone can be formed.[66, 67, 69, 70] Meanwhile, EC ossification does not require angiogenesis to occur since precursor chondrocytes can arise in lower oxygen tension environments compared to osteoblasts.[66, 67, 69, 70] This results in EC ossification occurring in the bulk of the defect space, where oxygen tension in the tissue is low due to absence of

established vasculature.[66, 67, 69, 70] In the current study, some evidence of regionalized ossification in the center of the defect space was observed with MicroCT and histological analysis. Although no cartilage tissue was identified in histological sections, active EC ossification may have ceased in the bulk of the defect space 8 weeks after implantation. This result was not desirable since full regeneration of the defect was incomplete.

Relative comparisons of the extent of bone regeneration in the defect space could be made by scoring MicroCT images (Table 5.1) according to a methodology reported by Spicer *et al*.[193] Although no significant differences were observed between tested groups, qualitatively it was evident that the colloidal formulations incorporating HA polymer exhibited more ossification in the defect. This could be due to increased retention of colloidal material at the defect site which builds upon previous work that identified injectable HA-HAP-ECM colloidal gel formulations possessing similar or superior viscoelastic properties, including G', τ_y, and $G'_{Recovery}$, compared to HAP formulations. Although this result supported our initial hypothesis, the primary goal of this assessment was to determine the efficacy of DCC and DBM in colloidal formulations. The presence of DCC and DBM did not result in a significantly higher ossification score compared to sham, HAP, or HA-HAP treatment groups. There was also no qualitative evidence that DCC or DBM contributed to active EC ossification *in vivo*, though evidence of ossification foci in the central, avascular portion of the defect space was present.

5. CONCLUSION

Despite supportive *in vitro* evidence that HA-HAP-DCC and HA-HAP-DBM colloidal gels could significantly influence gene expression associated with EC ossification and osteogenesis, incomplete regeneration of critical-sized rat calvarial defects was observed in animals treated with

colloidal implants. Furthermore, no significant differences were observed in defects treated with colloidal gel formulations compared to the negative sham control group. Evidence of ossification foci in the central region of the defect space, however, were only observed when animals were treated with colloidal gels. This may have been evidence of an enhanced EC ossification response, though notably not sufficient enough to regenerate the entire defect at 8 weeks post-implantation. This means that future HA-HAP and HA-HAP-ECM colloidal gels could be reformulated with increased viscoelastic properties, such as G' and τ_y, to increase retention of colloidal material in the tissue defect and to increase regenerative capacity of the implant. Additionally, many sources of cartilage ECM exist in the body including hyaline cartilage (e.g., femoral condyles and tibial plateau), fibrocartilage (e.g., temporomandibular joint disc and knee meniscus), elastic cartilage (e.g., nose and ear), and even hypertrophic cartilage (e.g., fetal bones and growth plates).[68] Fibrocartilage may provide an even better procallus mimetic tissue than hyaline cartilage since the procallus is fibrocartilaginous in nature. Additionally, fetal bones undergoing EC ossification during skeletogenesis may provide a primed hypertrophic cartilage template that could facilitate rapid ossification in a bone defect. Thus, there exists a range of DCC-derived tissues that may be explored in relation to EC ossification.

6. ABBREVIATIONS

ABG – Autologous Bone Grafting; Acan – Aggrecan; BMSC – Bone Mesenchymal Stem Cell; BMP – Bone Morphogenic Protein; BSP – Bone Sialoprotein; Col1A1 – Collagen Type 1; Col2A1 – Collagen Type 2; Col10A1 – Collagen Type 10; DBM – Demineralized Bone Matrix; DCC – Decellularized Cartilage; ECM – Extracellular Matrix; EC – Endochondral Ossification; FBS – Fetal Bovine Serum; GAG – glycosaminoglycan; HA – hyaluronic acid; HAP –

Hydroxyapatite; H&E – Hematoxylin and Eosin; HSS – hypertonic salt solution; IM – Intramembranous Ossification; LVE – linear viscoelastic region; MEM – Minimum Essential Medium; MicroCT – Micro Computed Tomography; PBS – phosphate buffered saline; Runx2 – Runt related transcription factor 2; RT-qPCR – reverse transcriptase quantitative polymerase chain reaction; SSD – shaded surface display; Saf-O – Safranin O; VRT – volume rendering display

CHAPTER 6: Conclusion

Predecessors to this work developed methods of creating self-assembling and shear-responsive colloidal gels from oppositely charged PLGA nanoparticles and demonstrated feasibility of the concept for tissue defect filling, controlled drug release, and *in vivo* stimulation of bone regeneration in rat calvarial defects.[10, 11] Within this thesis, colloidal gel materials were derived exclusively from native ECM components found in the bone healing environment. The majority of this work focused on the feasibility of combining these components, including HA, HAP, DCC, and DBM, to meet standards for surgical delivery and retention of material at the defect site. Pilot *in vitro* and *in vivo* studies furthermore characterized the regenerative potential of these viscoelastic materials within bone defects.

Extensive rheological and viscoelastic profiling of initial GAG-HAP colloids along with subsequent HA-ECM suspensions and HA-HAP-ECM colloids demonstrated that fluid parameters including G', τ_y, and $G'_{Recovery}$ could be readily modified by changing composition of colloidal formulations. The combination of GAG polymers and HAP particles led to a synergistic increase in both consistency index and storage modulus of fluids that was dependent on polymer concentration and molecular weight. This corresponded to changes in physical association of GAG and HAP observed during light scattering zeta potential measurements. Although GAGs increased electrostatic stability of HAP at dilute concentrations, it was hypothesized that at high concentrations, similar to those tested in rheological experiments, bridging flocculation occurred due to multivalent GAG polymers adsorbing simultaneously to multiple HAP particles in close proximity. The additional loading of ECM microparticles to HA-HAP colloidal formulations did not compromise the physical crosslinking or the viscoelastic properties of colloidal gels. Instead, all tested HA-ECM microparticle suspensions and HA-HAP-ECM colloidal gels exhibited either

equivalent or substantially higher storage modulus ($G' \approx$ 100-10,000 Pa), yield stress ($\tau_y \approx$ 100-1000 Pa), and viscoelastic recovery ($G'_{Recovery} \geq 87\%$) kinetics compared to HA, HAP, and HA-HAP control fluids. Most importantly, these colloidal formulations could be modified to facilitate injectability and retention of implant material in critical-sized bone tissue defects.

Preliminary *in vitro* evidence revealed that DCC could positively influence cell viability and direct gene expression profile of seeded rBMSCs toward hypertrophic chondrogenesis while both DBM and HAP colloidal formulations appeared to direct cell lineage down an osteogenic pathway in a temporal manner similar to expression profiles observed in native bone fracture healing.[66, 71] Meanwhile, two preliminary cell viability studies with DCC and HAP loaded colloidal gels provided conflicting evidence to support or reject their use in formulations. However, coupling these results with the corresponding gene expression studies showing positive signs of chondrogenic, hypertrophic, and osteogenic differentiation did provide evidence to support the hypothesis that HA-HAP-ECM colloidal formulations could influence EC ossification and potentially facilitate bone regeneration.

In vivo evidence revealed the presence of both EC and IM ossification foci in critical-sized calvarial defects treated with HA-HAP, HA-HAP-DCC and HA-HAP-DBM. Incomplete regeneration of the defect, however, was observed in all tested formulations 8 weeks following implantation. Furthermore, no significant differences were observed in defects treated with colloidal formulations compared to the negative sham control group. Qualitatively it was evident that the incorporation of HA into colloidal gels led to higher retention of implant material at the defect site and increased ossification, though notably not sufficient enough to regenerate the entire critical-sized defect space. Thus, definite advantages of using colloidal gel technology were

observed in these preliminary studies, but future iterations of the implant design may yield enhanced bone tissue regeneration.

The evidence presented in this thesis readily demonstrates that using native ECM colloidal gels to facilitate bone regeneration in non-load bearing calvarial defects is feasible and potentially efficacious. Improving the regenerative capacity of these injectable colloids may reside in exploring alternative native ECM sources and strategies that better resemble the bone healing microenvironment along with reformulation approaches to enhance retention of material at the defect site. Many sources of specialized cartilage ECM exist in the body that may provide a primed hypertrophic cartilage template to facilitate rapid ossification in a bone defect. Therefore, future HA-HAP and HA-HAP-ECM colloidal gels could be reformulated with enhanced regenerative capacity. The viscoelastic properties of colloidal gels, such as G' and τ_y, may also be increased by altering the physicochemical properties of individual components of the colloids. This could include modifying HAP morphology or surface chemistry along with changing GAG molecular weight. GAG polymers may also be chemically modified to possess dendritic structure or cross-linking moieties to yield desirable rheological properties for surgical delivery. Improving viscoelastic properties of colloidal formulations could improve retention of the implant at the tissue defect and ultimately improve implant efficacy. Although a wide array of colloidal gel formulations were evaluated in this thesis, there remain largely underexplored design spaces within colloidal technology that combine elements of the traditional tissue engineering triad (i.e., cells, signal, and scaffolds). The future of this scaffolding technology, however, may reside in adjacent tissue engineering applications outside of orthopedics. Self-assembling and shear-responsive colloidal gels may prove advantageous in many soft-tissue regeneration strategies. Ultimately, the idea of colloidal-based tissue implants has been taken from concept to practice, produced

promising results for the treatment of non-load bearing bone defects, and has precipitated numerous new areas of research to consider and challenges to meet.

APPENDIX A: TABLES

Table 2.1: HAP Dynamic Light Scattering data

Weight Ratio (GAG:HAP)	Size (nm)		Zeta Potential (mV)	
Pure HAP	430 ± 73		-26.3 ± 5.5	
CS:HAP (1:1)	524 ± 72		-49.5 ± 8.3	**
CS:HAP (10:1)	545 ± 113	*	-56.6 ± 6.2	**
Pure HAP	430 ± 73		-26.3 ± 5.5	
HA:HAP (1:1)	489 ± 96		-39.4 ± 7.4	**
HA:HAP (10:1)	475 ± 46		-45.8 ± 6.1	**

Significant differences between groups compared to pure HAP (ANOVA, post-hoc Tukey's HSD; $n = 15$; $p < 0.05$*; $p < 0.01$**).

Table 2.2: CS-HAP rheological properties estimated by H-B fluid model

[CS]	[HAP]		τ_y (Yield Stress) (Pa)			K (Consistency Index) (Pa-s^n)			n (Flow Behavior Index)			RMSE
(% w/v)	(% w/v)	ϕ (% v/v)	Average	±	95% CI	Average	±	95% CI	Average	±	95% CI	—
CS 10%	0%	0.0%	0.01	±	0.07	0.04	±	0.01	0.93	±	0.02	0.06
	5%	3.1%	0.05	±	0.10	0.14	±	0.01	0.86	±	0.01	0.10
	10%	6.1%	0.52	±	0.55	0.11	±	0.03	0.93	±	0.04	0.57
	20%	12.3%	0.96	±	0.61	0.24	±	0.05	0.85	±	0.03	0.61
	40%	24.6%	10.46	±	2.39	0.87	±	0.28	0.77	±	0.05	2.20
	80%	49.2%	1403.00	±	1193.00	38.34	±	52.66	0.28	±	2.84	286.60
CS 15%	0%	0.0%	-0.23	±	0.24	0.34	±	0.03	0.81	±	0.02	0.20
	7.5%	4.6%	0.24	±	0.54	0.30	±	0.04	0.86	±	0.02	0.53
	15%	9.2%	0.31	±	0.61	0.51	±	0.06	0.81	±	0.02	0.59
	30%	18.4%	2.33	±	0.72	1.52	±	0.10	0.73	±	0.01	0.63
	60%	36.9%	218.50	±	21.10	2.69	±	1.23	0.80	±	0.06	3.51
	—	—	—		—	—		—	—		—	—
CS 20%	0%	0.0%	0.13	±	0.16	0.43	±	0.02	0.85	±	0.01	0.14
	10%	6.1%	-0.65	±	0.65	1.08	±	0.07	0.78	±	0.01	0.60
	20%	12.3%	-0.72	±	0.84	2.23	±	0.13	0.71	±	0.01	0.73
	40%	24.6%	11.66	±	3.67	4.06	±	0.55	0.72	±	0.02	3.22
	80%	49.2%	1350.00	±	68.00	3.14	±	2.49	0.93	±	0.11	31.10
	—	—	—		—	—		—	—		—	—
CS 30%	0%	0.0%	0.15	±	1.48	1.34	±	0.13	0.83	±	0.01	1.44
	15%	9.2%	-2.23	±	1.27	4.02	±	0.19	0.73	±	0.01	1.11
	30%	18.4%	-2.06	±	3.67	7.97	±	0.56	0.72	±	0.01	3.18
	60%	36.9%	134.70	±	25.70	20.20	±	3.77	0.73	±	0.03	22.56
	—	—	—		—	—		—	—		—	—
	—	—	—		—	—		—	—		—	—
CS 40%	0%	0.0%	-1.86	±	1.26	3.19	±	0.13	0.80	±	0.01	1.19
	20%	12.3%	-11.56	±	8.84	10.39	±	1.37	0.71	±	0.02	7.65
	40%	24.6%	3.09	±	13.97	16.55	±	1.69	0.77	±	0.02	12.82
	80%	49.2%	958.80	±	368.20	382.40	±	205.90	0.52	±	0.10	125.80
	—	—	—		—	—		—	—		—	—
	—	—	—		—	—		—	—		—	—
CS 60%	0%	0.0%	-7.96	±	3.28	10.47	±	0.36	0.78	±	0.01	3.06
	30%	18.4%	-65.26	±	83.57	44.58	±	12.56	0.72	±	0.04	72.90
	60%	36.9%	112.60	±	47.50	199.30	±	17.20	0.68	±	0.02	24.16
	—	—	—		—	—		—	—		—	—
	—	—	—		—	—		—	—		—	—
	—	—	—		—	—		—	—		—	—
CS 80%	0%	0.0%	-81.25	±	101.09	48.17	±	18.46	0.74	±	0.06	79.21
	40%	24.6%	11.33	±	55.17	111.00	±	14.80	0.78	±	0.03	33.02
	—	—	—		—	—		—	—		—	—
	—	—	—		—	—		—	—		—	—
	—	—	—		—	—		—	—		—	—
	—	—	—		—	—		—	—		—	—

Individual points are reported (average ± 95% CI) from triplicate studies and overall model fit reported as root-mean-squared error (RMSE).

Table 2.3: HA-HAP rheological properties estimated by H-B fluid model

[HA]	[HAP]		τ_y (Yield Stress) (Pa)			K (Consistency Index) (Pa-s^n)			n (Flow Behavior Index)			RMSE
(% w/v)	(% w/v)	ϕ (% v/v)	Average	±	95% CI	Average	±	95% CI	Average	±	95% CI	—
HA 10%	0%	0.0%	0.26	±	0.21	0.11	±	0.01	0.98	±	0.02	0.21
	5%	3.1%	0.39	±	0.35	0.10	±	0.01	0.99	±	0.03	0.38
	10%	6.1%	0.52	±	0.50	0.06	±	0.01	1.05	±	0.04	0.56
	20%	12.3%	0.37	±	1.68	0.55	±	0.15	0.83	±	0.04	1.64
	40%	24.6%	7.24	±	2.94	0.85	±	0.22	0.86	±	0.04	2.94
	80%	49.2%	912.40	±	266.60	105.90	±	133.20	0.37	±	0.16	53.06
HA 15%	0%	0.0%	1.04	±	1.41	0.17	±	0.04	1.01	±	0.09	1.59
	7.5%	4.6%	1.41	±	1.31	0.34	±	0.05	1.01	±	0.02	1.43
	15%	9.2%	2.97	±	1.93	0.63	±	0.09	0.97	±	0.02	2.07
	30%	18.4%	7.41	±	0.09	2.32	±	0.09	0.87	±	0.01	1.18
	60%	36.9%	132.60	±	17.80	46.66	±	4.10	0.63	±	0.01	13.50
	—	—	—		—	—		—	—		—	—
HA 20%	0%	0.0%	1.10	±	1.44	0.49	±	0.05	1.03	±	0.01	1.59
	10%	6.1%	0.46	±	0.36	1.15	±	0.02	0.96	±	0.00	0.38
	20%	12.3%	-0.24	±	2.32	3.07	±	0.15	0.89	±	0.01	2.37
	40%	24.6%	-4.49	±	23.44	14.81	±	2.76	0.77	±	0.03	21.64
	80%	49.2%	263.00	±	521.90	759.90	±	373.10	0.39	±	0.08	113.10
	—	—	—		—	—		—	—		—	—
HA 30%	0%	0.0%	-5.02	±	6.54	3.40	±	0.32	0.95	±	0.01	6.93
	15%	9.2%	-32.50	±	44.75	12.94	±	4.32	0.81	±	0.05	43.00
	30%	18.4%	-17.48	±	28.59	22.31	±	3.69	0.82	±	0.03	24.54
	60%	36.9%	-22.98	±	111.90	234.10	±	44.40	0.65	±	0.04	53.53
	—	—	—		—	—		—	—		—	—
	—	—	—		—	—		—	—		—	—
HA 40%	0%	0.0%	-37.25	±	49.85	15.06	±	5.34	0.86	±	0.06	44.50
	20%	12.3%	-33.06	±	43.35	30.27	±	6.78	0.85	±	0.04	33.44
	40%	24.6%	-221.30	±	376.60	223.10	±	151.80	0.65	±	0.13	178.20
	—	—	—		—	—		—	—		—	—
	—	—	—		—	—		—	—		—	—
	—	—	—		—	—		—	—		—	—

Individual points are reported (Average ± 95% CI) from triplicate studies and overall model fit reported as root-mean-squared error (RMSE).

Table 2.4: Pure HAP rheological properties estimated by H-B fluid model

[HAP]		τ_y (Yield Stress) (Pa)			K (Consistency Index) (Pa-s^n)			n (Flow Behavior Index)			RMSE
(% w/v)	**ϕ (% v/v)**	Average	±	95% CI	Average	±	95% CI	Average	±	95% CI	—
0%	**0.0%**	0.00	±	0.00	0.001	±	0.00	0.95	±	0.18	0.01
5%	**3.1%**	-0.04	±	0.13	0.002	±	0.05	1.05	±	0.24	0.07
7.5%	**4.6%**	0.00	±	0.10	0.001	±	0.05	1.07	±	0.20	0.02
10%	**6.1%**	0.00	±	0.20	0.002	±	0.05	1.05	±	0.25	0.21
15%	**9.2%**	-0.06	±	0.18	0.01	±	0.02	0.90	±	0.19	0.16
20%	**12.3%**	-0.15	±	0.28	0.03	±	0.05	0.81	±	0.17	0.24
30%	**18.4%**	-9.57	±	18.69	0.97	±	18.05	0.91	±	0.15	0.92
40%	**24.6%**	-11.07	±	23.76	2.78	±	21.94	0.90	±	0.18	1.89
60%	**36.9%**	12.68	±	122.42	35.29	±	86.47	0.85	±	0.43	29.42
80%	**49.2%**	1124.87	±	1245.02	21.98	±	53.86	0.56	±	0.83	384.31

Individual points are reported (Average ± 95% CI) from triplicate studies and overall model fit reported as root-mean-squared error (RMSE).

Table 2.5: Viscoelastic recovery of GAG (15%) – HAP (60%) mixtures compared to pure components

	[GAG]	[HAP]	Phase I: Initial			Phase II: Disruption			Phase III: Recovery			G' Recovery
			G' (kPa)	G" (kPa)	δ (°)	G' (kPa)	G" (kPa)	δ (°)	G' (kPa)	G" (kPa)	δ (°)	(5 min) (%)
Pure CS	**15%**	**—**	8.00E-05	1.88E-03	88	2.40E-04	1.57E-03	81	8.00E-05	1.90E-03	88	100%
Mixture	**15%**	**60%**	7.8	1.9	14	9.75E-04	2.34E-02	88	4.95	1.42	16	64%
Pure HAP	**—**	**60%**	878	86.7	6	1.10E-03	1.12E-02	84	810	82.8	6	92%
Pure HA	**15%**	**—**	1.40E-04	1.70E-03	85	2.30E-04	1.79E-03	83	1.40E-04	1.73E-03	85	100%
Mixture	**15%**	**60%**	175	20.2	7	1.58E-03	1.39E-01	89	149	16.8	6	85%
Pure HAP	**—**	**60%**	878	86.7	6	1.10E-03	1.12E-02	84	810	82.8	6	92%

Table 3.1: Modulators of Chondrocyte Hypertrophy

Differentiation Pathway	Chemical	Physical	Mechanical
Chondrogenesis	TGF-β, BMPs, Dexamethasone	Low Oxygen Tension	Lower stiffness and Adhesion, Intermittent and cyclic compression load conditions
Hypertrophy and Osteogenesis	Vitamin D3, Retinoic Acid, Leptin, Insulin, Thyroxine, β-glycerophosphate, BMPs, MMPs, IL1-β, Calcium Ions	Normal Oxygen Tension	Higher stiffness and adhesion, Lower magnitude and higher fluid shear load conditions

Table 3.2: Priming *in vitro* chondrogenesis with BMSCs for *in vivo* EC ossification

Reference(s)	Year	Cell Source	Additional Materials	In Vitro Priming Method	Animal Model	Highlighted Results
Yamada, Y. et al.[159]	2003	BMSCs	Fibrin and Tricalcium Phosphate (beta-TCP)	Isolated rat BMSCs were chondrogenically primed on b-TCP blocks and implanted with fibrin glue.	Implanted subcutaneously in nude mice.	EC ossification was only seen in primed rBMSC constructs. Non-cellular and unprimed rBMSC scaffolds did not produce EC ossification.
Simmons, C.A. et al.[158]	2004	BMSCs	Alginate Matrix (RGD conjugation)	Isolated rat BMSCs were chondrogenically primed and implanted with dual growth factor encapsulation (BMP-2 and TGF-beta).	Implanted subcutaneously in nude mice.	Significantly higher amount of EC ossification was seen in scaffolds with dual GF compared to single GF and non-loaded controls.
Pelttari, K. et al.[131]	2006	BMSCs	Fibrin Matrix	Isolated human BMSCs were primed in chondrogenic medium for 4 to 7 weeks. Human ACs were isolated for implantation and a portion of hACs were expanded in chondrogenic medium.	Implanted subcutaneously in nude mice.	hBMSCs exhibited extensive EC ossification, while hACs remained stable cartilage. Chondrogenically expanded hACs did not undergo EC ossification, suggesting that they are locked into a stable cartilage phase.
Farrell, E. et al.[123]	2009	BMSCs	Collagen and Glycosaminoglycan (GAG)	Isolated human BMSCs were cultured for 21 days in chondrogenic medium. Three groups were cultured for 14 extra days in a) the same medium, b) mineralizing chondrogenic medium, or c) osteogenic medium. Unprimed control medium was also used.	Implanted subcutaneously in nude mice.	Chondrogenic priming led to collagen II and X production along with vessel ingrowth in vivo while osteogenic priming led to mineralized matrix, no vascularization, and poor cell viability. Unprimed control conditions yielded no bone. Mineralized chondrogenic priming severely diminished production of inductive growth factors.
Janicki, P. et al.[125]	2010	BMSCs	Tricalcium Phosphate (beta-TCP) or Hydroxyapatite (HA/TCP)	Isolated human BMSCs were primed in chondrogenic medium (6 weeks), in osteogenic medium, or unprimed in control medium.	Implanted subcutaneously in nude mice.	Osteogenic priming led to poor bone formation. Unprimed hBMSCs on betaTCP exhibited IM ossification. With chondrogenic priming, hBMSCs formed bone via EC ossification, while hematopoietic marrow formed from murine origin. This was hypothesized to be result of direct osteogenesis of cartilage-resident hBMSCs or transdifferentiation from chondrocytes to osteoblasts.
Scotti, C. et al.[133]	2010	BMSCs	None, direct pellet implantation	Isolated human BMSCs were primed to prechondrogenic, early hypertrophic, and late hypertrophic phase tissues	Implanted subcutaneously in nude mice.	Hypertrophic cartilage templates were required to form bone trabeculae. Pre-hypertrophic hBMSCs resorbed quickly and did not form bone. Results indicate that no external scaffolding was required to undergo EC ossification.
Farrell, E. et al.[122]	2011	BMSCs	Collagen and Glycosaminoglycan (GAG)	Isolated human BMSCs and rat BMSCs were cultured in osteogenic, chondrogenic, or control medium (28 days). In some cases, induced mineralization in chondrogenic medium lasted 7 days.	Implanted subcutaneously in nude co-isogenic hPLAP-transgenic F344 rats	Bone and bone marrow was observed in chondrogenic primed constructs but not in unprimed control and osteogenic primed constructs. Late switching (last 7 days) to osteogenic medium prevented bone formation, but beta-glycophosphate induced mineralization did not prevent bone formation in chondrogenic primed constructs. Osteoblasts in formed bone were almost entirely of host origin, but osteocytes were both host and donor origin.

Table 3.2 (continued): Priming *in vitro* chondrogenesis with BMSCs for *in vivo* EC ossification

Reference(s)	Year	Cell Source	Additional Materials	In Vitro Priming Method	Animal Model	Highlighted Results
Scotti, C. et al.[132]	2013	BMSCs	Collagen Type I Meshes	Isolated human BMSCs were primed to hypertrophic stage and seeded onto collagen type I meshes.	Implanted subcutaneously in nude mice.	Functional bone was formed heterotopically with cortical-like bone originating from host murine cells, and inner trabecular-like bone from EC ossification and originating from hBMSC primed hypertrophic cartilage constructs.
Sheehy, E.J. et al.[119]	2013	BMSCs	Agarose	Isolated porcine chondrocytes and BMSCs were cultured and chondrogenically primed prior to seeding on bilayer osteochondral scaffolds.	Implanted subcutaneously in nude mice.	EC ossification was restricted to the BMSC primed layer of the scaffold in vivo, while primed chondrocytes maintained chondrogenic phenotype. This led to a bilayer osteochondral construct.
Sheehy, E.J. et al.[162]	2014	BMSCs	Agarose and 'Channeled' Agarose	Isolated porcine BMSCs were chondrogenically primed for 5 weeks followed by hypertrophic priming for an additional week.	Implanted subcutaneously in nude mice.	EC ossification was observed in hypertrophic primed pBMSCs encapsulated in agarose gel. Additionally, channeled agarose gels with pBMSCs showed increased vascularization and mineralization compared to solid agarose counterparts, which indicated that EC ossification may be enhanced with improved vascular support.
Bahney, C.S. et al.[165]	2014	BMSCs	None, direct pellet implantation	Isolated human BMSCs were chondrogenically primed for three weeks. Additionally, cartilage grafts were isolated from healing callus 7 days after fracture and re-implanted in vivo. Implants were compared to living isografts, devitalized allografts, and sham groups.	Implanted into mid-tibia diaphysis osteotomy in nude mice.	Cartilage grafts and primed hBMSC pellets produce well vascularized and integrated bone regenerate via EC ossification; however, hBMSC pellets did not integrate with each other *in vivo*. Cartilage graft was equally likely to integrate with adjacent bone as bone isografts and outperformed devitalized allografts. Osteocytes in regenerated bone were primarily of donor origin rather than host recruited cells.
van der Stok, J. et al.[161]	2014	BMSCs	None, direct pellet implantation	Isolated human BMSCs were chondrogenically primed for three weeks and compared to hBMSCs cultured in chondrogenic media for only 3 days.	Implanted in 6mm mid-femur diaphysis defects in RNU rats.	Significantly higher EC ossification was observed in 21 day chondrogenically primed hBMSC pellets compared to 3 day undifferentiated hBMSC controls. Primed hBMSC can result in complete bridging of the 6 mm defect; however, the effect was donor dependent.
Harada, N. et al.[160]	2014	BMSCs	Poly(lactic-co-glycolic) acid (PLGA)	Isolated rat BMSCS were chondrogenically primed for 21 days and compared to rBMSCS that were cultured in standard medium. Implants were also compared to cell-free scaffolds and contralateral femur controls.	Implanted into 5mm and 15mm mid-femur diaphysis defects in Fischer 344 rats.	Significantly higher EC ossification was observed in chondrogenically primed rBMSCs seeded onto PLGA scaffolds compared to undifferentiated rBMSC controls. Histological, micro-CT, and mechanical analysis of primed cell scaffolds revealed functionalized bone regeneration as early as 2 weeks following implantation in both 5 and 15 mm defect models. By 8 weeks, mechanical strength of primed cell scaffolds were statistically equivalent to contralateral femur controls in 5 mm defects while scaffolds implanted in 15 mm defects exhibited 75% of the mean strength of native bone.

Table 3.3: Priming *in vitro* chondrogenesis with ESCs, SDSCs, ACs, and iPSCs for *in vivo* EC ossification

Reference(s)	Year	Cell Source	Additional Materials	In Vitro Priming Method	Animal Model	Highlighted Results
Montufar-Solis, D. et al.[86]	2004	ESCs	None, direct pellet implantation	Isolated murine ESC constructs were chondrogenically primed for 3 weeks.	Implanted adjacent to and within murine skull defects of same lineage.	Implants placed both adjacently and directly into skull defects exhibited EC ossification while control groups without primed implants did not.
Doan, L. et al.[121]	2010	ESCs	None, direct pellet implantation	Isolated murine ESC constructs were chondrogenically primed for 3 weeks.	Implanted into murine skull defects of same lineage.	EC Ossification was only seen in rBMSC primed cartilage implants.
Shoji, T. et al.[163]	2010	ADSCs	Collagen	Isolated human ADSCs expanded from SVF	Implanted in nude rat femurs	hADSCs exhibited greater EC ossification than PBS and hFB (fibroblast) implant controls in collagen matrix.
Case, N.D. et al.[120]	2003	ACs	Polyglycolic Acid (PGA)	Isolated rabbit chondrocytes from patellar groove and femoral condyles were chondrogenically primed on PGA scaffolds for 4 weeks.	Implanted into empty bone chambers in rabbit femoral metaphyses.	Cell loaded constructs exhibited EC ossification and led to increased bone formation compared to devitalized constructs. Thus, cells had significant impact on outcome.
Oliveira, S.M. et al.[129, 130]	2009	ACs	Chitosan Sponge	Isolated chondrocytes from chicken embryo sterna expanded on chitosan sponge and hypertrophically primed for 3 weeks. Control chondrocytes taken from caudal region of sternum while transient chondrocytes taken from cephalic region of sternum.	Implanted subcutaneously in nude mice.	Maturation and hypertrophy seen in treated chondrocyte-chitosan scaffolds. EC ossification was only seen in transient cartilage templates compared to permanent cartilage scaffold (control).
Tam, W.L. et al.[164]	2014	iChons	CopiOs (Zimmer) Bone Void Filler	Induced chondrocytes (iChons) were directly reprogrammed from murine dermal fibroblasts by two methods iChon(Con) and iChon(Ind). Following induction, cells were chondrogenically primed for 7 days, and hypertrophically primed for 14 days.	Implanted subcutaneously in nude mice.	Both induced cell sources underwent chondrogenic differentiation in vitro, but hypertrophic differentiation was only seen in iChon(Ind) cells. In vivo, iChon(Con) cells formed stable cartilage, while iChon(Ind) cells exhibited EC ossification markers. Osteoblasts in formed bone were of host origin, while chondrocytes were of both donor and host origin.

Table 3.4: Comparing *in vitro* chondrogenically primed cell sources for *in vivo* EC ossification

Reference(s)	Year	Cell Source	Additional Materials	In Vitro Priming Method	Animal Model	Highlighted Results
Dickhut, A. et al.[136]	2008	BMSCs, ADSCs, SDSCs and ACs	None, direct pellet implantation	Isolated human BMSCs, ADSCs, SDSCs, and ACs were cultured in chondrogenic medium (5 weeks).	Implanted subcutaneously in nude mice.	Chondrogenic priming led to similar collagen type II vs. type I levels and were positive for type X in all cells. SDSCs and ACs had significantly lower levels of ALP activity after priming, which correlated with poor EC ossification after implantation. While primed BMSCs and ADSCs exhibited EC ossification *in vivo*, SDSCs and ACs exhibited fibrous dedifferentiation and degradation.
Jukes, J.M. et al.[126]	2008	ESCs, BMSCs, and ACs	Ceramic particles	Isolated goat and human BMSCs were osteogenically primed for 7 or 21 days. Additionally, these cells along with murine ESCs and goat ACs were chondrogenically primed up to 21 days.	Implanted into nude mouse skull defects.	Osteogenic priming led only to direct IM ossification. Chondrogenic priming was necessary for EC ossification, but not sufficient since only mESCs underwent EC ossification. Goat and human BMSCs underwent only marginal EC ossification and goat ACs didn't exhibit any EC ossification when cultured in similar fashion.
Tortelli, F. et al.[166]	2009	BMSCs and OBs	Hydroxyapatite (HAP)	Isolated rate BMSCs and OBs were cultured in standard medium.	Implanted subcutaneously in nude mice.	The capacity to recruit host cells and the ossification pathway were dependent on donor cell commitment. rBMSC implants led to formation of bone from host cells through the EC ossification pathway, and donor rOBs exhibited direct IM ossification. No studies were conducted with chondrogenically primed cells.
Both, S.K. et al.[135]	2011	BMSCs and ESCs	Biphasic Calcium Phosphate (BCP)	Isolated human BMSCs, rat ESCs, and human ESCs were cultured in a series of differentiation mediums including chondrogenic priming followed by osteogenic priming. Cells were seeded on BCP scaffolds.	Implanted subcutaneously in nude mice.	ESCs were indistinguishable from BMSCs following in vitro osteogenic priming. Osteogenic priming of BMSCs led to direct (IM) osteogenesis and extensive bone formation. Both rESCs and hESCs did not form substantial bone but did exhibit signs of limited EC ossification.
Vinardell, T. et al.[134]	2012	BMSCs, FPSCs, SDSCs and ACs	Agarose	Isolated porcine BMSCs, SDSCs, FPSCs, and ACs were chondrogenically primed (3 weeks). An additional group was primed in hypertrophic medium for 4 weeks.	Implanted subcutaneously in nude mice.	Only BMSCs exhibited EC ossification. SDSCs and FPSCs underwent fibrous dedifferentiation and resorption, and ACs appeared to maintain chondrogenic stability.

Table 4.1: Formulations for HA Molecular Weight Viscoelastic Studies

	Concentration (% w/v)	Mass Fraction (%)					Volume Fraction (%)			
Group	**HA**	**HA**	**HAP**	**DCC**	**DBM**	**Media**	**HAP**	**DCC**	**DBM**	**Media**
HA(35)-HAP	10%	8%	41%			51%	32%			68%
HA(350)-HAP	3%	3%	43%			54%	32%			68%
HA(1500)-HAP	1%	1%	44%			55%	32%			68%

Table 4.2: Formulations for HA-ECM and HA-HAP-ECM Viscoelastic Studies

	Concentration (% w/v)	Mass Fraction (%)					Volume Fraction (%)			
Group	**HA**	**HA**	**HAP**	**DCC**	**DBM**	**Media**	**HAP**	**DCC**	**DBM**	**Media**
HA(1500)	2%	2%				98%				100%
HAP			44%			56%	32%			68%
HA(1500)-HAP	1%	2%	44%			55%	32%			68%
HA(1500)-HAP-DCC (Φ = 0.15)	1%	1%	43%	3%		53%	32%	15%		53%
HA(1500)-HAP-DCC (Φ = 0.30)	1%	1%	42%	5%		52%	31%	30%		39%
HA(1500)-HAP-DCC (Φ = 0.45)	1%	1%	41%	8%		51%	30%	45%		25%
HA(1500)-DCC (Φ = 0.15)	2%	2%		3%		95%		15%		85%
HA(1500)-DCC (Φ = 0.30)	2%	2%		6%		92%		30%		70%
HA(1500)-DCC (Φ = 0.45)	2%	2%		9%		89%		45%		55%
HA(1500)-HAP-DBM (Φ = 0.05)	1%	1%	43%		3%	53%	31%		5%	64%
HA(1500)-HAP-DBM (Φ = 0.10)	1%	1%	42%		5%	52%	31%		10%	60%
HA(1500)-HAP-DBM (Φ = 0.15)	1%	1%	41%		8%	51%	30%		15%	55%
HA(1500)-DBM (Φ = 0.05)	2%	2%			3%	95%			5%	95%
HA(1500)-DBM (Φ = 0.10)	2%	2%			6%	92%			10%	90%
HA(1500)-DBM (Φ = 0.15)	2%	2%			9%	89%			15%	85%
HA(1500)-DBM (Φ = 0.30)	2%	2%			19%	80%			30%	70%
HA(1500)-DBM (Φ = 0.45)	2%	2%			28%	70%			45%	55%

Table 4.3: HAP Size and Zeta Potential

	Effective Diameter (nm)				Zeta Potential (mV)			
Pure HAP	476.7	±	106.6		-26.7	±	6.8	
HA (35) - HAP (1:1)	537.6	±	103.0		-31.1	±	7.3	
HA (350) - HAP (1:1)	639.4	±	106.3	**	-42.9	±	7.3	**
HA (1500) - HAP (1:1)	666.6	±	101.6	**	-46.7	±	5.3	**

Significant differences between individual groups compared to pure HAP (ANOVA with post-hoc Tukey's HSD test) ($n = 15$; $p < 0.05$*; $p < 0.01$**).

Table 5.1: In vitro and in vivo HA-ECM and HA-HAP-ECM Formulations

	Mass Fraction (%)					Volume Fraction (%)				Cranial Defect Score		
Group	**HA**	**HAP**	**DCC**	**DBM**	**Media**	**HAP**	**DCC**	**DBM**	**Media**	**Average**	**±**	**SD**
SHAM										2.33	±	0.58
HAP		44%			56%	32%			68%	1.67	±	0.58
HA-HAP	2%	44%			55%	32%			68%	2.67	±	0.58
HA-DCC (Φ = 0.15)	2%		3%		95%		15%		85%			
HA-HAP-DCC (Φ = 0.15)	1%	43%	3%		53%	32%	15%		53%	2.33	±	0.58
HA-DBM (Φ = 0.05)	2%			3%	95%			5%	95%			
HA-HAP-DBM (Φ = 0.05)	1%	43%		3%	53%	31%		5%	64%	1.67	±	0.58

APPENDIX B: FIGURES

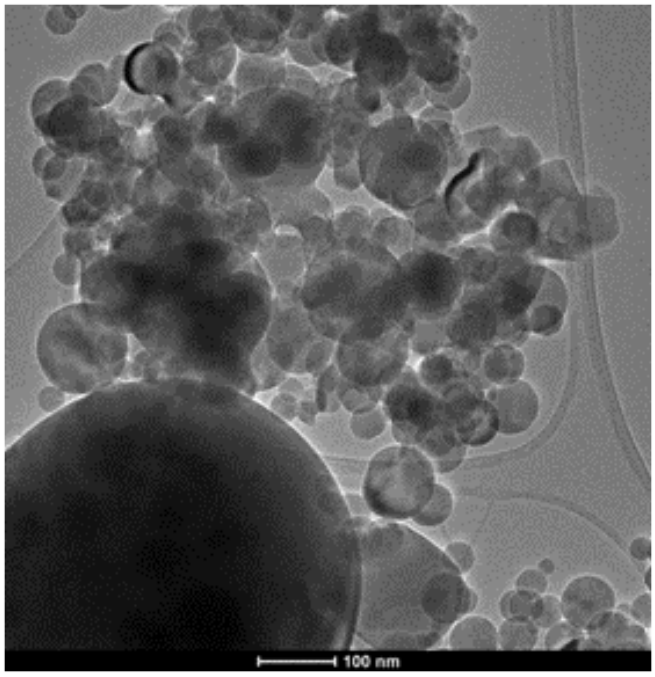

Figure 2.1: TEM image of HAP particles (scale bar = 100 nm).

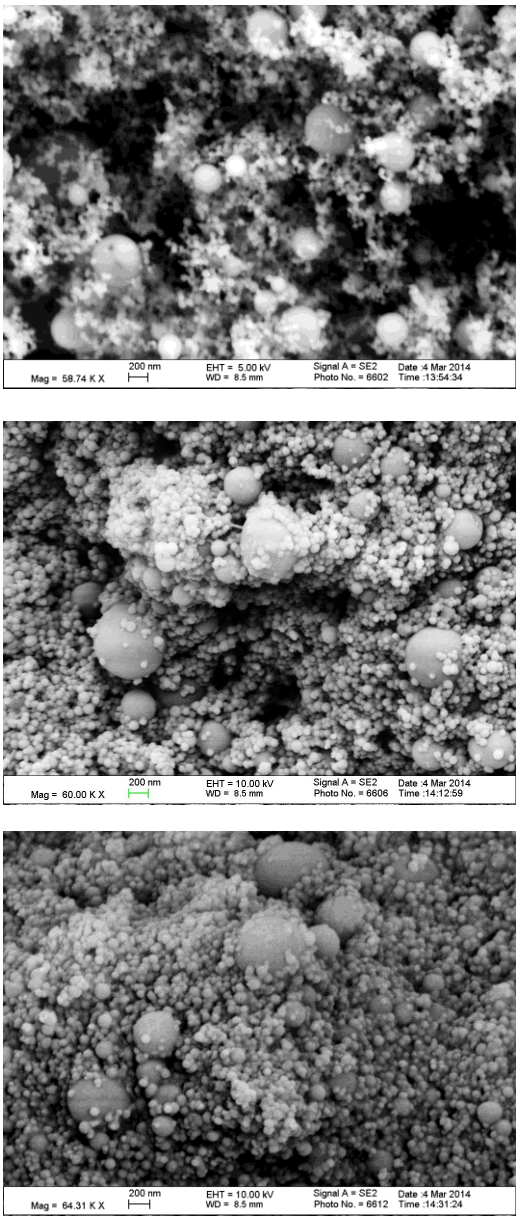

Figure 2.2A-C: SEM images of A) HAP particles (60% w/v), B) CS-HAP (15%-60% w/v), and C) HA-HAP (15%-60% w/v) colloidal gels (scale bar = 200 nm).

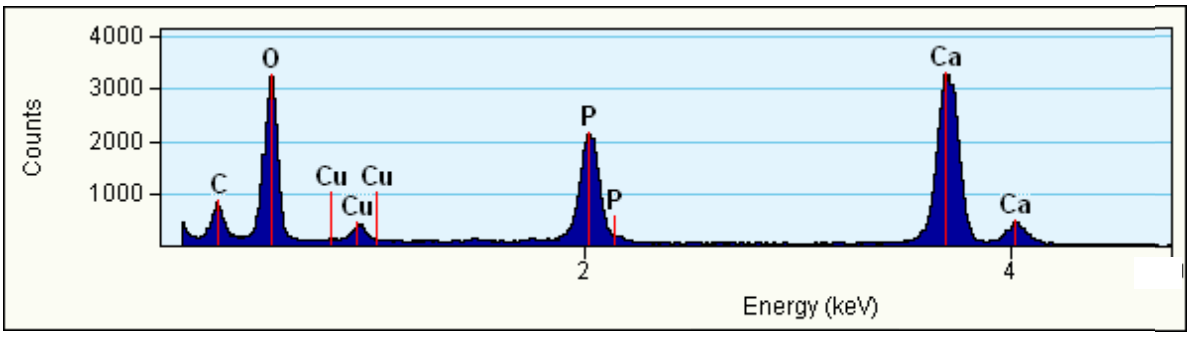

Figure 2.3: EDS spectra of HAP particles

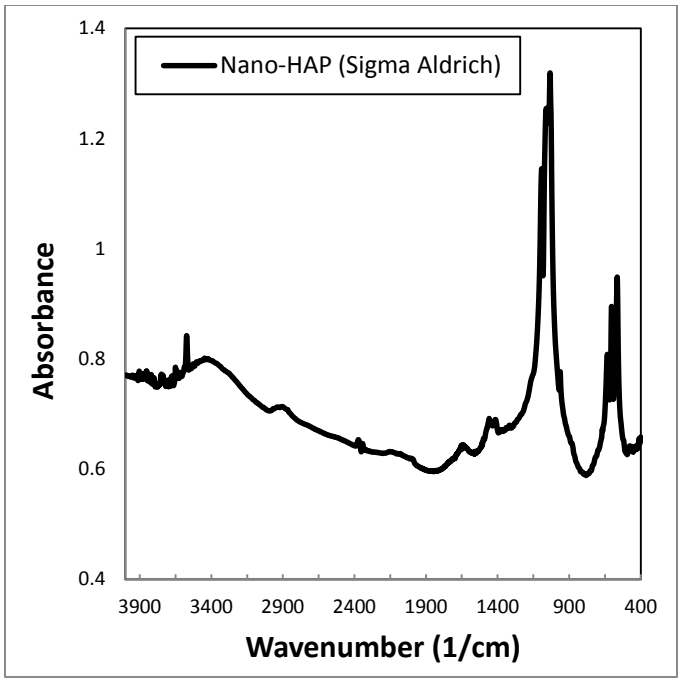

Figure 2.4: FTIR spectra of HAP particles. [21, 22]

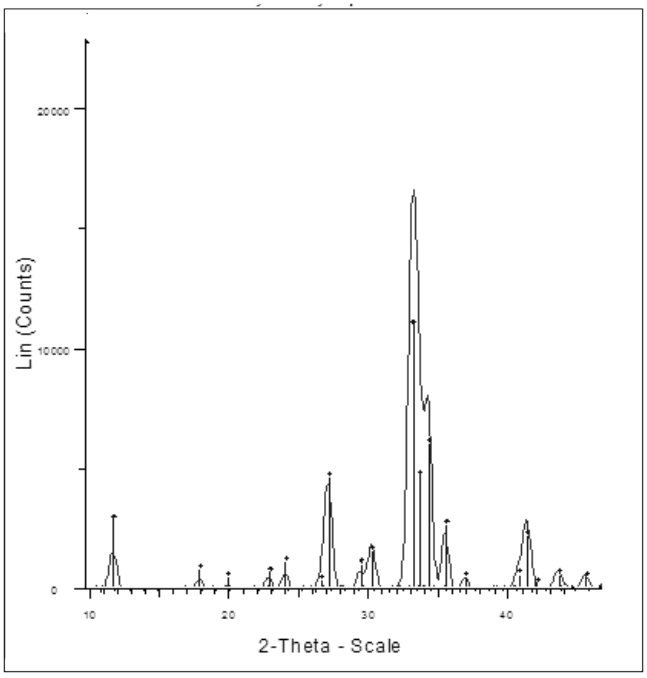

Figure 2.5: XRD of HAP particles (curve) compared to ICDD (vertical lines) HAP standard. [21, 22]

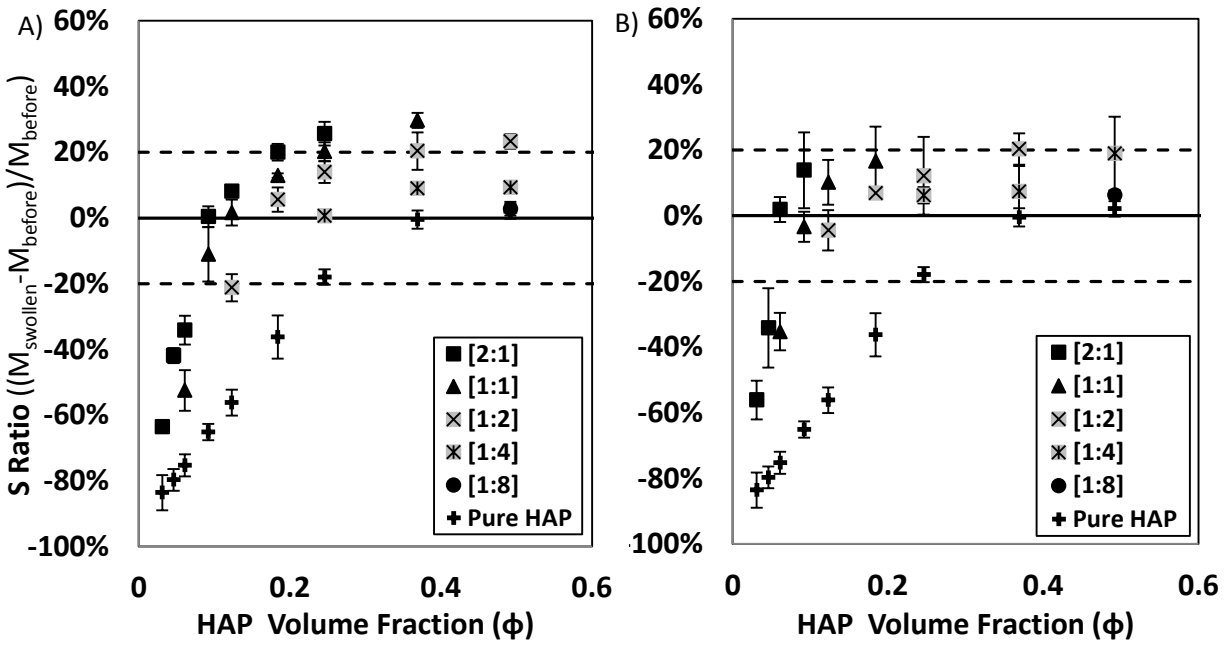

Figure 2.6A-B: Swelling ratio of A) CS-HAP and B) HA-HAP gels plotted versus HAP Φ. Data sets represent GAG:HAP ratios (w:w) compared to pure HAP. No swelling change was desired ($S \approx 0$), and success criteria for the gels were established by setting swelling tolerances (dashed lines; $0 \pm 20\%$). Individual points are reported (average ± SD) from triplicate studies.

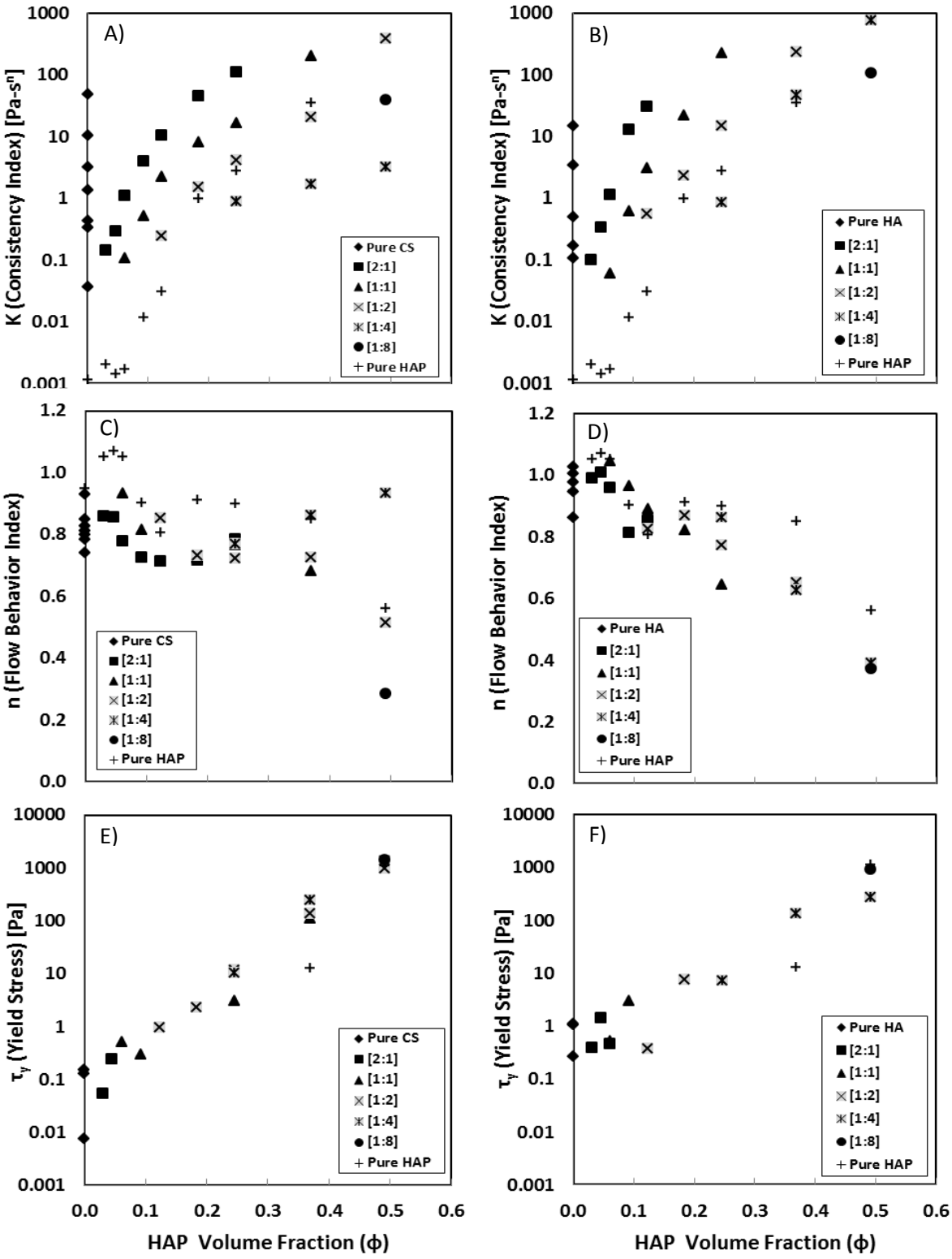

Figure 2.7A-F: Trends in modeled H-B fluid parameters for *K* (A, B), *n* (C, D), and τ_y (E, F) plotted versus HAP Φ for CS-HAP (left) and HA-HAP (right) at various [GAG:HAP] ratios [w:w].

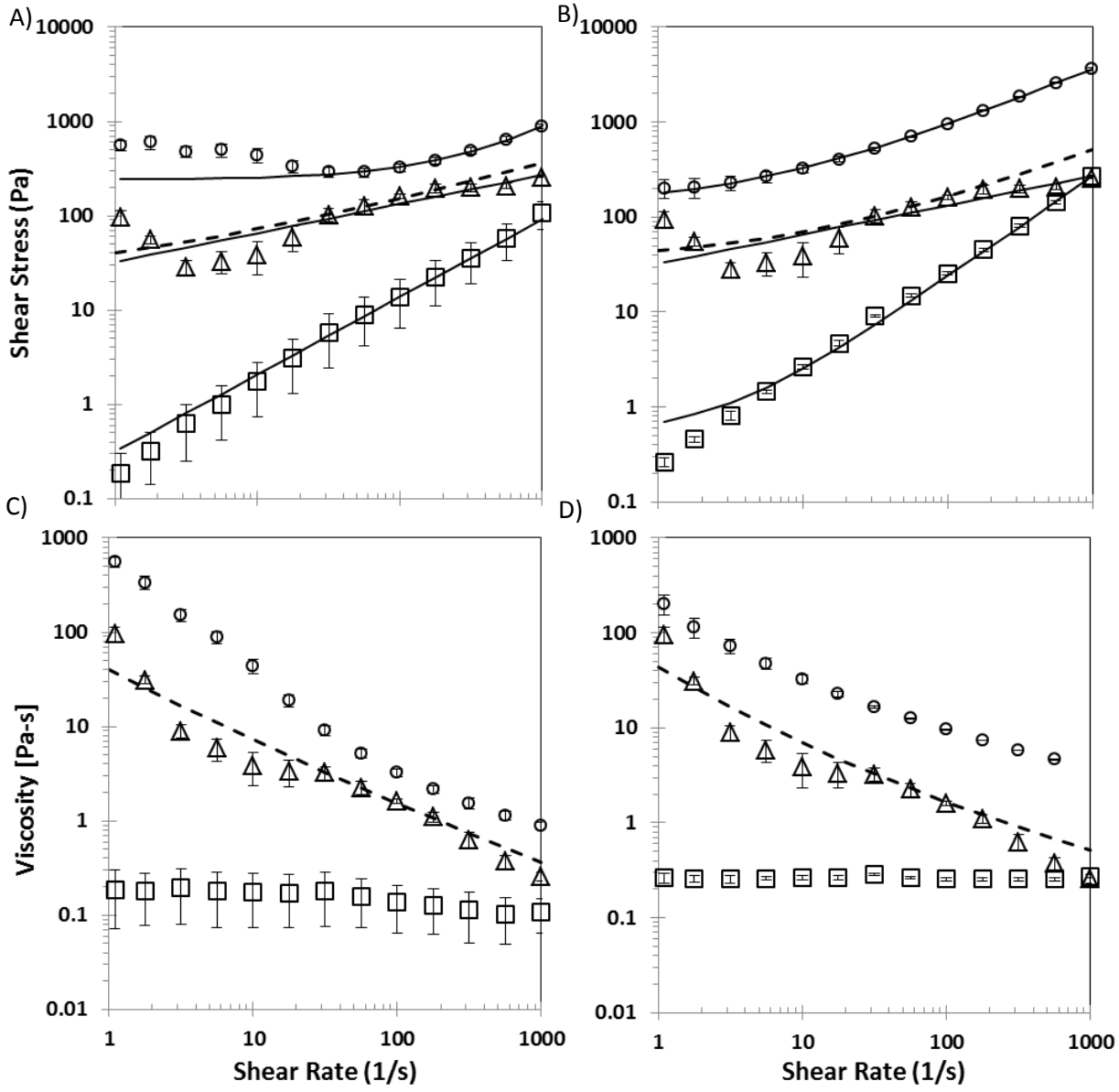

Figure 2.8A-D: Examples of shear stress and viscosity profiles of CS 15% - HAP 60% (A, C) and HA 15% - HAP 60% (B, D) colloidal gels (circles) compared to pure components GAG 15% (squares) and HAP 60% (triangles). Displayed solid trend lines were calculated using a three-parameter fit to the H-B fluid model, and individual data points represent experimental average ± SD from triplicate studies. Dashed lines represent the H-B fit of experimental data from the addition of pure components GAG 15% and HAP 60%.

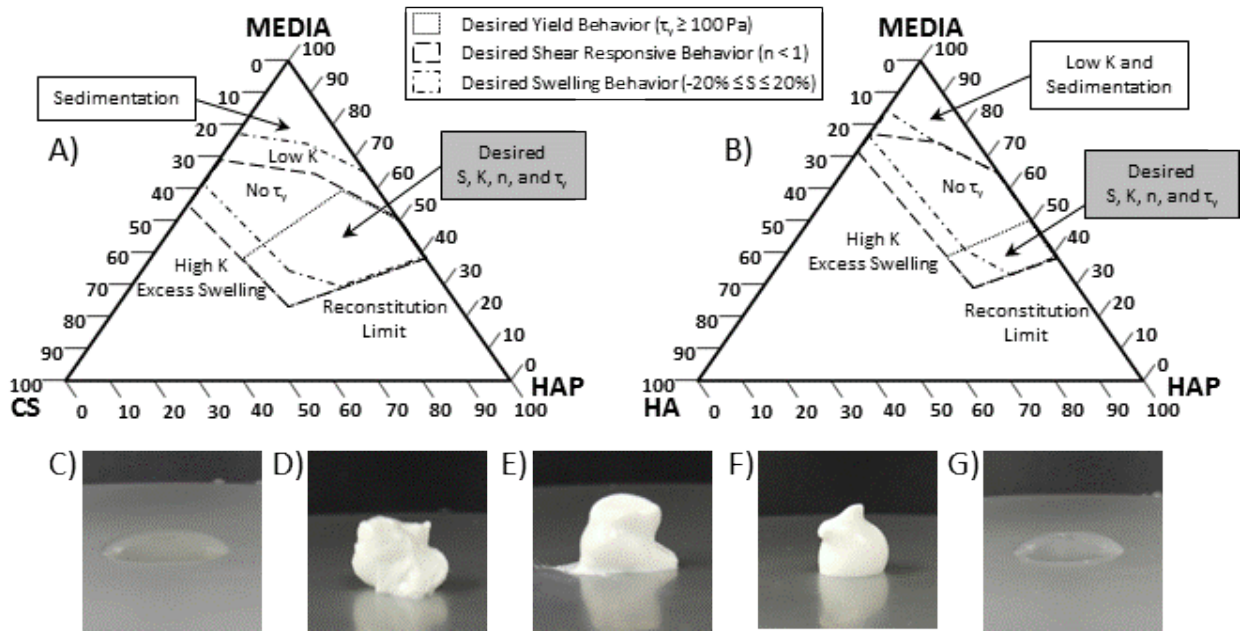

Figure 2.9A-B: Ternary diagrams (weight %) for A) CS-HAP and B) HA-HAP colloidal mixtures identifying overlay of desirable regions of rheological yield (dotted line), shear-response (dashed line), and swelling properties (dot-dashed line). Images of extruded mixtures (via 21-gauge needle) of C) Pure CS (15%), D) CS-HAP (15-60%), E) Pure HAP (60%), F) HA-HAP (15-60%), and G) Pure HA (15%) (w/v).

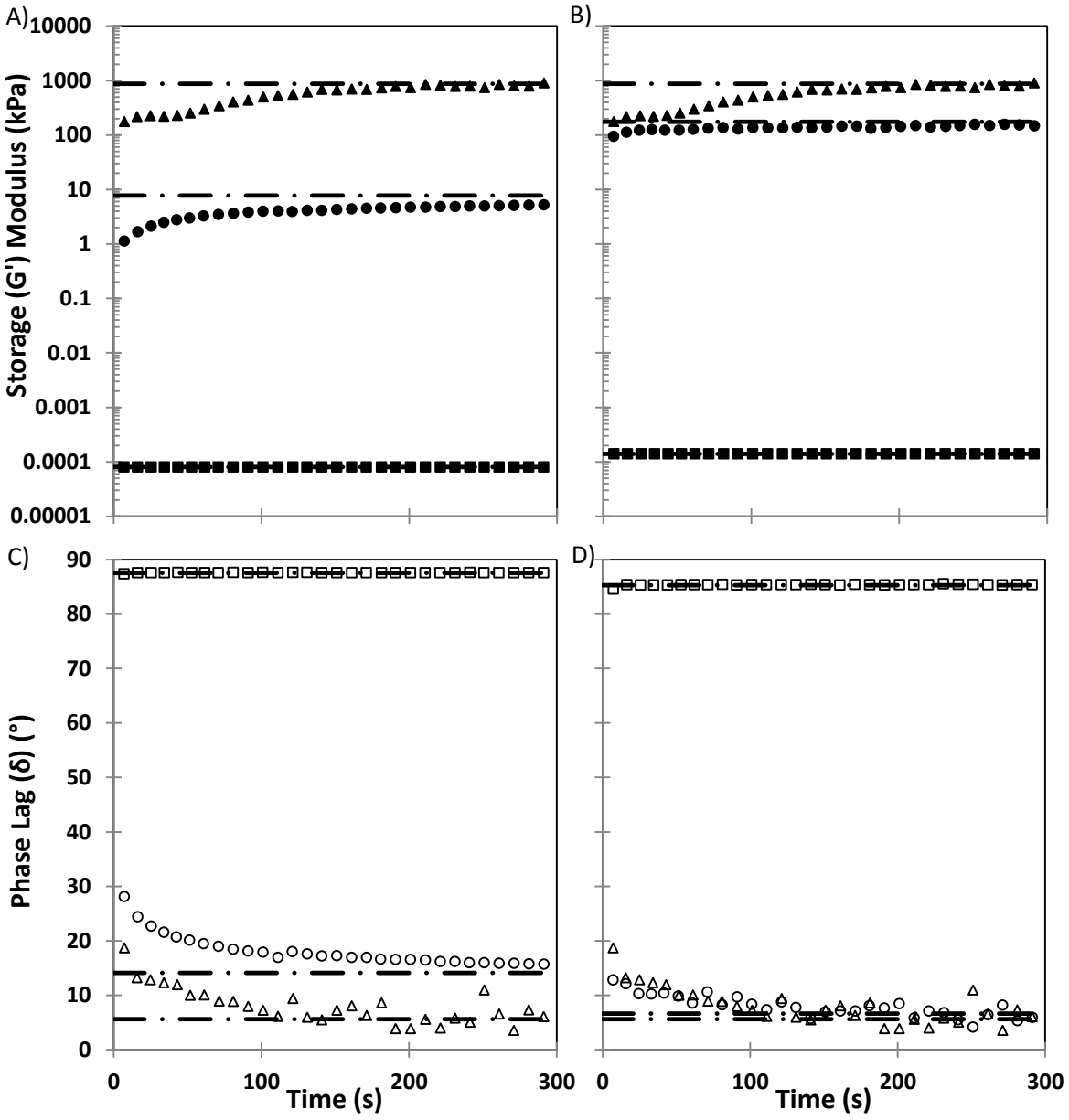

Figure 2.10A-D: Viscoelastic recovery profiles of CS 15% - HAP 60% (A, C) and HA 15% - HAP 60% (B, D) gels (circles) were compared to pure components, GAG 15% (squares) and HAP (triangles) 60%. G′ (solid symbols), G″ (not shown), and δ (open symbols) were measured every 3 seconds (n = 5) following a high oscillatory disruption phase. Recovery was assessed relative to a baseline low oscillatory stress profile for each group (dashed lines).

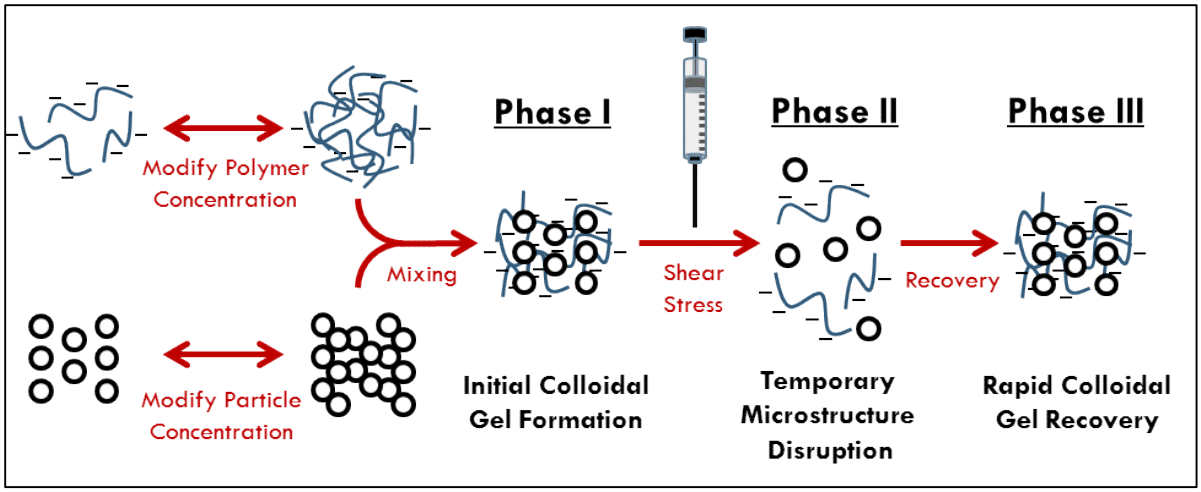

Figure 2.11: Schematic depicting the formulation parameters and rheological fluid properties of GAG-HAP colloidal gels.

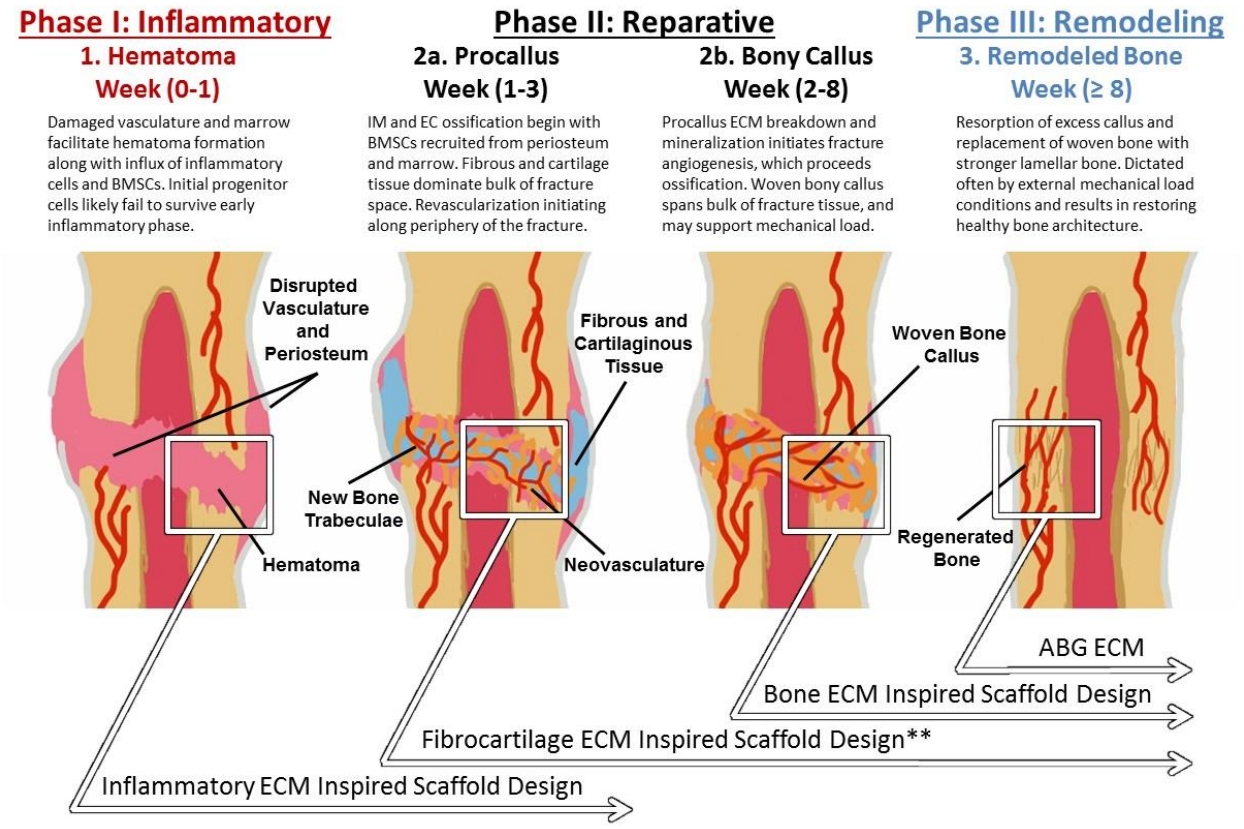

Figure 3.1: Both IM and EC ossification occur during the bone healing process in three overlapping regeneration phases. Critical-sized bone defects favor EC ossification over direct IM ossification primarily due to the large, avascular nature of these defects. Four ECM based biomaterial strategies (boxes) are highlighted with regard to bone regeneration. The intermediate fibrocartilaginous ECM remains underexplored (**) as a strategy to potentially enhance quality and extent of EC ossification and overall bone regeneration.

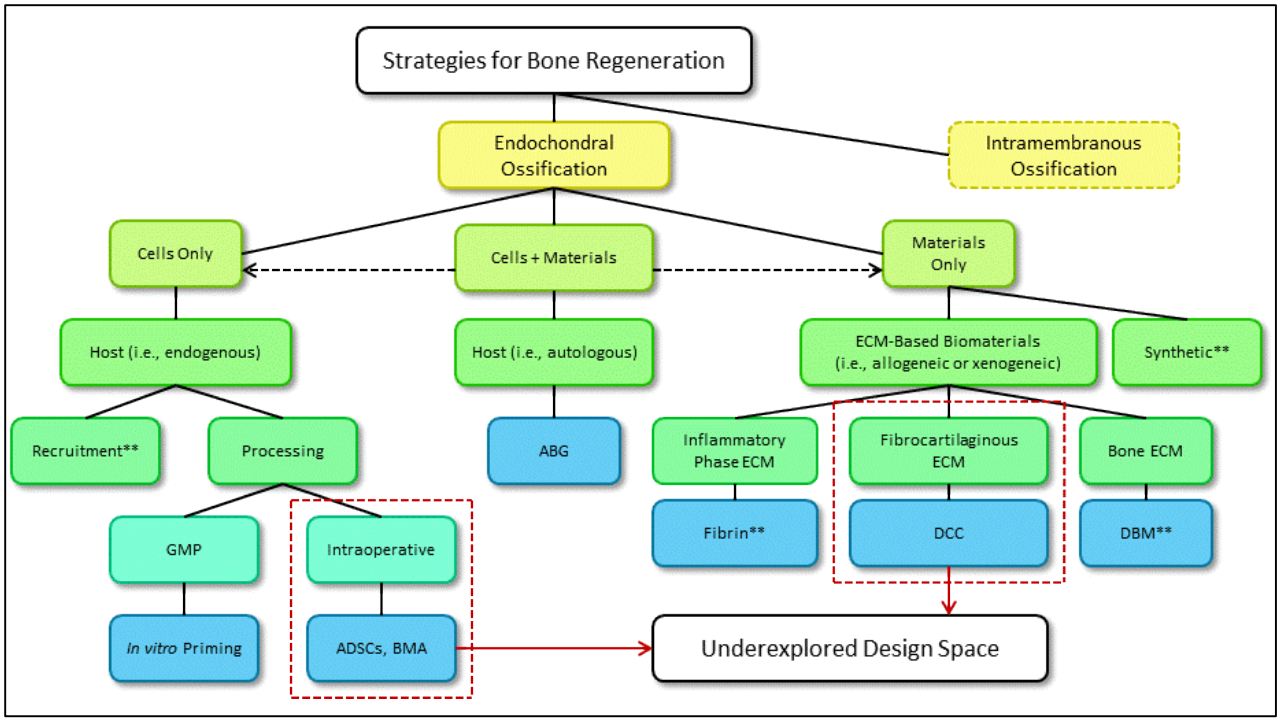

Figure 3.2: Current landscape of EC ossification strategies (blue boxes) along with underexplored design space (dashed outlines) highlighted in this review. Some combined cell and material strategies are not shown explicitly (dashed arrows). This includes several *in vitro* priming studies that utilized cell and material approaches (**) and is further explored elsewhere (Table 3.2-3.4). All strategies will be critically evaluated with regard to technical, regulatory, and commercial challenges. ABG = Autologous Bone Grafting; ADSCs = Adipose Derived Stem Cells; BMA = Bone Marrow Aspirate; DBM = Demineralized Bone Matrix; DCC = Decellularized Cartilage; ECM = Extracellular Matrix; GMP = Good Manufacturing Practice

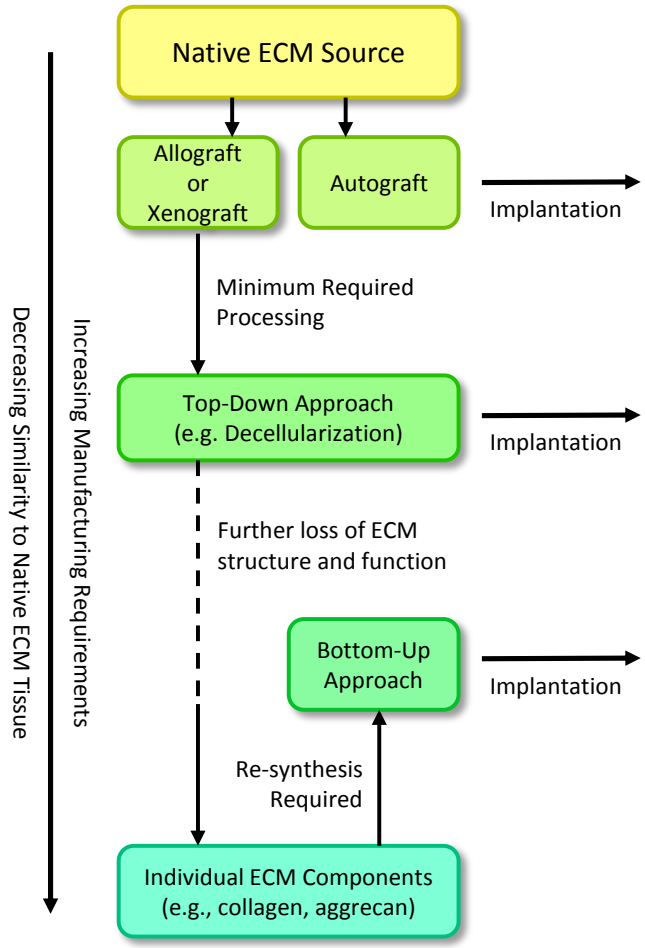

Figure 3.3: Top-down approaches to mimic native ECM tissue require less processing before implantation and retain more of the ECM's physicochemical composition, structure and function compared to bottom-up re-synthesis approaches.

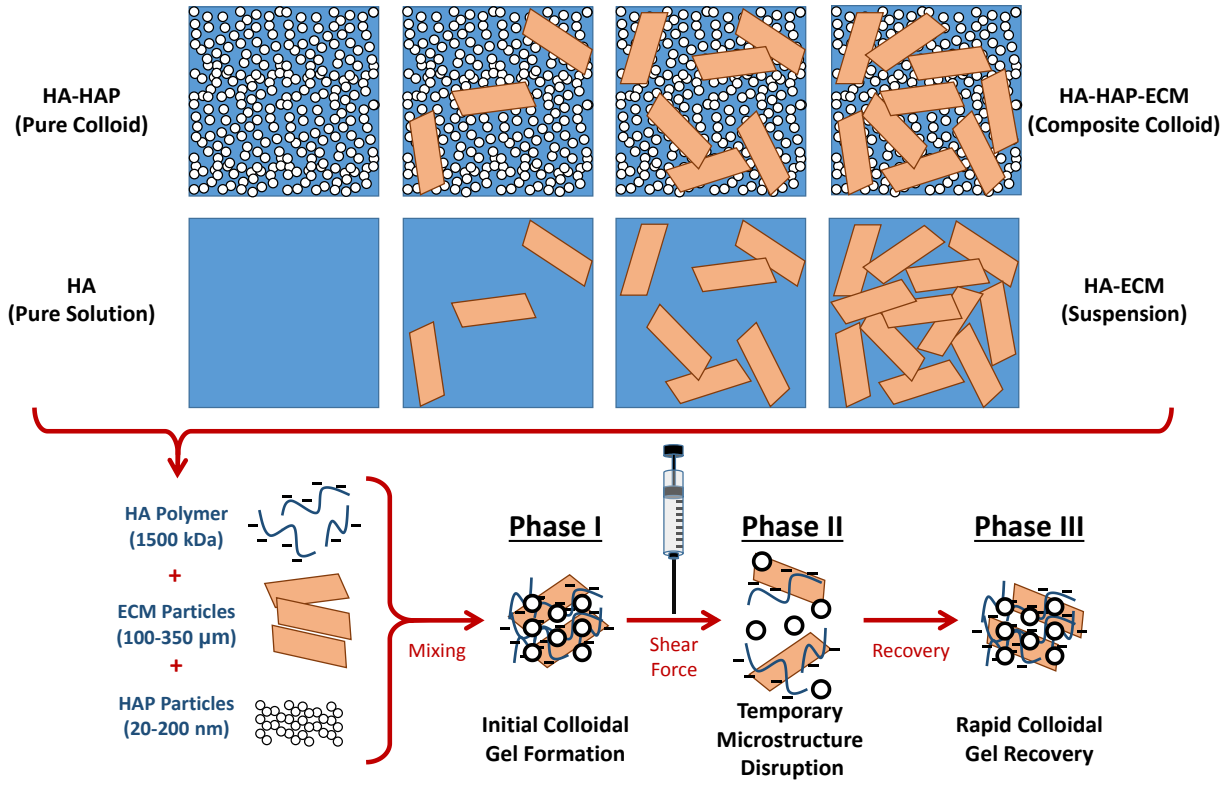

Figure 4: Schematic depicting the formulation parameters and rheological fluid properties of HA-ECM microparticle suspensions and HA-HAP-ECM colloidal gels.

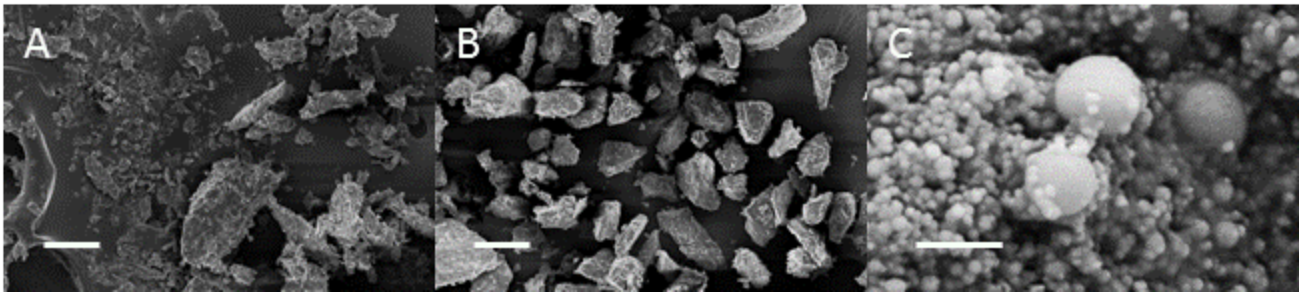

Figure 4.1: SEM images of sieved (< 350 μm) ECM microparticles A) DBM and B) DCC as well as C) HAP nanoparticles. Scale bars for images A and B were (100 μm) and for image C (500 nm).

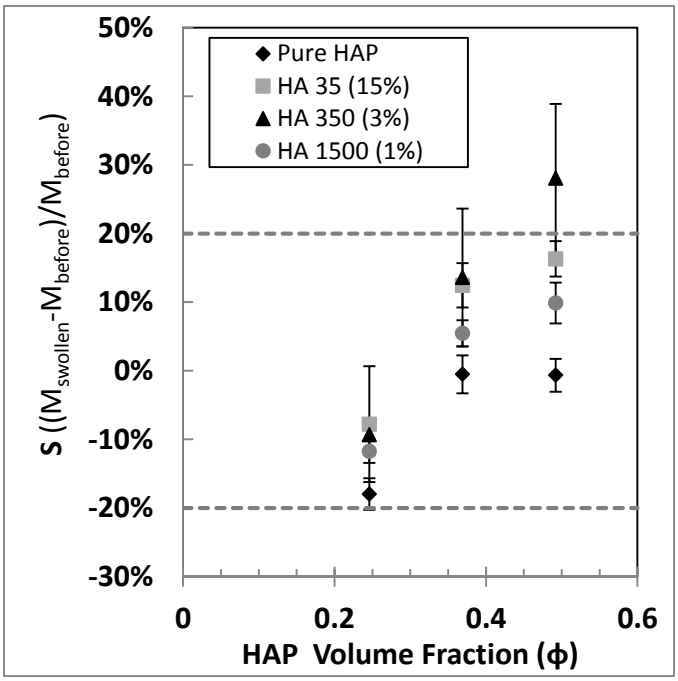

Figure 4.2: Swelling ratio (*S*) of HA-HAP gels plotted versus HAP Φ. Data sets represent colloids comprised of different molecular weight HA (35, 350, and 1500 kDa) compared to pure HAP. No swelling change was desired (S-ratio ≈ 0), and success criteria for the gels were established by setting S-ratio tolerances (dashed lines; 0 ± 20%). Individual points are reported (average ± SD) from triplicate studies.

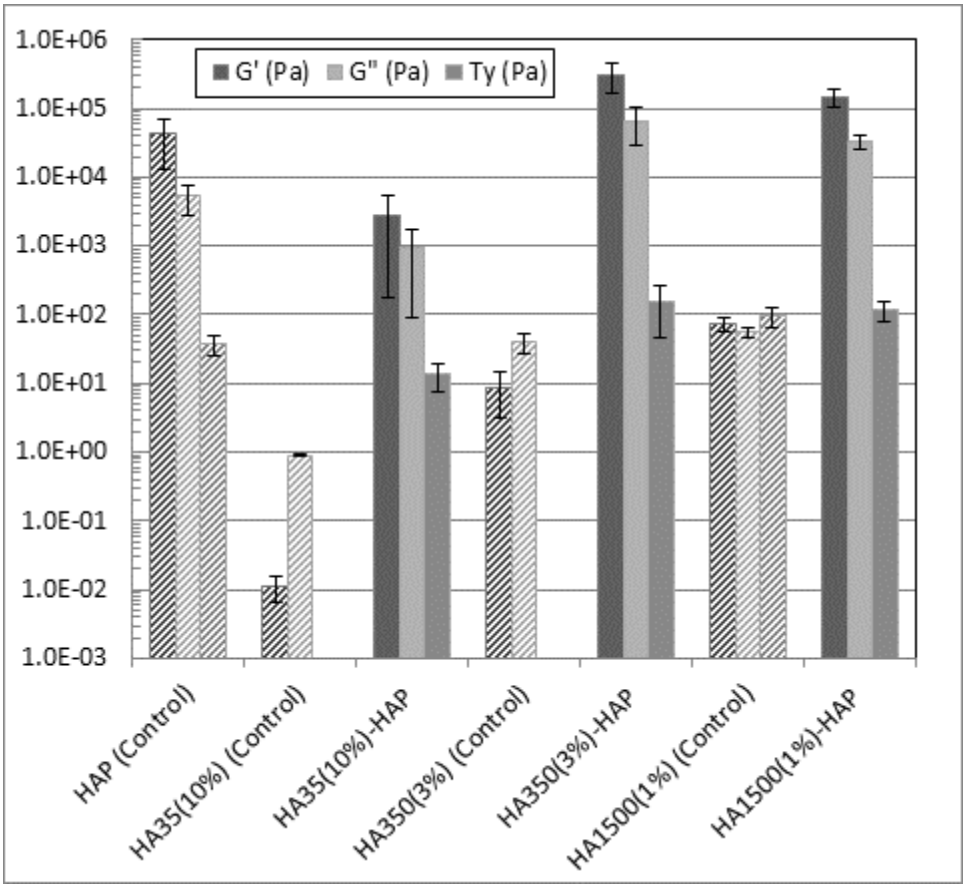

Figure 4.3: LVE region viscoelastic properties from controlled stress sweeps (1-10,000 Pa) at constant frequency (1 Hz) of HA-HAP colloids composed of 35 kDa (10% w/v), 350 kDa (3% w/v), and 1500 kDa (1% w/v) HA polymers and compared to HAP and HA control fluids, respectively. Averaged values for G′, G″, and τ_y (Pa) are displayed from triplicate studies. Error bars represent 95% CI of the mean.

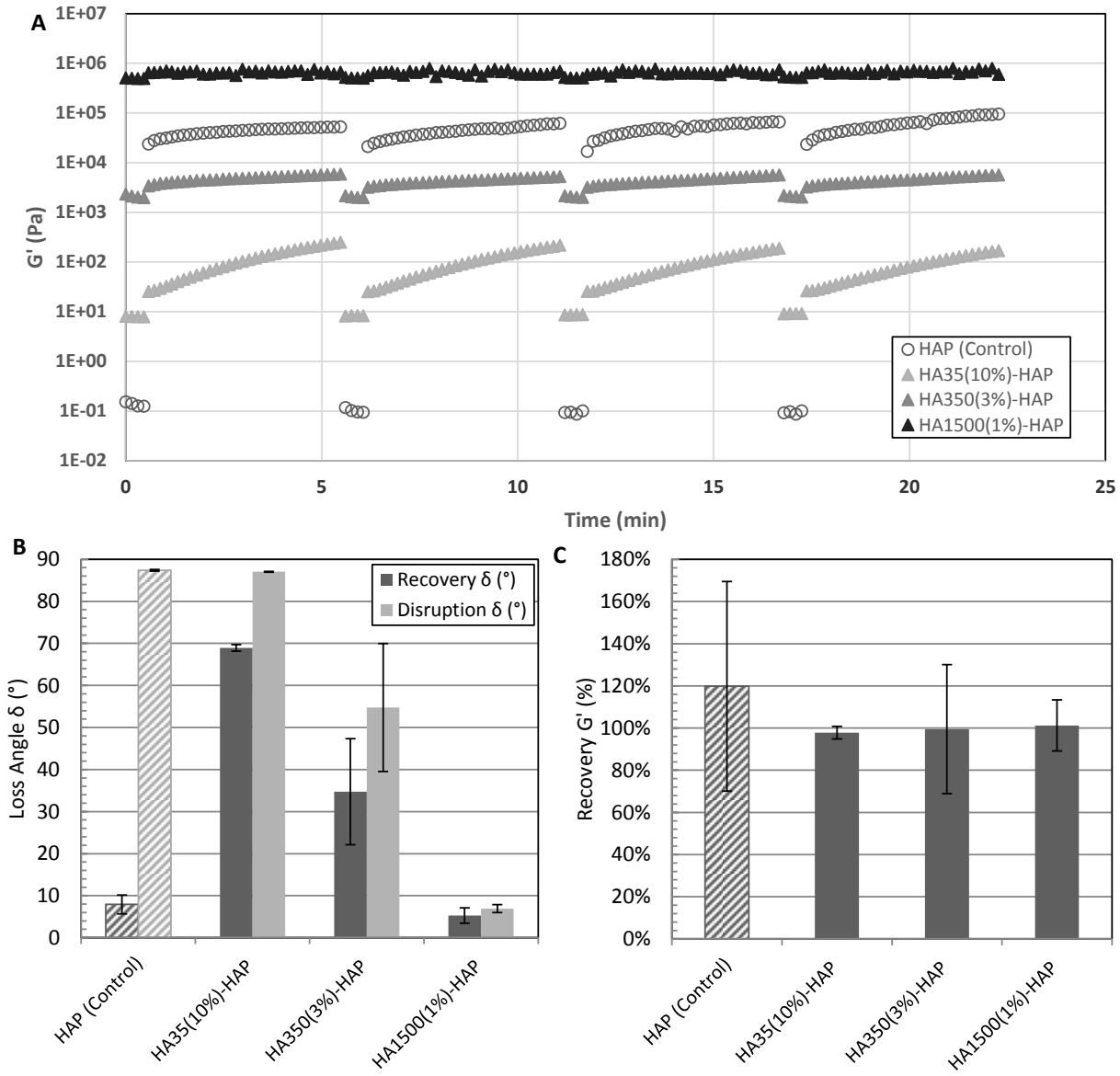

Figure 4.4 A-C: A) Viscoelastic $G'_{Recovery}$ profiles of HA-HAP colloids composed of 35 kDa (10% w/v), 350 kDa (3% w/v), and 1500 kDa (1% w/v) HA polymers and compared to HAP and HA control fluids, respectively. Measurements were made every 10 seconds during four alternating rounds of intense disruption (30 s, 1000 Pa, 1 Hz) and recovery (5 min, low stress in LVE regime, 1 Hz) oscillatory time sweeps at 37°C. B) Average δ (°) value of oscillatory recovery and disruption sweeps, and C) average $G'_{Recovery}$ (%) following 5 minutes of recovery time (n = 3). Error bars represent 95% CI of the mean.

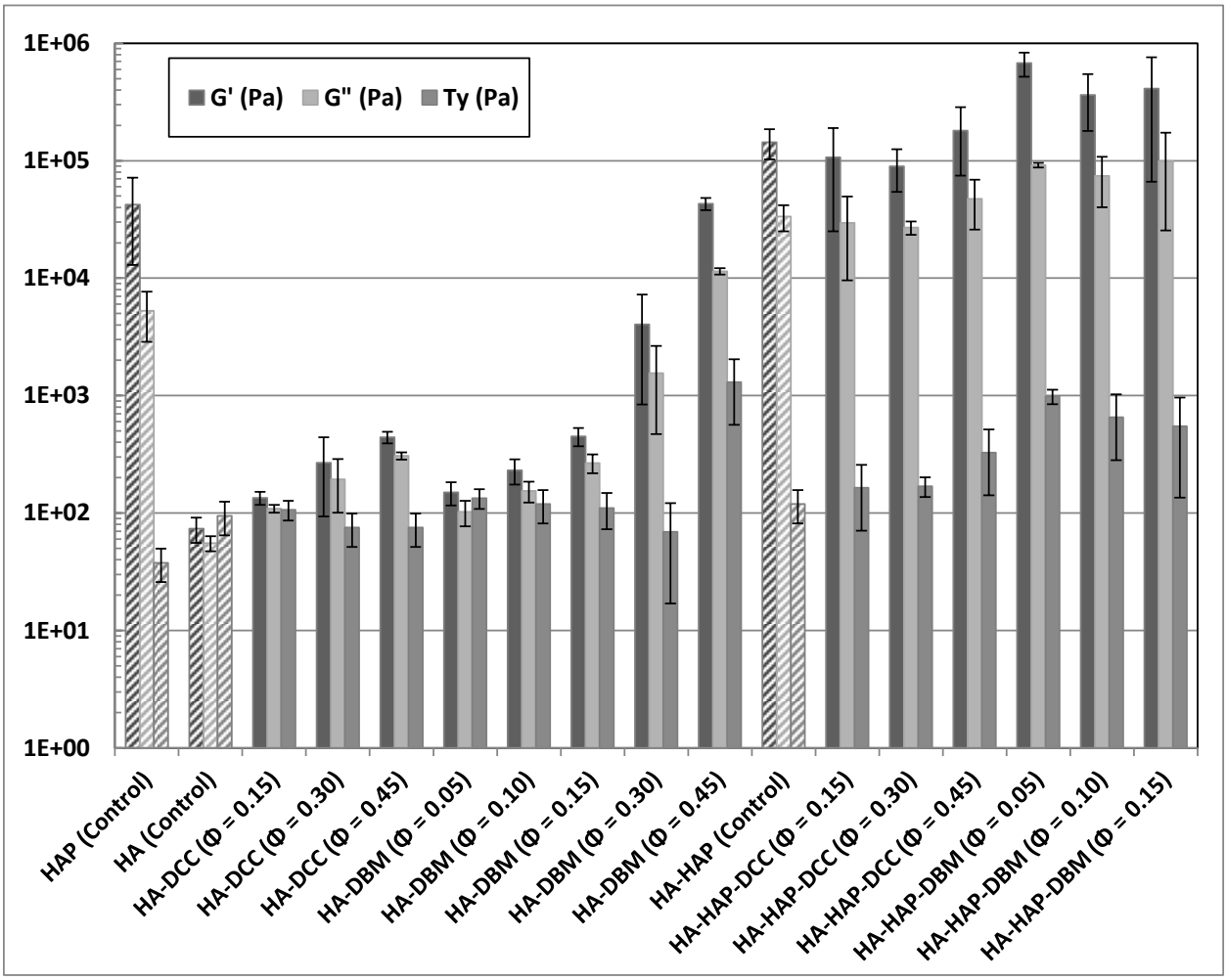

Figure 4.5: LVE region viscoelastic properties from controlled stress sweeps (1-10,000 Pa) at constant frequency (1 Hz) of HA-ECM suspensions and HA-HAP-ECM colloids compared to HA, HAP, and HA-HAP control fluids, respectively. HA-HAP-DBM colloids ($\Phi_{DBM} \geq 30\%$) exhibited incomplete hydration, fractured when tested with the rheometer, and thus could not be measured. Averaged values for G′, G″, and τ_y (Pa) are displayed from triplicate studies. Error bars represent 95% CI of the mean.

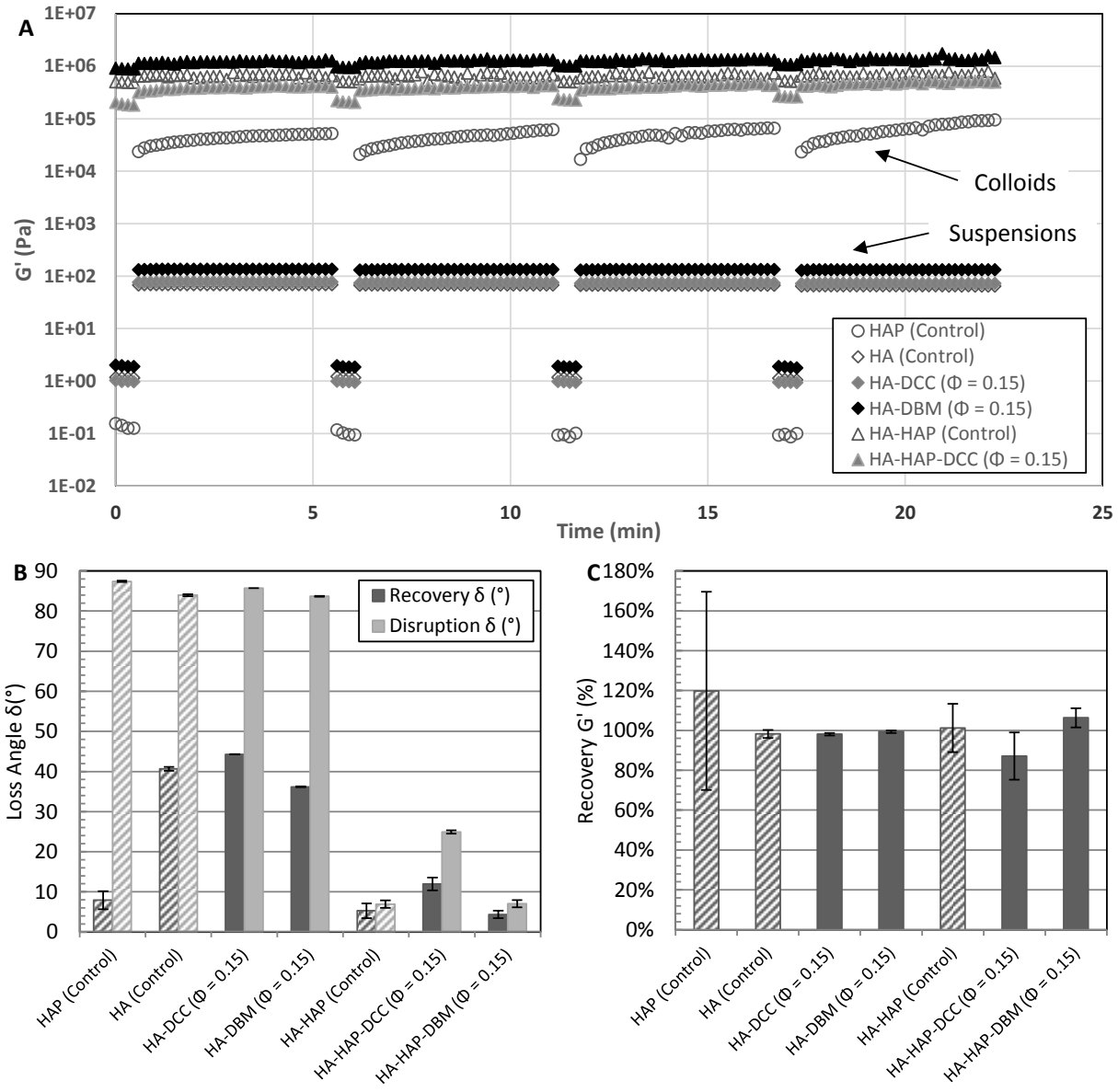

Figure 4.6 A-C: A) Viscoelastic $G'_{Recovery}$ profiles of HA-ECM suspensions and HA-HAP-ECM colloids compared to HA, HAP, and HA-HAP control fluids, respectively. Measurements were made every 10 seconds during four alternating rounds of intense disruption (30 s, 1000 Pa, 1 Hz) and recovery (5 min, low stress in LVE regime, 1 Hz) oscillatory time sweeps at 37°C. B) Average δ (°) value of oscillatory recovery and disruption sweeps, and C) average $G'_{Recovery}$ (%) following 5 minutes of recovery time (n = 3). Error bars represent 95% CI of the mean.

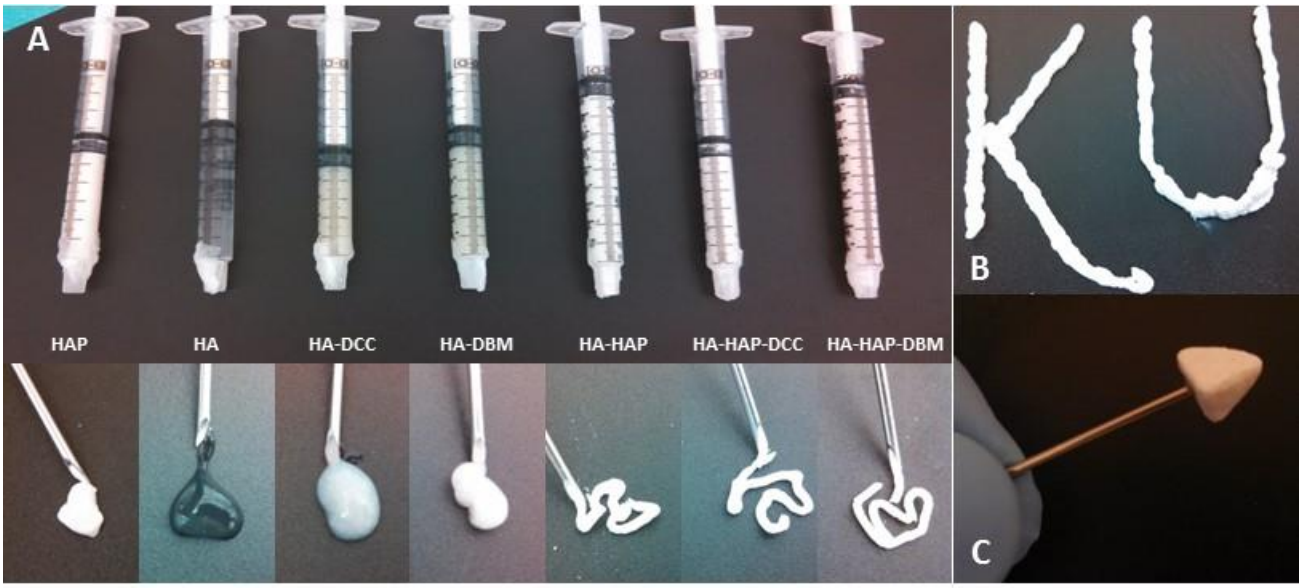

Figure 4.7 A-C: A) All tested HA-ECM and HA-HAP-ECM fluids could readily be loaded into 1 ml syringes and subsequently be extruded through 18-gauge needles. Colloidal ECM formulations could be shaped B) during extrusion and C) maintained form following handling. HA-HAP-DBM ($\Phi_{DBM} = 0.15$) was shown above in image B and C.

FIGURES AND TABLES

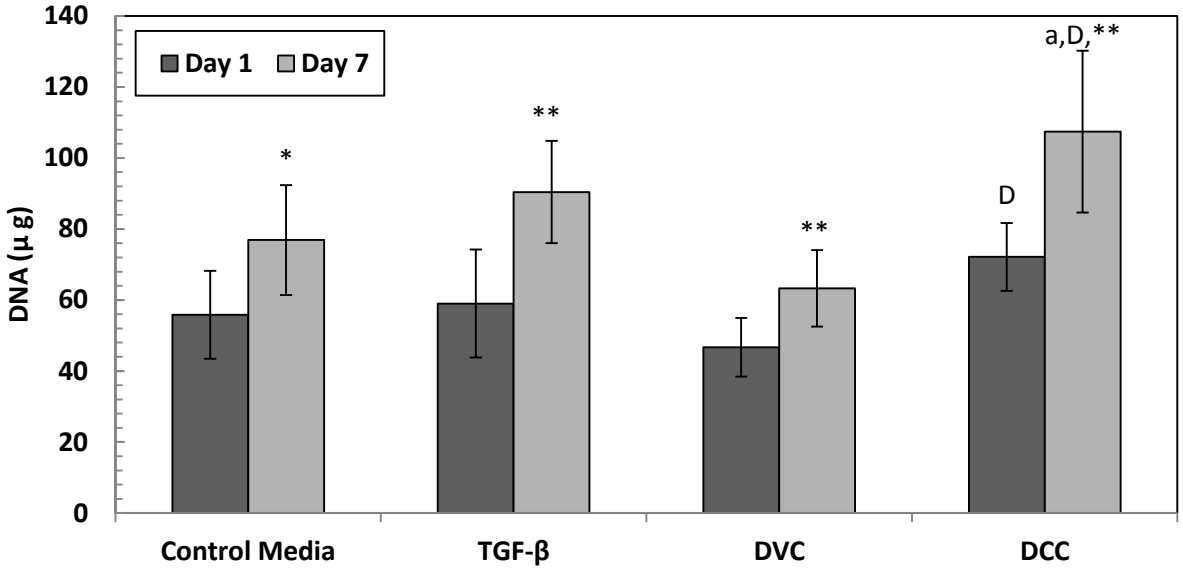

Figure 5.1: One week cell attachment (Day 1) and viability (Day 7) study comparing DCC treated cells to control media, chondrogenic media (TGF-β), and DVC. Initial seeding density was 500,000 cells/well. Overall DNA mass significantly increased for all groups from day 1 to day 7 (* = $p < 0.05$; ** = $p < 0.01$) (n = 6). DCC exhibited significantly higher DNA than DVC (Day 1) (d = $p < 0.05$; D = $p < 0.01$) and compared to control (Day 7) (a = $p < 0.05$; A = $p < 0.01$) and DVC groups. No significant difference was observed between DCC and TGF-β (b = $p < 0.05$; B = $p < 0.01$). Values represent averages ± 95% confidence intervals.

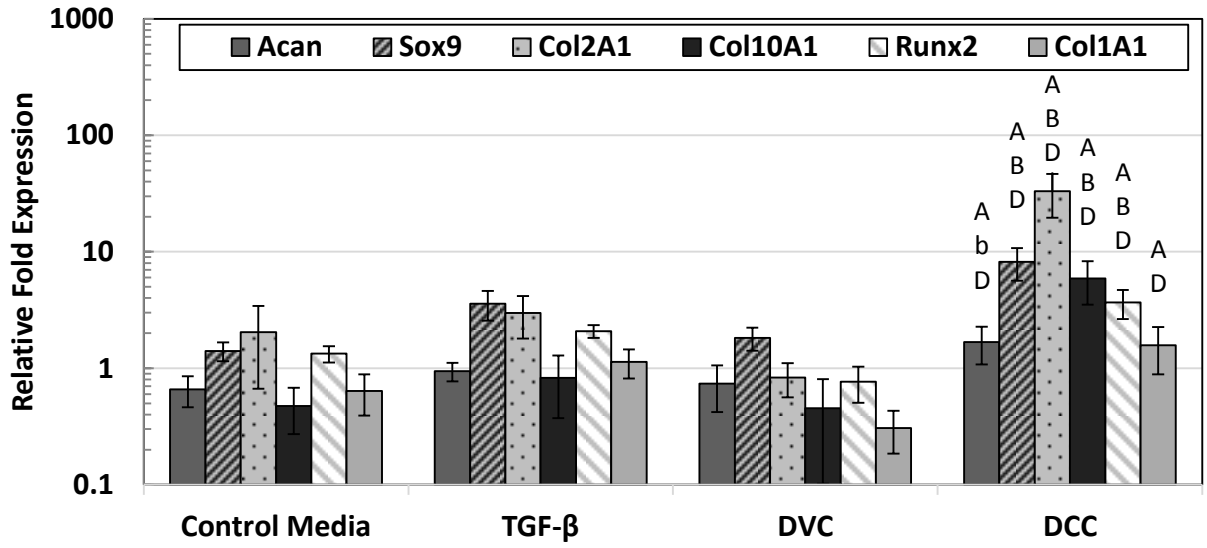

Figure 5.2: Endochondral gene expression profiles of BMSCs treated with DCC compared to control media, chondrogenic media (TGF-β), and DVC averaged over a one week span (Day 1, 3, and 7) (n = 15). DCC exhibited significantly higher expression for all tested genes compared to control media (a = $p < 0.05$; A = $p < 0.01$), TGF-β (b = $p < 0.05$; B = $p < 0.01$), and DVC (d = $p < 0.05$; D = $p < 0.01$) with the exception of *Col1A1* expression compared to TGF-β. DCC, DVC, and TGF-β all exhibited significantly higher *Sox9* expression relative to *RunX2* ($p < 0.01$). Values represent averages ± 95% confidence intervals.

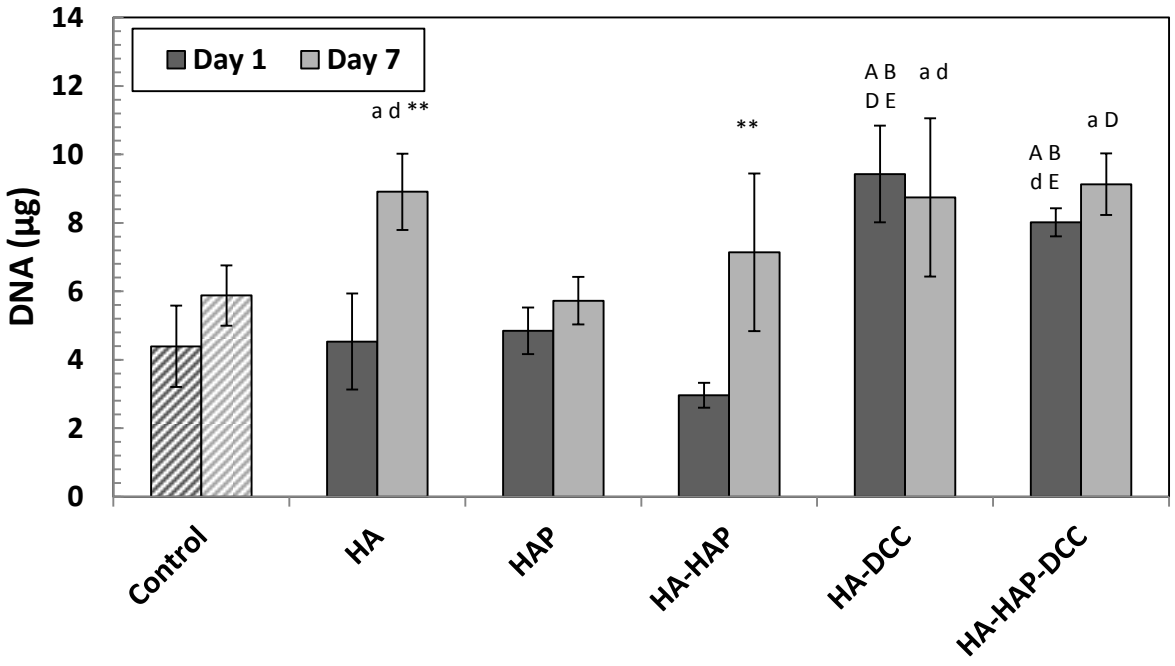

Figure 5.3: One week cell attachment (Day 1) and viability (Day 7) study comparing the effects of HA, HAP, and DCC compared to control media. Initial seeding density was 95,000 cells/well. Overall DNA mass was statistically equivalent or significantly higher for all groups from day 1 to day 7 (* = $p < 0.05$; ** = $p < 0.01$) (n = 6). DCC treated groups exhibited significantly higher DNA mass at Day 1 and Day 7 compared to control media (a = $p < 0.05$; A = $p < 0.01$), HA (b = $p < 0.05$; B = $p < 0.01$), HAP (d = $p < 0.05$; D = $p < 0.01$), and HA-HAP (e = $p < 0.05$; E = $p < 0.01$). Values represent averages ± 95% confidence intervals.

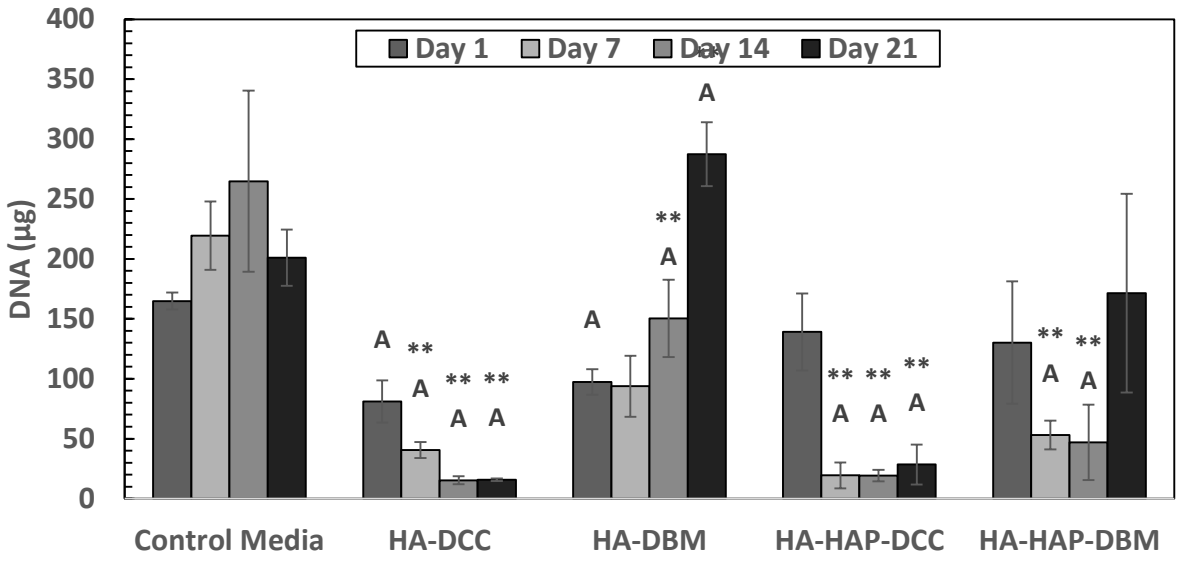

Figure 5.4: Three week cell attachment (Day 1) and viability (Day 7, 14, and 21) study comparing the effects of HAP, DCC, and DBM compared to control media. Initial seeding density was $1x10^6$ cells/well (n = 6). Overall DNA mass for each group was compared to Day 1 (* = $p < 0.05$; ** = $p < 0.01$). Only DBM loaded groups exhibited DNA increase over 21 days. All groups exhibited significantly lower DNA mass compared to control media on a treated culture plate (a = $p < 0.05$; A = $p < 0.01$) except for HA-DBM at day 21. Values represent averages ± 95% confidence intervals.

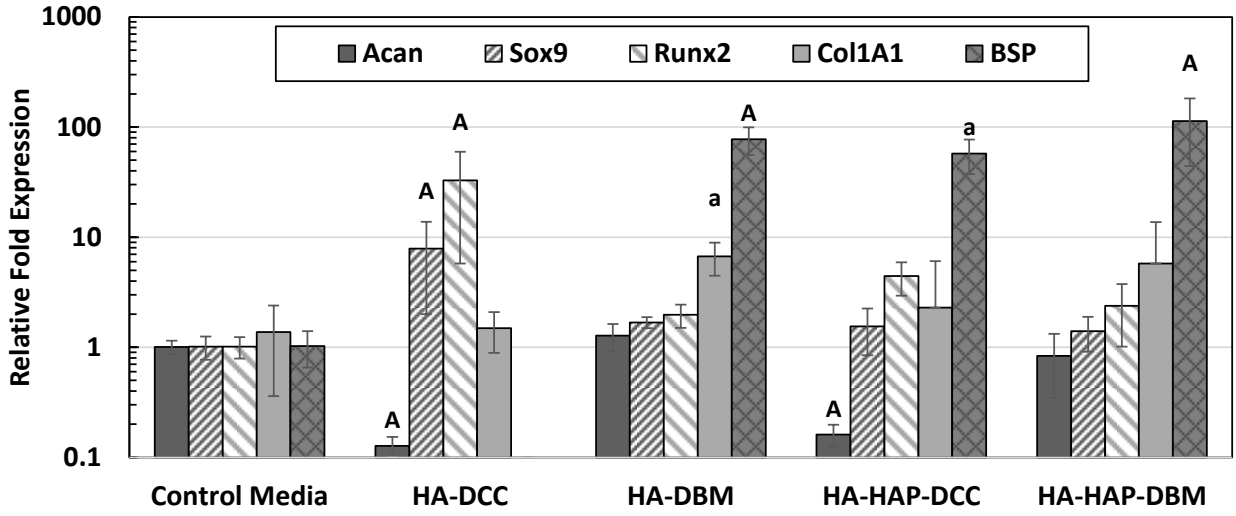

Figure 5.5: Endochondral gene expression profiles comparing the effects of DCC, DBM, and HAP to control media. Values represent averages ± 95% confidence intervals taken two weeks (Day 14) after initial cell seeding (n = 5). Poor RNA isolation from various groups prevented RT-qPCR data from being obtained on days 1, 7, and 21. HA-DCC exhibited significantly higher expression of *Sox9* and *Runx2* and significantly lower *Acan* expression compared to control media (a = $p < 0.05$; A = $p < 0.01$), suggesting that cells may be undergoing intermediate hypertrophic changes. HA-DBM exhibited significantly higher *Col1A1* and *BSP* expression compared to control media, indicating that cells might be osteogenic. The presence of HAP in both HA-HAP-DCC and HA-HAP-DBM also appeared to direct cells toward an osteogenic lineage compared to control.

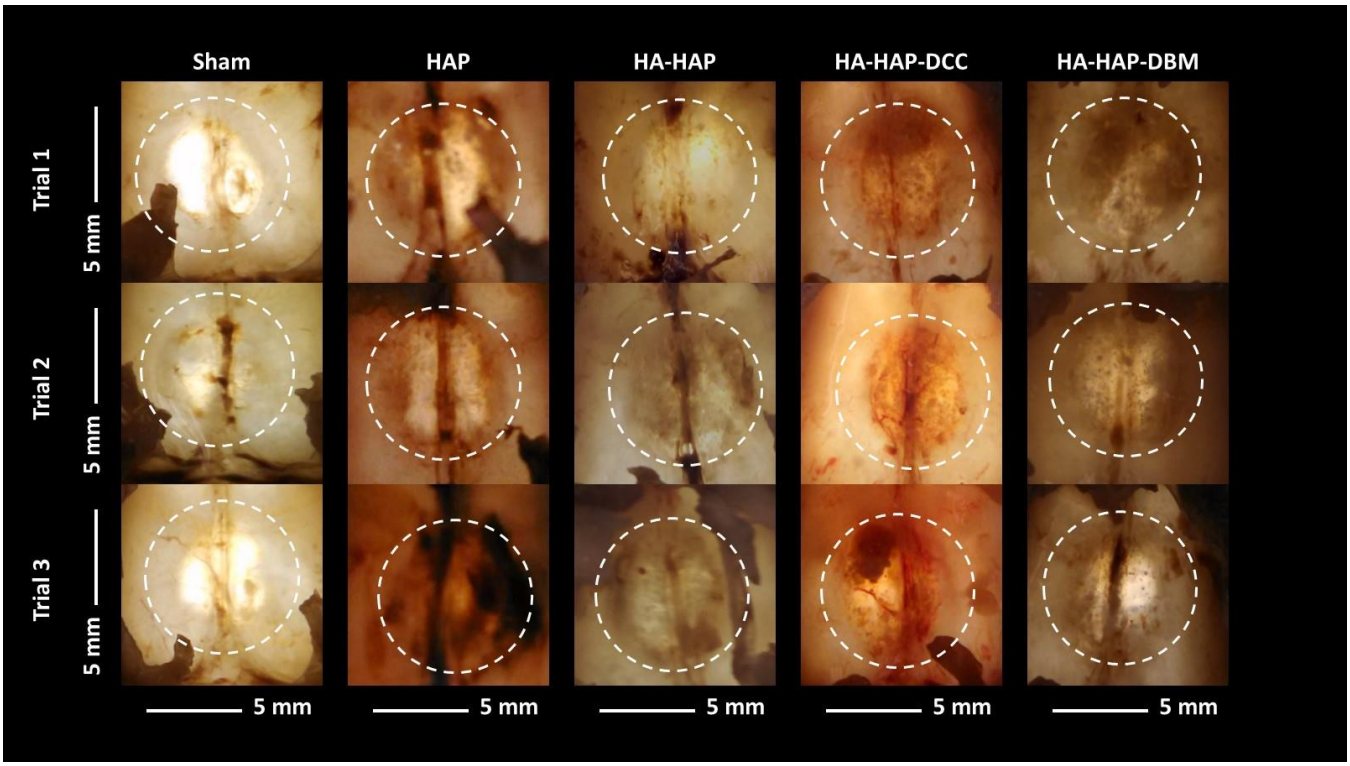

Figure 5.6: Gross anatomy images of rat calvarial defects harvested 8 weeks post-operation performed with a trephine (D = 8 mm). Images are inferior views of the defect space following dermal tissue (superior to defect) and brain tissue (inferior to defect) removal. Images are backlit to aid visualization of the defect site, and the resulting visual image was mirrored to match the superior view MicroCT images. The dotted line represents an estimation of the original defect site (D = 8 mm). The scale bar for all images was 5 mm.

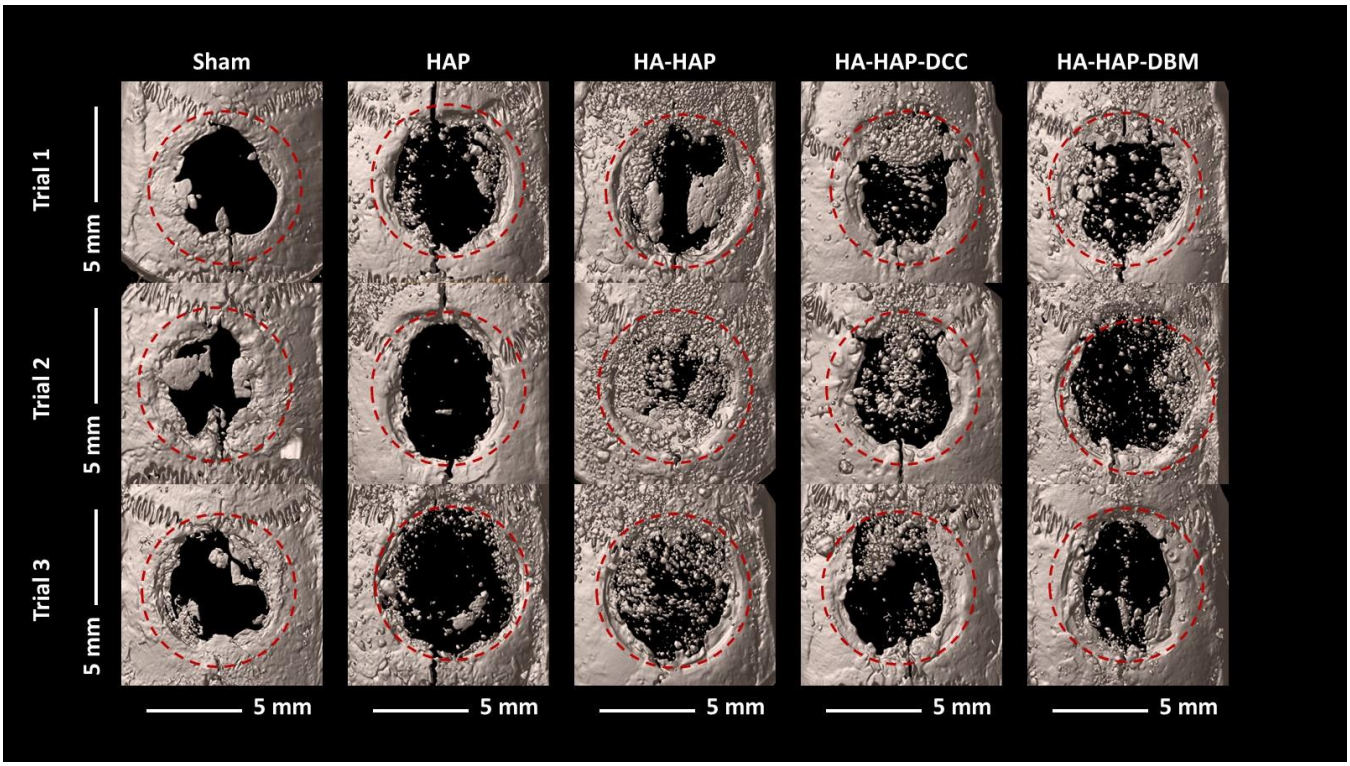

Figure 5.7: MicroCT images of rat calvarial defects performed with a trephine (D = 8 mm) and harvested 8 weeks post-operation. Images are superior views of the defect space and are virtually rendered using a shaded surface display (SSD) visualization mode. Threshold values for virtual surfaces were constant across all samples. The dotted line represents an estimation of the original defect site (D = 8 mm). The scale bar for all images was 5 mm.

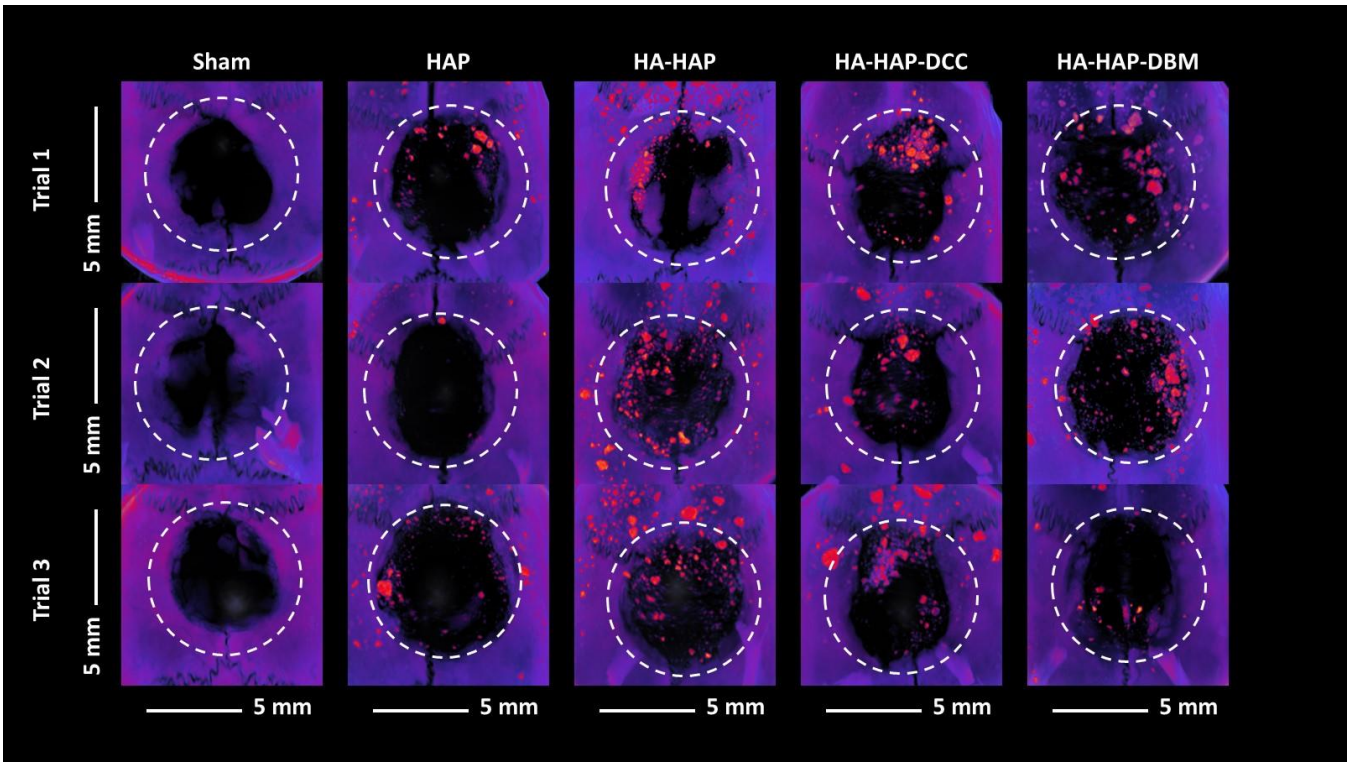

Figure 5.8: MicroCT images of rat calvarial defects performed with a trephine (D = 8 mm) and harvested 8 weeks post-operation. Images are superior views of the defect space and are virtually rendered using a volume rendering technique (VRT) visualization mode. Color and transparency mapping of virtual surfaces was controlled with a transfer function in the software (Xradia TXM3DViewer), which was held constant across all samples. The dotted line represents an estimation of the original defect site (D = 8 mm). The scale bar for all images was 5 mm.

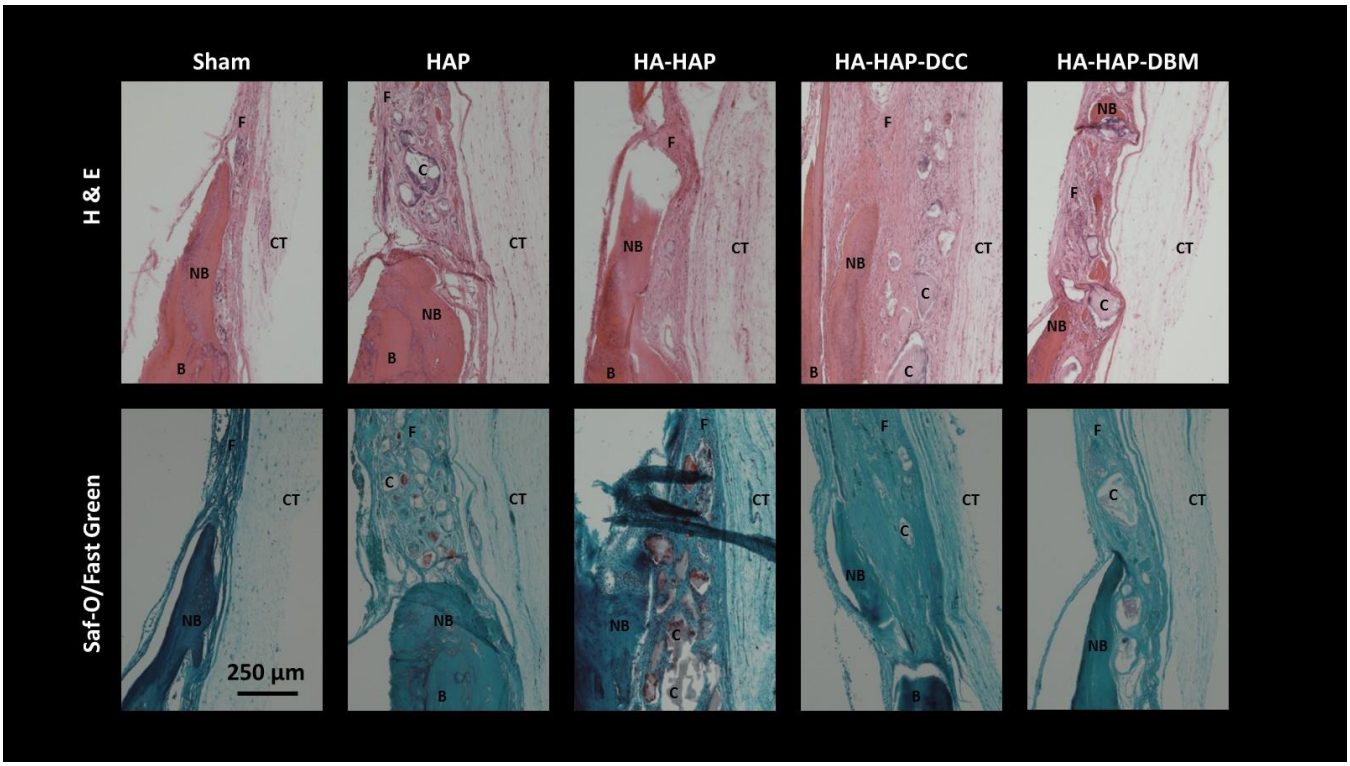

Figure 5.9: H&E and Saf-O/Fast Green histological images of rat calvarial defects corresponding to previous gross anatomy and MicroCT images (Trial 1). Images are sagittal cross-sections of the border between the defect space and native bone with left-to-right orientation representing inferior-to-superior direction. All treatment groups including sham exhibited areas of newly ossified bone, but no relative comparisons were made with histological analysis. B = native bone, C = colloidal implant material, CT = connective tissue, F = fibrous tissue, NB = new bone. The scale bar for all images was 250 µm.

APPENDIX C: REFERENCES

1. Burg, K.J., Porter, S., andKellam, J.F. Biomaterial developments for bone tissue engineering. Biomaterials **21**, 2347, 2000.

2. Frohlich, M., Grayson, W.L., Wan, L.Q., Marolt, D., Drobnic, M., andVunjak-Novakovic, G. Tissue engineered bone grafts: biological requirements, tissue culture and clinical relevance. Current stem cell research & therapy **3**, 254, 2008.

3. Mistry, A.S., andMikos, A.G. Tissue engineering strategies for bone regeneration. Advances in biochemical engineering/biotechnology **94**, 1, 2005.

4. Bohner, M. Design of ceramic-based cements and putties for bone graft substitution. European cells & materials **20**, 1, 2010.

5. Gruskin, E., Doll, B.A., Futrell, F.W., Schmitz, J.P., andHollinger, J.O. Demineralized bone matrix in bone repair: history and use. Advanced drug delivery reviews **64**, 1063, 2012.

6. Roux, R., Ladaviere, C., Montembault, A., andDelair, T. Particle assemblies: Toward new tools for regenerative medicine. Materials science & engineering C, Materials for biological applications **33**, 997, 2013.

7. Temenoff, J.S., andMikos, A.G. Injectable biodegradable materials for orthopedic tissue engineering. Biomaterials **21**, 2405, 2000.

8. Guvendiren, M., Lu, H.D., Burdick, J.A. Shear-thinning hydrogels for biomedical applications. Soft matter **8**, 260, 2012.

9. Abd El-Ghaffar, M.A., Hashem, M.S., El-Awady, M.K., andRabie, A.M. pH-sensitive sodium alginate hydrogels for riboflavin controlled release. Carbohydrate polymers **89**, 667, 2012.

10. Wang, Q., Jamal, S., Detamore, M.S., andBerkland, C. PLGA-chitosan/PLGA-alginate nanoparticle blends as biodegradable colloidal gels for seeding human umbilical cord mesenchymal stem cells. Journal of biomedical materials research Part A **96**, 520, 2011.

11. Wang, Q., Wang, J., Lu, Q., Detamore, M.S., andBerkland, C. Injectable PLGA based colloidal gels for zero-order dexamethasone release in cranial defects. Biomaterials **31**, 4980, 2010.

12. Lin, Y., Boker, A., He, J., Sill, K., Xiang, H., Abetz, C., Li, X., Wang, J., Emrick, T., Long, S., Wang, Q., Balazs, A., andRussell, T.P. Self-directed self-assembly of nanoparticle/copolymer mixtures. Nature **434**, 55, 2005.

13. Cunningham, E., Dunne, N., Walker, G., andBuchanan, F. High-solid-content hydroxyapatite slurry for the production of bone substitute scaffolds. Proceedings of the Institution of Mechanical Engineers Part H, Journal of engineering in medicine **223**, 727, 2009.

14. Huber, F.X., McArthur, N., Heimann, L., Dingeldein, E., Cavey, H., Palazzi, X., Clermont, G., andBoutrand, J.P. Evaluation of a novel nanocrystalline hydroxyapatite paste Ostim in comparison to Alpha-BSM - more bone ingrowth inside the implanted material with Ostim compared to Alpha BSM. BMC musculoskeletal disorders **10**, 164, 2009.

15. Kilfoil, M.L., Pashkovski, E.E., Masters, J.A., andWeitz, D.A. Dynamics of weakly aggregated colloidal particles. Philosophical transactions Series A, Mathematical, physical, and engineering sciences **361**, 753, 2003.

16. Wang, H., Hansen, M.B., Lowik, D.W., van Hest, J.C., Li, Y., Jansen, J.A., andLeeuwenburgh, S.C. Oppositely charged gelatin nanospheres as building blocks for injectable and biodegradable gels. Advanced materials **23**, H119, 2011.

17. Van Tomme, S.R., van Nostrum, C.F., de Smedt, S.C., andHennink, W.E. Degradation behavior of dextran hydrogels composed of positively and negatively charged microspheres. Biomaterials **27**, 4141, 2006.

18. Van Tomme, S.R., van Steenbergen, M.J., De Smedt, S.C., van Nostrum, C.F., andHennink, W.E. Self-gelling hydrogels based on oppositely charged dextran microspheres. Biomaterials **26**, 2129, 2005.

19. Wang, H., Boerman, O.C., Sariibrahimoglu, K., Li, Y., Jansen, J.A., andLeeuwenburgh, S.C. Comparison of micro- vs. nanostructured colloidal gelatin gels for sustained delivery of osteogenic proteins: Bone morphogenetic protein-2 and alkaline phosphatase. Biomaterials **33**, 8695, 2012.

20. Wang, H., Zou, Q., Boerman, O.C., Nijhuis, A.W., Jansen, J.A., Li, Y., andLeeuwenburgh, S.C. Combined delivery of BMP-2 and bFGF from nanostructured colloidal gelatin gels and its effect on bone regeneration in vivo. Journal of controlled release : official journal of the Controlled Release Society **166**, 172, 2013.

21. Detsch, R., Hagmeyer, D., Neumann, M., Schaefer, S., Vortkamp, A., Wuelling, M., Ziegler, G., andEpple, M. The resorption of nanocrystalline calcium phosphates by osteoclast-like cells. Acta biomaterialia **6**, 3223, 2010.

22. Dorozhkin, S.V. Nanosized and nanocrystalline calcium orthophosphates. Acta biomaterialia **6**, 715, 2010.

23. Huber, F.X., Hillmeier, J., Kock, H.J., McArthur, N., Huber, C., Diwo, M., Baier, M., andMeeder, P.J. [Filling of metaphyseal defects with nanocrystalline hydroxyapatite (Ostim) for fractures of the radius]. Zentralblatt fur Chirurgie **133**, 577, 2008.

24. Tadic, D., andEpple, M. A thorough physicochemical characterisation of 14 calcium phosphate-based bone substitution materials in comparison to natural bone. Biomaterials **25**, 987, 2004.

25. Thorwarth, M., Schultze-Mosgau, S., Kessler, P., Wiltfang, J., andSchlegel, K.A. Bone regeneration in osseous defects using a resorbable nanoparticular hydroxyapatite. Journal of oral and maxillofacial surgery : official journal of the American Association of Oral and Maxillofacial Surgeons **63**, 1626, 2005.

26. Zhao, L., Weir, M.D., andXu, H.H. An injectable calcium phosphate-alginate hydrogel-umbilical cord mesenchymal stem cell paste for bone tissue engineering. Biomaterials **31**, 6502, 2010.

27. Habib, M., Baroud, G., Gitzhofer, F., andBohner, M. Mechanisms underlying the limited injectability of hydraulic calcium phosphate paste. Part II: particle separation study. Acta biomaterialia **6**, 250, 2010.

28. Verma, N.P., andSinha, A. Effect of solid to liquid ratio on the physical properties of injectable nanohydroxyapatite. Journal of materials science Materials in medicine **24**, 53, 2013.

29. Balazs, A.C., Emrick, T., andRussell, T.P. Nanoparticle polymer composites: where two small worlds meet. Science **314**, 1107, 2006.

30. Huang, Z., Tian, J., Yu, B., Xu, Y., andFeng, Q. A bone-like nano-hydroxyapatite/collagen loaded injectable scaffold. Biomedical materials **4**, 055005, 2009.

31. Laurati, M., Petekidis, G., Koumakis, N., Cardinaux, F., Schofield, A.B., Brader, J.M., Fuchs, M., andEgelhaaf, S.U. Structure, dynamics, and rheology of colloid-polymer mixtures: from liquids to gels. The Journal of chemical physics **130**, 134907, 2009.

32. Sundaram, H., Voigts, B., Beer, K., andMeland, M. Comparison of the rheological properties of viscosity and elasticity in two categories of soft tissue fillers: calcium hydroxylapatite and hyaluronic acid. Dermatologic surgery : official publication for American Society for Dermatologic Surgery [et al] **36 Suppl 3**, 1859, 2010.

33. Surve, M., Pryamitsyn, V., andGanesan, V. Polymer-bridged gels of nanoparticles in solutions of adsorbing polymers. The Journal of chemical physics **125**, 64903, 2006.

34. Surve, M., Pryamitsyn, V., andGanesan, V. Universality in structure and elasticity of polymer-nanoparticle gels. Physical review letters **96**, 177805, 2006.

35. Surve, M., Pryamitsyn, V., andGanesan, V. Nanoparticles in solutions of adsorbing polymers: pair interactions, percolation, and phase behavior. Langmuir : the ACS journal of surfaces and colloids **22**, 969, 2006.

36. Tian, X.Y., Li, M.G., Cao, N., Li, J.W., andChen, X.B. Characterization of the flow behavior of alginate/hydroxyapatite mixtures for tissue scaffold fabrication. Biofabrication **1**, 045005, 2009.

37. Berriaud, N., Milas, M., andRinaudo, M. Rheological study on mixtures of different molecular weight hyaluronates. International journal of biological macromolecules **16**, 137, 1994.

38. Matteini, P., Dei, L., Carretti, E., Volpi, N., Goti, A., andPini, R. Structural behavior of highly concentrated hyaluronan. Biomacromolecules **10**, 1516, 2009.

39. Seyrek, E., andDubin, P. Glycosaminoglycans as polyelectrolytes. Advances in colloid and interface science **158**, 119, 2010.

40. Volpi, N., Schiller, J., Stern, R., andSoltes, L. Role, metabolism, chemical modifications and applications of hyaluronan. Current medicinal chemistry **16**, 1718, 2009.

41. Roux, R., Ladaviere, C., Montembault, A., David, L., andDelair, T. Shear Thinning Three-Dimensional Colloidal Assemblies of Chitosan and Poly(lactic acid) Nanoparticles. The journal of physical chemistry B **117**, 7455, 2013.

42. Stocks, D., Sundaram, H., Michaels, J., Durrani, M.J., Wortzman, M.S., andNelson, D.B. Rheological evaluation of the physical properties of hyaluronic acid dermal fillers. Journal of drugs in dermatology : JDD **10**, 974, 2011.

43. Silbert, J.E., andSugumaran, G. Biosynthesis of chondroitin/dermatan sulfate. IUBMB life **54**, 177, 2002.

44. Buzzega, D., Maccari, F., andVolpi, N. Determination of molecular mass values of chondroitin sulfates by fluorophore-assisted carbohydrate electrophoresis (FACE). Journal of pharmaceutical and biomedical analysis **51**, 969, 2010.

45. Lim, J.J., Hammoudi, T.M., Bratt-Leal, A.M., Hamilton, S.K., Kepple, K.L., Bloodworth, N.C., McDevitt, T.C., andTemenoff, J.S. Development of nano- and microscale chondroitin sulfate particles for controlled growth factor delivery. Acta biomaterialia **7**, 986, 2011.

46. Lu, H.D., Charati, M.B., Kim, I.L., andBurdick, J.A. Injectable shear-thinning hydrogels engineered with a self-assembling Dock-and-Lock mechanism. Biomaterials **33**, 2145, 2012.

47. Holland, T.A., Tabata, Y., andMikos, A.G. In vitro release of transforming growth factor-beta 1 from gelatin microparticles encapsulated in biodegradable, injectable oligo(poly(ethylene glycol) fumarate) hydrogels. Journal of controlled release : official journal of the Controlled Release Society **91**, 299, 2003.

48. Ozbas, B., Rajagopal, K., Haines-Butterick, L., Schneider, J.P., andPochan, D.J. Reversible stiffening transition in beta-hairpin hydrogels induced by ion complexation. The journal of physical chemistry B **111**, 13901, 2007.

49. Moller, P.C.F., Mewis, J., andBonn, D. Yield stress and thixotropy: on the difficulty of measuring yield stresses in practice. Soft matter **2**, 274, 2006.

50. LeGeros, R.Z. Properties of osteoconductive biomaterials: calcium phosphates. Clinical orthopaedics and related research, 81, 2002.

51. Supova, M. Problem of hydroxyapatite dispersion in polymer matrices: a review. Journal of materials science Materials in medicine **20**, 1201, 2009.

52. Swetha, M., Sahithi, K., Moorthi, A., Srinivasan, N., Ramasamy, K., andSelvamurugan, N. Biocomposites containing natural polymers and hydroxyapatite for bone tissue engineering. International journal of biological macromolecules **47**, 1, 2010.

53. Bao, X.a.P., Y. X. Influence of temperature, ripening time and calcination on the morphology and crystallinity of hydroxyapatite nanoparticles. Journal of the European Ceramic Society **23**, 1697, 2002.

54. Murugan, R., andRamakrishna, S. Bioresorbable composite bone paste using polysaccharide based nano hydroxyapatite. Biomaterials **25**, 3829, 2004.

55. Bao, Y., Senos, A.M., Almeida, M., andGauckler, L.J. Rheological behavior of aqueous suspensions of hydroxyapatite (HAP). Journal of materials science Materials in medicine **13**, 639, 2002.

56. Gardini, D., Galassi, C. Rheology of Hydoxyapatite Dispersions. Journal of the American Ceramic Society **88**, 271, 2005.

57. Larson, R.G. The Structure and Rheology of Complex Fluids. New York, New York: Oxford University Press; 1999.

58. Asakura, S., andOosawa, F. Interaction between Particles Suspended in Solutions of Macromolecules. J Polym Sci **33**, 183, 1958.

59. Jenkins, P., andSnowden, M. Depletion flocculation in colloidal dispersions. Advances in colloid and interface science **68**, 57, 1996.

60. Otsubo, Y. Rheology Control of Suspensions by Soluble Polymers. Langmuir : the ACS journal of surfaces and colloids **11**, 1893, 1995.

61. Wen, Y.H., Lin, P.C., Lee, C.Y., Hua, C.C., andLee, T.C. Reduced colloidal repulsion imparted by adsorbed polymer of particle dimensions. Journal of colloid and interface science **349**, 134, 2010.

62. Segre, P.N., Meeker, S.P., Pusey, P.N., andPoon, W.C.K. Viscosity and Structural Relaxation in Suspensions of Hard-Sphere Colloids. Physical review letters **75**, 958, 1995.

63. Roux, R., Ladaviere, C., Montembault, A., Delair T. Paricle Assemblies: Toward new tools for regenerative medicine. Materials Science and Engineering C **33**, 997, 2013.

64. Choi, G.N., andKrieger, I.M. Rheological Studies on Sterically Stabilized Dispersions of Uniform Colloidal Spheres. Journal of colloid and interface science **113**, 94, 1986.

65. Einhorn, T.A. The science of fracture healing. Journal of orthopaedic trauma **19**, S4, 2005.

66. Gerstenfeld, L.C., Cullinane, D.M., Barnes, G.L., Graves, D.T., andEinhorn, T.A. Fracture healing as a post-natal developmental process: molecular, spatial, and temporal aspects of its regulation. J Cell Biochem **88**, 873, 2003.

67. Kalfas, I.H. Principles of bone healing. Neurosurgical focus **10**, E1, 2001.

68. Meyer, U., Weismann, H. P. . Bone and Cartilage. Bone and Cartilage Engineering. New York, NY: Springer; 2006. pp. 7.

69. Miclau, T., Schneider, R.A., Eames, B.F., Helms, J.A. Common Molecular Mechanisms Regulating Fetal Bone Formation and Adult Fracture Repair. In: Lieberman J.R., Friedlaender, G.

E., ed. Bone Regeneration and Repair: Biology and Clinical Application. Totowa, NJ: Humana Press Inc.; 2005. pp. 45.

70. Sfeir, C., Ho, L., Doll, B.A., Azari, K., Hollinger, J.O. Fracture Repair. In: Lieberman J.R., Friedlaender, G. E., ed. Bone Regeneration and Repair: Biology and Clinical Applications. Totowa, NJ: Humana Press Inc.; 2005. pp. 21.

71. Mehta, M., Schmidt-Bleek, K., Duda, G.N., andMooney, D.J. Biomaterial delivery of morphogens to mimic the natural healing cascade in bone. Advanced drug delivery reviews **64**, 1257, 2012.

72. Schindeler, A., McDonald, M.M., Bokko, P., andLittle, D.G. Bone remodeling during fracture repair: The cellular picture. Seminars in cell & developmental biology **19**, 459, 2008.

73. Mackie, E.J., Ahmed, Y.A., Tatarczuch, L., Chen, K.S., andMirams, M. Endochondral ossification: how cartilage is converted into bone in the developing skeleton. The international journal of biochemistry & cell biology **40**, 46, 2008.

74. Lu, C., Miclau, T., Hu, D., Hansen, E., Tsui, K., Puttlitz, C., andMarcucio, R.S. Cellular basis for age-related changes in fracture repair. Journal of orthopaedic research : official publication of the Orthopaedic Research Society **23**, 1300, 2005.

75. Jaklenec, A., Stamp, A., Deweerd, E., Sherwin, A., andLanger, R. Progress in the tissue engineering and stem cell industry "are we there yet?". Tissue engineering Part B, Reviews **18**, 155, 2012.

76. Badylak, S.F. The extracellular matrix as a biologic scaffold material. Biomaterials **28**, 3587, 2007.

77. Benders, K.E., van Weeren, P.R., Badylak, S.F., Saris, D.B., Dhert, W.J., andMalda, J. Extracellular matrix scaffolds for cartilage and bone regeneration. Trends in biotechnology **31**, 169, 2013.

78. Gilbert, T.W., Sellaro, T.L., andBadylak, S.F. Decellularization of tissues and organs. Biomaterials **27**, 3675, 2006.

79. Renth, A.N., andDetamore, M.S. Leveraging "raw materials" as building blocks and bioactive signals in regenerative medicine. Tissue engineering Part B, Reviews **18**, 341, 2012.

80. Tsang, K.Y., Cheung, M.C., Chan, D., andCheah, K.S. The developmental roles of the extracellular matrix: beyond structure to regulation. Cell and tissue research **339**, 93, 2010.

81. Lenas, P., Moos, M., andLuyten, F.P. Developmental engineering: a new paradigm for the design and manufacturing of cell-based products. Part II: from genes to networks: tissue engineering from the viewpoint of systems biology and network science. Tissue engineering Part B, Reviews **15**, 395, 2009.

82. Lenas, P., Moos, M., andLuyten, F.P. Developmental engineering: a new paradigm for the design and manufacturing of cell-based products. Part I: from three-dimensional cell growth to biomimetics of in vivo development. Tissue engineering Part B, Reviews **15**, 381, 2009.

83. Hollister, S.J., andMurphy, W.L. Scaffold translation: barriers between concept and clinic. Tissue engineering Part B, Reviews **17**, 459, 2011.

84. Jakob, M., Saxer, F., Scotti, C., Schreiner, S., Studer, P., Scherberich, A., Heberer, M., andMartin, I. Perspective on the evolution of cell-based bone tissue engineering strategies. European surgical research Europaische chirurgische Forschung Recherches chirurgicales europeennes **49**, 1, 2012.

85. Oakes, D.A., Lee, C.C., andLieberman, J.R. An evaluation of human demineralized bone matrices in a rat femoral defect model. Clinical orthopaedics and related research, 281, 2003.

86. Montufar-Solis, D., Nguyen, H.C., Nguyen, H.D., Horn, W.N., Cody, D.D., andDuke, P.J. Using cartilage to repair bone: an alternative approach in tissue engineering. Annals of biomedical engineering **32**, 504, 2004.

87. Rabie, A.B., Chay, S.H., andWong, A.M. Healing of autogenous intramembranous bone in the presence and absence of homologous demineralized intramembranous bone. American journal of orthodontics and dentofacial orthopedics : official publication of the American Association of Orthodontists, its constituent societies, and the American Board of Orthodontics **117**, 288, 2000.

88. Wang, J., Glimcher, M.J., Mah, J., Zhou, H.Y., andSalih, E. Expression of bone microsomal casein kinase II, bone sialoprotein, and osteopontin during the repair of calvarial defects. Bone **22**, 621, 1998.

89. Rabie, A.B., Dan, Z., andSamman, N. Ultrastructural identification of cells involved in the healing of intramembranous and endochondral bones. International journal of oral and maxillofacial surgery **25**, 383, 1996.

90. Rabie, A.B., andLie Ken Jie, R.K. Integration of endochondral bone grafts in the presence of demineralized bone matrix. International journal of oral and maxillofacial surgery **25**, 311, 1996.

91. Rabie, A.B., Wong, R.W., andHagg, U. Composite autogenous bone and demineralized bone matrices used to repair defects in the parietal bone of rabbits. The British journal of oral & maxillofacial surgery **38**, 565, 2000.

92. Dimitriou, R., Tsiridis, E., andGiannoudis, P.V. Current concepts of molecular aspects of bone healing. Injury **36**, 1392, 2005.

93. Studer, D., Millan, C., Ozturk, E., Maniura-Weber, K., andZenobi-Wong, M. Molecular and Biophysical Mechanisms Regulating Hypertrophic Differentiation in Chondrocytes and Mesenchymal Stem Cells. European cells & materials **24**, 118, 2012.

94. Carmeliet, P., andJain, R.K. Molecular mechanisms and clinical applications of angiogenesis. Nature **473**, 298, 2011.

95. Centola, M., Abbruzzese, F., Scotti, C., Barbero, A., Vadala, G., Denaro, V., Martin, I., Trombetta, M., Rainer, A., andMarsano, A. Scaffold-based delivery of a clinically relevant anti-angiogenic drug promotes the formation of in vivo stable cartilage. Tissue engineering Part A **19**, 1960, 2013.

96. des Rieux, A., Ucakar, B., Mupendwa, B.P., Colau, D., Feron, O., Carmeliet, P., andPreat, V. 3D systems delivering VEGF to promote angiogenesis for tissue engineering. Journal of controlled release : official journal of the Controlled Release Society **150**, 272, 2011.

97. Zhou, Z., Apte, S.S., Soininen, R., Cao, R., Baaklini, G.Y., Rauser, R.W., Wang, J., Cao, Y., andTryggvason, K. Impaired endochondral ossification and angiogenesis in mice deficient in membrane-type matrix metalloproteinase I. Proceedings of the National Academy of Sciences of the United States of America **97**, 4052, 2000.

98. Malda, J., Klein, T.J., andUpton, Z. The roles of hypoxia in the in vitro engineering of tissues. Tissue engineering **13**, 2153, 2007.

99. Sheehy, E.J., Buckley, C.T., andKelly, D.J. Oxygen tension regulates the osteogenic, chondrogenic and endochondral phenotype of bone marrow derived mesenchymal stem cells. Biochemical and biophysical research communications **417**, 305, 2012.

100. Gawlitta, D., Farrell, E., Malda, J., Creemers, L.B., Alblas, J., andDhert, W.J. Modulating endochondral ossification of multipotent stromal cells for bone regeneration. Tissue engineering Part B, Reviews **16**, 385, 2010.

101. Lewis, M.C., Macarthur, B.D., Malda, J., Pettet, G., andPlease, C.P. Heterogeneous proliferation within engineered cartilaginous tissue: the role of oxygen tension. Biotechnology and bioengineering **91**, 607, 2005.

102. Scotti, C., Osmokrovic, A., Wolf, F., Miot, S., Peretti, G.M., Barbero, A., andMartin, I. Response of human engineered cartilage based on articular or nasal chondrocytes to interleukin-1beta and low oxygen. Tissue engineering Part A **18**, 362, 2012.

103. Scott, C.K., andHightower, J.A. The matrix of endochondral bone differs from the matrix of intramembranous bone. Calcified tissue international **49**, 349, 1991.

104. Discher, D.E., Mooney, D.J., andZandstra, P.W. Growth factors, matrices, and forces combine and control stem cells. Science **324**, 1673, 2009.

105. Anitua, E., Sanchez, M., andOrive, G. Potential of endogenous regenerative technology for in situ regenerative medicine. Advanced drug delivery reviews **62**, 741, 2010.

106. Chen, F.M., Zhang, J., Zhang, M., An, Y., Chen, F., andWu, Z.F. A review on endogenous regenerative technology in periodontal regenerative medicine. Biomaterials **31**, 7892, 2010.

107. Dare, E.V., Griffith, M., Poitras, P., Wang, T., Dervin, G.F., Giulivi, A., andHincke, M.T. Fibrin sealants from fresh or fresh/frozen plasma as scaffolds for in vitro articular cartilage regeneration. Tissue engineering Part A **15**, 2285, 2009.

108. Eyrich, D., Brandl, F., Appel, B., Wiese, H., Maier, G., Wenzel, M., Staudenmaier, R., Goepferich, A., andBlunk, T. Long-term stable fibrin gels for cartilage engineering. Biomaterials **28**, 55, 2007.

109. Eyrich, D., Gopferich, A., andBlunk, T. Fibrin in tissue engineering. Advances in experimental medicine and biology **585**, 379, 2006.

110. Grageda, E. Platelet-rich plasma and bone graft materials: a review and a standardized research protocol. Implant dentistry **13**, 301, 2004.

111. Kaufman, M.R., Westreich, R., Ammar, S.M., Amirali, A., Iskander, A., andLawson, W. Autologous cartilage grafts enhanced by a novel transplant medium using fibrin sealant and fibroblast growth factor. Archives of facial plastic surgery **6**, 94, 2004.

112. Mazor, Z., Peleg, M., Garg, A.K., andLuboshitz, J. Platelet-rich plasma for bone graft enhancement in sinus floor augmentation with simultaneous implant placement: patient series study. Implant dentistry **13**, 65, 2004.

113. Santos, S.G., Lamghari, M., Almeida, C.R., Oliveira, M.I., Neves, N., Ribeiro, A.C., Barbosa, J.N., Barros, R., Maciel, J., Martins, M.C.L., Goncalves, R.M., andBarbosa, M.A. Adsorbed fibrinogen leads to improved bone regeneration and correlates with differences in the systemic immune response. Acta biomaterialia **9**, 7209, 2013.

114. Singh, M., Berkland, C., andDetamore, M.S. Strategies and applications for incorporating physical and chemical signal gradients in tissue engineering. Tissue engineering Part B, Reviews **14**, 341, 2008.

115. Lee, S.H., andShin, H. Matrices and scaffolds for delivery of bioactive molecules in bone and cartilage tissue engineering. Advanced drug delivery reviews **59**, 339, 2007.

116. Pelttari, K., Steck, E., andRichter, W. The use of mesenchymal stem cells for chondrogenesis. Injury **39 Suppl 1**, S58, 2008.

117. Jukes, J.M., Moroni, L., van Blitterswijk, C.A., andde Boer, J. Critical Steps toward a tissue-engineered cartilage implant using embryonic stem cells. Tissue engineering Part A **14**, 135, 2008.

118. Sundelacruz, S., andKaplan, D.L. Stem cell- and scaffold-based tissue engineering approaches to osteochondral regenerative medicine. Seminars in cell & developmental biology **20**, 646, 2009.

119. Sheehy, E.J., Vinardell, T., Buckley, C.T., andKelly, D.J. Engineering osteochondral constructs through spatial regulation of endochondral ossification. Acta biomaterialia **9**, 5484, 2013.

120. Case, N.D., Duty, A.O., Ratcliffe, A., Muller, R., andGuldberg, R.E. Bone formation on tissue-engineered cartilage constructs in vivo: effects of chondrocyte viability and mechanical loading. Tissue engineering **9**, 587, 2003.

121. Doan, L., Kelley, C., Luong, H., English, J., Gomez, H., Johnson, E., Cody, D., andDuke, P.J. Engineered cartilage heals skull defects. American journal of orthodontics and dentofacial orthopedics : official publication of the American Association of Orthodontists, its constituent societies, and the American Board of Orthodontics **137**, 162 e1, 2010.

122. Farrell, E., Both, S.K., Odorfer, K.I., Koevoet, W., Kops, N., O'Brien, F.J., Baatenburg de Jong, R.J., Verhaar, J.A., Cuijpers, V., Jansen, J., Erben, R.G., andvan Osch, G.J. In-vivo generation of bone via endochondral ossification by in-vitro chondrogenic priming of adult human and rat mesenchymal stem cells. BMC musculoskeletal disorders **12**, 31, 2011.

123. Farrell, E., van der Jagt, O.P., Koevoet, W., Kops, N., van Manen, C.J., Hellingman, C.A., Jahr, H., O'Brien, F.J., Verhaar, J.A., Weinans, H., andvan Osch, G.J. Chondrogenic priming of human bone marrow stromal cells: a better route to bone repair? Tissue engineering Part C, Methods **15**, 285, 2009.

124. Janicki, P., Boeuf, S., Steck, E., Egermann, M., Kasten, P., andRichter, W. Prediction of in vivo bone forming potency of bone marrow-derived human mesenchymal stem cells. European cells & materials **21**, 488, 2011.

125. Janicki, P., Kasten, P., Kleinschmidt, K., Luginbuehl, R., andRichter, W. Chondrogenic pre-induction of human mesenchymal stem cells on beta-TCP: enhanced bone quality by endochondral heterotopic bone formation. Acta biomaterialia **6**, 3292, 2010.

126. Jukes, J.M., Both, S.K., Leusink, A., Sterk, L.M., van Blitterswijk, C.A., andde Boer, J. Endochondral bone tissue engineering using embryonic stem cells. Proceedings of the National Academy of Sciences of the United States of America **105**, 6840, 2008.

127. Jukes, J.M., van Blitterswijk, C.A., andde Boer, J. Skeletal tissue engineering using embryonic stem cells. Journal of tissue engineering and regenerative medicine **4**, 165, 2010.

128. Li, J., andPei, M. Optimization of an in vitro three-dimensional microenvironment to reprogram synovium-derived stem cells for cartilage tissue engineering. Tissue engineering Part A **17**, 703, 2011.

129. Oliveira, S.M., Amaral, I.F., Barbosa, M.A., andTeixeira, C.C. Engineering endochondral bone: in vitro studies. Tissue engineering Part A **15**, 625, 2009.

130. Oliveira, S.M., Mijares, D.Q., Turner, G., Amaral, I.F., Barbosa, M.A., andTeixeira, C.C. Engineering endochondral bone: in vivo studies. Tissue engineering Part A **15**, 635, 2009.

131. Pelttari, K., Winter, A., Steck, E., Goetzke, K., Hennig, T., Ochs, B.G., Aigner, T., andRichter, W. Premature induction of hypertrophy during in vitro chondrogenesis of human mesenchymal stem cells correlates with calcification and vascular invasion after ectopic transplantation in SCID mice. Arthritis Rheum **54**, 3254, 2006.

132. Scotti, C., Piccinini, E., Takizawa, H., Todorov, A., Bourgine, P., Papadimitropoulos, A., Barbero, A., Manz, M.G., andMartin, I. Engineering of a functional bone organ through endochondral ossification. Proceedings of the National Academy of Sciences of the United States of America **110**, 3997, 2013.

133. Scotti, C., Tonnarelli, B., Papadimitropoulos, A., Scherberich, A., Schaeren, S., Schauerte, A., Lopez-Rios, J., Zeller, R., Barbero, A., andMartin, I. Recapitulation of endochondral bone formation using human adult mesenchymal stem cells as a paradigm for developmental engineering. Proceedings of the National Academy of Sciences of the United States of America **107**, 7251, 2010.

134. Vinardell, T., Sheehy, E.J., Buckley, C.T., andKelly, D.J. A comparison of the functionality and in vivo phenotypic stability of cartilaginous tissues engineered from different stem cell sources. Tissue engineering Part A **18**, 1161, 2012.

135. Both, S.K., van Apeldoorn, A.A., Jukes, J.M., Englund, M.C., Hyllner, J., van Blitterswijk, C.A., andde Boer, J. Differential bone-forming capacity of osteogenic cells from either embryonic stem cells or bone marrow-derived mesenchymal stem cells. Journal of tissue engineering and regenerative medicine **5**, 180, 2011.

136. Dickhut, A., Pelttari, K., Janicki, P., Wagner, W., Eckstein, V., Egermann, M., andRichter, W. Calcification or dedifferentiation: requirement to lock mesenchymal stem cells in a desired differentiation stage. Journal of cellular physiology **219**, 219, 2009.

137. Gauci, S.J., Golub, S.B., Tutolo, L., Little, C.B., Sims, N.A., Lee, E.R., Mackie, E.J., andFosang, A.J. Modulating chondrocyte hypertrophy in growth plate and osteoarthritic cartilage. Journal of musculoskeletal & neuronal interactions **8**, 308, 2008.

138. Hattori, T., Muller, C., Gebhard, S., Bauer, E., Pausch, F., Schlund, B., Bosl, M.R., Hess, A., Surmann-Schmitt, C., von der Mark, H., de Crombrugghe, B., andvon der Mark, K. SOX9 is a major negative regulator of cartilage vascularization, bone marrow formation and endochondral ossification. Development **137**, 901, 2010.

139. Inada, M., Wang, Y., Byrne, M.H., Rahman, M.U., Miyaura, C., Lopez-Otin, C., andKrane, S.M. Critical roles for collagenase-3 (Mmp13) in development of growth plate cartilage and in endochondral ossification. Proceedings of the National Academy of Sciences of the United States of America **101**, 17192, 2004.

140. Mumme, M., Scotti, C., Papadimitropoulos, A., Todorov, A., Hoffmann, W., Bocelli-Tyndall, C., Jakob, M., Wendt, D., Martin, I., andBarbero, A. Interleukin-1beta modulates endochondral ossification by human adult bone marrow stromal cells. European cells & materials **24**, 224, 2012.

141. Ortega, N., Behonick, D.J., andWerb, Z. Matrix remodeling during endochondral ossification. Trends in cell biology **14**, 86, 2004.

142. Ortega, N., Wang, K., Ferrara, N., Werb, Z., andVu, T.H. Complementary interplay between matrix metalloproteinase-9, vascular endothelial growth factor and osteoclast function drives endochondral bone formation. Disease models & mechanisms **3**, 224, 2010.

143. Page-McCaw, A., Ewald, A.J., andWerb, Z. Matrix metalloproteinases and the regulation of tissue remodelling. Nature reviews Molecular cell biology **8**, 221, 2007.

144. Stickens, D., Behonick, D.J., Ortega, N., Heyer, B., Hartenstein, B., Yu, Y., Fosang, A.J., Schorpp-Kistner, M., Angel, P., andWerb, Z. Altered endochondral bone development in matrix metalloproteinase 13-deficient mice. Development **131**, 5883, 2004.

145. Boskey, A.L., andRoy, R. Cell culture systems for studies of bone and tooth mineralization. Chemical reviews **108**, 4716, 2008.

146. Hessle, L., Johnson, K.A., Anderson, H.C., Narisawa, S., Sali, A., Goding, J.W., Terkeltaub, R., andMillan, J.L. Tissue-nonspecific alkaline phosphatase and plasma cell membrane glycoprotein-1 are central antagonistic regulators of bone mineralization. Proceedings of the National Academy of Sciences of the United States of America **99**, 9445, 2002.

147. Johnson, K., Moffa, A., Chen, Y., Pritzker, K., Goding, J., andTerkeltaub, R. Matrix vesicle plasma cell membrane glycoprotein-1 regulates mineralization by murine osteoblastic MC3T3 cells. J Bone Miner Res **14**, 883, 1999.

148. Mahmoudifar, N., andDoran, P.M. Chondrogenesis and cartilage tissue engineering: the longer road to technology development. Trends in biotechnology **30**, 166, 2012.

149. Puetzer, J.L., Petitte, J.N., andLoboa, E.G. Comparative review of growth factors for induction of three-dimensional in vitro chondrogenesis in human mesenchymal stem cells isolated from bone marrow and adipose tissue. Tissue engineering Part B, Reviews **16**, 435, 2010.

150. Crapo, P.M., Gilbert, T.W., andBadylak, S.F. An overview of tissue and whole organ decellularization processes. Biomaterials **32**, 3233, 2011.

151. Evans, C.H. Barriers to the clinical translation of orthopedic tissue engineering. Tissue engineering Part B, Reviews **17**, 437, 2011.

152. Ye, K., Felimban, R., Moulton, S.E., Wallace, G.G., Di Bella, C., Traianedes, K., Choong, P.F.M., andMyers, D.E. Bioengineering of articular cartilage: past, present and future. Regenerative medicine **8**, 333, 2013.

153. Schwarz, S., Koerber, L., Elsaesser, A.F., Goldberg-Bockhorn, E., Seitz, A.M., Durselen, L., Ignatius, A., Walther, P., Breiter, R., andRotter, N. Decellularized cartilage matrix as a novel biomatrix for cartilage tissue-engineering applications. Tissue engineering Part A **18**, 2195, 2012.

154. Sutherland, A.J., Converse, G.L., Hopkins, R.A., andDetamore, M.S. The Bioactivity of Cartilage Extracellular Matrix in Articular Cartilage Regeneration. Advanced healthcare materials 2014.

155. Wang, Q., Gu, Z., Jamal, S., Detamore, M.S., andBerkland, C. Hybrid Hydroxyapatite Nanoparticle Colloidal Gels are Injectable Fillers for Bone Tissue Engineering. Tissue engineering Part A 2013.

156. Loh, Q.L., andChoong, C. Three-dimensional scaffolds for tissue engineering applications: role of porosity and pore size. Tissue engineering Part B, Reviews **19**, 485, 2013.

157. Gamie, Z., Tran, G.T., Vyzas, G., Korres, N., Heliotis, M., Mantalaris, A., andTsiridis, E. Stem cells combined with bone graft substitutes in skeletal tissue engineering. Expert opinion on biological therapy **12**, 713, 2012.

158. Simmons, C.A., Alsberg, E., Hsiong, S., Kim, W.J., andMooney, D.J. Dual growth factor delivery and controlled scaffold degradation enhance in vivo bone formation by transplanted bone marrow stromal cells. Bone **35**, 562, 2004.

159. Yamada, Y., Boo, J.S., Ozawa, R., Nagasaka, T., Okazaki, Y., Hata, K., andUeda, M. Bone regeneration following injection of mesenchymal stem cells and fibrin glue with a biodegradable scaffold. Journal of cranio-maxillo-facial surgery : official publication of the European Association for Cranio-Maxillo-Facial Surgery **31**, 27, 2003.

160. Harada, N., Watanabe, Y., Sato, K., Abe, S., Yamanaka, K., Sakai, Y., Kaneko, T., andMatsushita, T. Bone regeneration in a massive rat femur defect through endochondral

ossification achieved with chondrogenically differentiated MSCs in a degradable scaffold. Biomaterials **35**, 7800, 2014.

161. van der Stok, J., Koolen, M.K., Jahr, H., Kops, N., Waarsing, J.H., Weinans, H., andvan der Jagt, O.P. Chondrogenically differentiated mesenchymal stromal cell pellets stimulate endochondral bone regeneration in critical-sized bone defects. European cells & materials **27**, 137, 2014.

162. Sheehy, E.J., Vinardell, T., Toner, M.E., Buckley, C.T., andKelly, D.J. Altering the architecture of tissue engineered hypertrophic cartilaginous grafts facilitates vascularisation and accelerates mineralisation. PloS one **9**, e90716, 2014.

163. Shoji, T., Ii, M., Mifune, Y., Matsumoto, T., Kawamoto, A., Kwon, S.M., Kuroda, T., Kuroda, R., Kurosaka, M., andAsahara, T. Local transplantation of human multipotent adipose-derived stem cells accelerates fracture healing via enhanced osteogenesis and angiogenesis. Laboratory Investigation **90**, 637, 2010.

164. Tam, W.L., O, D.F., Hiramatsu, K., Tsumaki, N., Luyten, F.P., andRoberts, S.J. Sox9 reprogrammed dermal fibroblasts undergo hypertrophic differentiation in vitro and trigger endochondral ossification in vivo. Cellular reprogramming **16**, 29, 2014.

165. Bahney, C.S., Hu, D.P., Taylor, A.J., Ferro, F., Britz, H.M., Hallgrimsson, B., Johnstone, B., Miclau, T., andMarcucio, R.S. Stem cell-derived endochondral cartilage stimulates bone healing by tissue transformation. J Bone Miner Res **29**, 1269, 2014.

166. Tortelli, F., andCancedda, R. Three-dimensional cultures of osteogenic and chondrogenic cells: a tissue engineering approach to mimic bone and cartilage in vitro. European cells & materials **17**, 1, 2009.

167. Helder, M.N., Knippenberg, M., Klein-Nulend, J., andWuisman, P.I.J.M. Stem cells from adipose tissue allow challenging new concepts for regenerative medicine. Tissue engineering **13**, 1799, 2007.

168. Follmar, K.E., Prichard, H.L., DeCroos, F.C., Wang, H.T., Levin, L.S., Klitzman, B., Olbrich, K.C., andErdmann, D. Combined bone allograft and adipose-derived stem cell autograft in a rabbit model. Annals of plastic surgery **58**, 561, 2007.

169. Muller, A.M., Mehrkens, A., Schafer, D.J., Jaquiery, C., Guven, S., Lehmicke, M., Martinetti, R., Farhadi, I., Jakob, M., Scherberich, A., andMartin, I. Towards an intraoperative engineering of osteogenic and vasculogenic grafts from the stromal vascular fraction of human adipose tissue. European cells & materials **19**, 127, 2010.

170. Mehrkens, A., Saxer, F., Guven, S., Hoffmann, W., Muller, A.M., Jakob, M., Weber, F.E., Martin, I., andScherberich, A. Intraoperative engineering of osteogenic grafts combining freshly harvested, human adipose-derived cells and physiological doses of bone morphogenetic protein-2. European cells & materials **24**, 308, 2012.

171. Evans, C.H., Palmer, G.D., Pascher, A., Porter, R., Kwong, F.N., Gouze, E., Gouze, J.N., Liu, F., Steinert, A., Betz, O., Betz, V., Vrahas, M., andGhivizzani, S.C. Facilitated endogenous repair: making tissue engineering simple, practical, and economical. Tissue engineering **13**, 1987, 2007.

172. Kitamura, S., Ohgushi, H., Hirose, M., Funaoka, H., Takakura, Y., andIto, H. Osteogenic differentiation of human bone marrow-derived mesenchymal cells cultured on alumina ceramics. Artificial organs **28**, 72, 2004.

173. Lee, M.H., Arcidiacono, J.A., Bilek, A.M., Wille, J.J., Hamill, C.A., Wonnacott, K.M., Wells, M.A., andOh, S.S. Considerations for tissue-engineered and regenerative medicine product

development prior to clinical trials in the United States. Tissue engineering Part B, Reviews **16**, 41, 2010.

174. Hing, K.A., Wilson, L.E., andBuckland, T. Comparative performance of three ceramic bone graft substitutes. Spine Journal **7**, 475, 2007.

175. Dennis, S.C., Detamore, M.S., Kieweg, S.L., andBerkland, C.J. Mapping glycosaminoglycan-hydroxyapatite colloidal gels as potential tissue defect fillers. Langmuir : the ACS journal of surfaces and colloids **30**, 3528, 2014.

176. Wang, Q., Gu, Z., Jamal, S., Detamore, M.S., andBerkland, C. Hybrid hydroxyapatite nanoparticle colloidal gels are injectable fillers for bone tissue engineering. Tissue engineering Part A **19**, 2586, 2013.

177. Detamore, M.S., Dennis, S.C., Berkland, C., andBonewald, L. Endochondral Ossification for Enhancing Bone Regeneration: Converging Native ECM Biomaterials and Developmental Engineering in vivo. Tissue engineering Part B, Reviews 2014.

178. Converse, G.L., Armstrong, M., Quinn, R.W., Buse, E.E., Cromwell, M.L., Moriarty, S.J., Lofland, G.K., Hilbert, S.L., andHopkins, R.A. Effects of cryopreservation, decellularization and novel extracellular matrix conditioning on the quasi-static and time-dependent properties of the pulmonary valve leaflet. Acta biomaterialia **8**, 2722, 2012.

179. Shih, W.Y., Shih, W.H., andAksay, I.A. Elastic and yield behavior of strongly flocculated colloids. Journal of the American Ceramic Society **82**, 616, 1999.

180. Walls, H.J., Caines, S.B., Sanchez, A.M., andKhan, S.A. Yield stress and wall slip phenomena in colloidal silica gels. J Rheol **47**, 847, 2003.

181. Fakhari, A., andBerkland, C. Applications and emerging trends of hyaluronic acid in tissue engineering, as a dermal filler and in osteoarthritis treatment. Acta biomaterialia **9**, 7081, 2013.

182. Fakhari, A., Phan, Q., andBerkland, C. Hyaluronic acid colloidal gels as self-assembling elastic biomaterials. Journal of biomedical materials research Part B, Applied biomaterials **102**, 612, 2014.

183. Israelachvili, J.N., andMcguiggan, P.M. Effect of Ions and Surface Lattice Mismatch Angle on Adhesion and Hydration Forces between Mica Surfaces in Electrolyte-Solutions. Abstr Pap Am Chem S **201**, 245, 1991.

184. Leong, Y.K., Boger, D.V., Scales, P.J., Healy, T.W., andBuscall, R. Control of the Rheology of Concentrated Aqueous Colloidal Systems by Steric and Hydrophobic Forces. J Chem Soc Chem Comm, 639, 1993.

185. Garboczi, E.J., Snyder, K.A., Douglas, J.F., andThorpe, M.F. Geometrical Percolation-Threshold of Overlapping Ellipsoids. Phys Rev E **52**, 819, 1995.

186. Khan, S.A., Prudhomme, R.K., andLarson, R.G. Comparison of the Rheology of Polymer Melts in Shear, and Biaxial and Uniaxial Extensions. Rheol Acta **26**, 144, 1987.

187. Buscall, R., Mcgowan, J.I., andMortonjones, A.J. The Rheology of Concentrated Dispersions of Weakly Attracting Colloidal Particles with and without Wall Slip. J Rheol **37**, 621, 1993.

188. Buscall, R., Mills, P.D.A., andYates, G.E. Viscoelastic Properties of Strongly Flocculated Polystyrene Latex Dispersions. Colloid Surface **18**, 341, 1986.

189. Hamed, E., Novitskaya, E., Li, J., Chen, P.Y., Jasiuk, I., andMcKittrick, J. Elastic moduli of untreated, demineralized and deproteinized cortical bone: Validation of a theoretical model of bone as an interpenetrating composite material. Acta biomaterialia **8**, 1080, 2012.

190. Dormer, N.H., Qiu, Y., Lydick, A.M., Allen, N.D., Mohan, N., Berkland, C.J., andDetamore, M.S. Osteogenic differentiation of human bone marrow stromal cells in hydroxyapatite-loaded microsphere-based scaffolds. Tissue engineering Part A **18**, 757, 2012.

191. Bustin, S.A., Benes, V., Garson, J.A., Hellemans, J., Huggett, J., Kubista, M., Mueller, R., Nolan, T., Pfaffl, M.W., Shipley, G.L., Vandesompele, J., andWittwer, C.T. The MIQE guidelines: minimum information for publication of quantitative real-time PCR experiments. Clinical chemistry **55**, 611, 2009.

192. Karlen, Y., McNair, A., Perseguers, S., Mazza, C., andMermod, N. Statistical significance of quantitative PCR. BMC bioinformatics **8**, 131, 2007.

193. Spicer, P.P., Kretlow, J.D., Young, S., Jansen, J.A., Kasper, F.K., andMikos, A.G. Evaluation of bone regeneration using the rat critical size calvarial defect. Nature protocols **7**, 1918, 2012.